# Diverse synaptic mechanisms underlying the processing of peripheral vestibular information in mammals

by

Zhou Yu

A dissertation submitted to The Johns Hopkins University in conformity with the requirements for the degree of Doctor of Philosophy

Baltimore, Maryland

March, 2016

# Abstract

Sensation of head position through the vestibular system is critical for maintaining balance and various physiological functions. To provide head movement information with high fidelity, unique synaptic circuitry has evolved in the mammalian peripheral vestibular epithelium. Among sensory receptors, the hair cells (HCs), type I HCs are completely ensheathed by calyx-like afferent terminals, and type II HCs are contacted by conventional bouton-like afferent terminals. Type II HCs and afferents are also regulated by efferent inputs originating from the brain stem. It is intriguing to know how those specialized neuronal elements work in concert to mediate the peripheral vestibular function. Here, in the first part of this thesis, I investigated synaptic signals generated at synapses between HCs and calyx-containing afferents. I found that output signals from type I HCs were distinct from signals produced by type II HCs, as the former had more tonic waveform and were resistant to glutamate receptor blockade while the later resembled conventional signals resulting from quantal vesicular glutamate synaptic transmission. While both types of signals were excitatory, I showed that those unusual Type I HC signals alone could strongly drive firing rate increases in calyx-containing afferents and mediate vestibular-ocular reflexes (Dr. Kodama performed behavior tests). Therefore, this study demonstrates that peripheral vestibular function is mediated by highly distinct signals at type I and type II HC synapses. Because of their fast onset kinetics, signals generated at the type I HC to calyx synapses may facilitate the detection of quick head movements. In the second part of this thesis, I investigated how efferents modulate the peripheral vestibular function at individual types of synapses. Those efferent synapses showed strong short-term facilitation, indicating that they could

provide powerful modulation during high-level activities. However, efferents were found to inhibit type II HC through α9 nicotinic acetylcholine receptors (nAChRs) and SK potassium channels while exciting calyx-containing afferents through neuronal type nAChRs. Such distinct effects possibly provide a mechanism for efferents to fine tune the gain and sensitivity of the vestibular periphery. By illustrating functional properties of diverse synaptic signals, this study has greatly contributed to our understanding of peripheral vestibular functions.

**Thesis advisor: Elisabeth Glowatzki, Ph.D.**

**Thesis reader: Paul Albert Fuchs, Ph.D.**

# Acknowledgements

The whole journey of this thesis research can be summarized as “exploring the unknowns”. However, there is an old saying in China, if translated into English, it would be: “the life is short while the process of exploring the unknowns is endless. Spending the limited lifetime in solving something infinite – it is dangerous.” Indeed, I have to say that even a tiny bit new scientific knowledge can take a lot of time and efforts to obtain. If this thesis work contributes anything worthy to our knowledge, it could not be completed without support from my family and friends, my mentor and colleagues. I am grateful to have the opportunity here to address my acknowledgements to them, in no particular order.

There have been a lot of ups and downs during my graduate school time. As a young person, the pain caused by the gap between my ambition and achievements can be overwhelming. But even at the most difficult moment, my family and friends always stand behind me no matter what I experience. Especially my parents, I doubt whether they can understand why such scientific discovery would be worth their daughter spending eight years abroad, but I know they will give me full support and understanding just because it is my choice. As I am the only child in the family and they are getting old, it is a huge sacrifice from them that I work abroad for years, yet they always encourage me to pursuit my dream no matter what the outcome is. The best thing happened during my graduate school is to meet my husband. With him, my life becomes more beautiful and colorful. He is the one that I can share with my deepest fear and the one who cheers me up. While I was writing this thesis under time pressure, an accident flooded the apartment and I had to move out. It was him who took the next flight to Baltimore and

helped me take care of the accident. During graduate school, I have been very fortunate to also have quite a few friends. They generously provide their help and keep me accompany. We have had great time together playing board games, trying out restaurants, playing sports and etc.

None of these discoveries made in this thesis study would happen without my mentor Elisabeth Glowatzki. I was forced to leave my previous lab and that could be the end of my scientific career. It was her and David Ginty, who was the director of the training program at that time, made it possible for me to continue studying neuroscience and performing research. During the training in her lab, I learnt a lot from her, for example, how to start a project, how to manage the risks of experiments, how to wrap up a study and etc, and also received enormous amount of support from her. Under her guidance, I had my first meeting presentation, my first fellowship, first publication and manuscript. It is not exaggerating to say that she is my scientific mother. Although I will form my own style one day, her mentorship has profound impact on my scientific career and I am very grateful to have someone so generous, kind and caring as my mentor.

Other faculties, especially my thesis committee members also provide lots of help to my thesis research. They give me not only great suggestions to improve my research, but also advice to handle all kinds of crisis in graduate school. Paul Fuchs has spent a lot of his time to help keep my research project on track, particularly during the last half-year of the thesis study. Mike Caterina and King-Wai Yau also have worked closely with me to ensure that progress has been made to the thesis work. Eric Young is directly involved in computational work for this thesis. There are many others that I can turn to whenever

help is needed, although I can not list all of them, I very appreciate their help over these years.

Last but not least, I owe a lot of thanks to my fellow graduate students, postdocs and technicians. I still remember that it was Yuichi Makino who helped me make the first successful whole-cell recording, Martin Paukert who helped me set up the electrical stimulation for the first time, Donggen Luo who helped me solve the overflow of the bath which eliminated all electrical signals, Soroush Sadeghi who showed me dissection of vestibular tissue, Hakim Hiel who helped me with the cryo-sectioning, Takashi Kodama who helped me with the optogenetic stimulation, and etc. I also want to thank all past and present members in the Glowatzki lab (Chang Liu, Charlene Batrel, Isabelle Roux, Sherry Wu, Ye-Hyun Kim, Soroush Sadeghi, Rodrigo Martinez, Shilpa Chatlani) for working together to overcome difficulties in research. Especially I want to thank Sherry Wu for helping me taking care of some mice and trouble-shooting together for immunohistochemistry experiments. As she and I are both graduate students in the same lab, we have experienced many challenges together, and her encouragement gives us a lot of support. I also want to thank our technician Fatima Chakir for performing genotyping work to all transgenic mice used in this research without a single mistake.

Although I am very proud of scientific discoveries made through this thesis research, there is no standard objective value for them. It could be important for the field at this time, but many years later, it could be just one line in the text book or just a citation in future research, or forgotten. Compared to the whole body of our knowledge, this study is like a drop of water in the sea, or a piece of sand in the desert. However, this thesis study is an important chapter of my limited lifetime not only because the science

but also because all pain and joy in the process. I am fortunate to have this journey with all beloved ones in my life, and that is what makes this thesis study meaningful. Therefore, I dedicate this thesis to my family, my friends, my mentor and colleagues.

# Table of Contents

# List of Figures

# List of Tables

# Chapter 1 Introduction

## 1.1 The sense of balance and the vestibular system.

The existence of the vestibular function barely reaches our consciousness unless it goes wrong. Then, many seemingly simple everyday tasks become impossible. John Crawford, a physician who suffered from a bilateral loss of vestibular function once wrote (Crawford, 1964) – "During walking, there was too much motion in my visual picture of the surroundings to permit recognition of fine detail. I learned that I must stop and stand still in order to read letters on a sign. These early excursions taught me a habit foreign to my New England background – that of greeting anybody who happened to pass. Being unable to distinguish the familiar from the unfamiliar faces when walking the obvious solution was to pretend to recognize everybody." And that was after a long period of compensation and recovery after his loss of vestibular function. At the early phase, he had to brace his head between two metal bars at the head of the bed to minimize "the effect of the pulse beat that made the letters on the page jump and blur " while reading a book.

These impaired functions – reading while walking or lying on bed - would be considered as to be entirely through the visual system. How can it be affected by vestibular dysfunctions? Let's focus on the visual pathway first. High visual acuity is limited to the central 1-degree of the visual filed, the fovea of the retina. Additionally, the retina processing is slow and not able to follow rapid changes of visual images. Therefore, any small head movements would impose challenges to the retina to convey

high acuity visual information of the rapid changing visual field. In fact, to accomplish such tasks, it must engage the vestibular system. The vestibular system can detect the head motions in all six degrees of freedoms (x,y,z, pitch, roll and yaw). Therefore, during head movement, it can drive an eye movement to compensate for the change of the head position and therefore stabilize the image in the fovea of the retina. This process is called the vestibular-ocular reflex (VOR), which is essential for the ability to view images during head movements. And the impairment of this reflex explains the difficulties encountered by John Crawford who had vestibular dysfunctions.

Many physiological functions are executed in a spatial context of oneself and the surrounding environment. From the example of the involvement of the vestibular system in the visual function, perhaps one can appreciate the importance of integrating the spatial information. And a critical component of the spatial information - head motion – is detected and processed by the vestibular system. Indeed, other than the VOR, the vestibular system is involved in many everyday activities by cooperating with other sensory and motor systems. For example, vestibulocollic reflexes can stabilize the head through the neck muscle. Another example is the vestibular-cardiovascular reflexes, which enables the maintaining of cerebral blood pressure during a rapid change of posture. Furthermore, the central vestibular neuro-anatomy also supports the profound impact of the vestibular system on the proper execution of numerous functions. The vestibular nuclei are reciprocally connected with autonomic centers for controlling cardiovascular, visceral and respiratory functions, with the cerebellum for controlling fine

motor movements, and with the thalamus, cerebral cortex and the limbic system for spatial orientation perception.

Therefore, although always acting in the background and in concert with other sensory and motor system, the vestibular function is vital for many behaviors. Impaired vestibular sensation can cause dizziness, vertigo, nausea or a sense of imbalance. It is no exaggeration that many scientists consider the vestibular system together with other proprioceptive systems as a sixth sense.

**1.2 The structure of the vestibular neuronal circuitry.**

The peripheral vestibular system resides in the inner ear bilaterally. It consists of three semicircular canals (anterior, horizontal, and posterior), utricle and saccule (Figure 1.1). All of these end organs are part of a membranous labyrinth. Each canal lies within a single plane and the three canal planes are nearly orthogonal to each other. And the canals of two sides form pairs that have nearly parallel canal planes. This arrangement allows the three canals to cover the detection of three dimensional angular head movements. And the bilateral pairs of canals respond to angular forces in opposite directions and their differences could provide information regarding the angular movement amplitude in that plane. Utricle and saccule are relatively flat and in horizontal and vertical planes respectively. Their function is mainly for detecting linear movement.

Each of these vestibular end organs contains an accessory structure and neuroepithelium (Figure 1.1). For the three semicircular canals, the neuroepithelium is

located at the bottom of the canal where the canal duct is enlarged and gradually merges into the utricle. Because the neuroepithelium is saddle-shaped and has a crest in the middle in the sagittal plane view, it is called the crista ampullaris or crista. A gelatinous accessory structure called the cupula sits on top of each crista and covers the hair bundles of sensory receptors – hair cells in the epithelium. For the utricle and saccule, the neuroepithelium is a flattened and round-shape structure, and is referred to as the macula. On top of the macula, there is a flattened accessory structure called the otoconial or otolithic membrane, as it has calcium carbonate crystals embedded. The accessory structures, cupula and otolithic membrane, couple the mechanical force to the movement of hair bundles. In a common form of vestibular disorder, benign paroxysmal positional vertigo, the calcium carbonate crystals in the utricle travel to the canal duct. The misplacement of those crystals can cause abnormal excitation of canals and result in vestibular dysfunction. One distinct feature of utricle macula and saccular macular is that they have a dividing line around which the orientation of the knocilium of hair cells reverses. For each hair cell, the hair bundle is composed of a single knocilium and many stereocilia. The directions of kinocilia relative to stereocilia are opposite at the two sides of the dividing line. However, such a dividing line is not found in the cristae of semicircular canals.

The neuroepithelium in all vertebrate vestibular end organs are similarly composed of hair cells, supporting cells, vestibular afferent and efferent endings, so here the structure of the neuroepithelium is introduced for all end organs in a generalized

fashion. In the amniotic vertebrates, reptiles, mammals and birds, there are two types of hair cells identified by their postsynaptic afferent contacts (Figure 1.2). Type I hair cells are defined as those completely ensheathed by calyx-like afferent terminals, while type II hair cells are defined as those lacking calyx terminals. Although hair cells serve as sensory receptors in other organs such as the cochlea and lateral lines, the calyx shaped synaptic specialization is unique to the vestibular end organs. Interestingly, the appearance of this specialization is late in evolution, coinciding with the time when vertebrates migrated from water to land. Possibly, this synaptic structure serves special functions to help vertebrates adapt to the land environment. As the main emphasis of this thesis study is on the mammalian vestibular system, only the vestibular periphery with calyx terminals and type I hair cells is introduced here. Other than the existence of calyx-terminals, morphologically, type I and type II hair cells have subtle differences in the diameters of mitochondria and stereocilia and the distribution of nuclear chromatin (reviewed in (Eatock et al., 1998)). It is worth pointing out that many early studies distinguish hair cells solely based on whether they have a narrowing in the apical part – "neck" and classify those that have "necks" as type I hair cells and others as type II hair cells. Such a method may be largely correct but is not entirely accurate. Numerous cases encountered in my study and other studies showed that type I and type II hair cells could not be reliably distinguished based on the degree of narrowing in the apical part. The numbers of type I hair cells and type II hair cells are roughly equal in rodents (Desai et al., 2005a), but have a 3:1 ratio in old world monkeys (Rhesus Monkey, *Macaca mulatta*)

(Lysakowski, 1996) and in new world monkey (Squirrel Monkey, *Saimiri sciureus*) (Lysakowski and Goldberg, 2008), possibly reflecting a increasing predominance of type I hair cells.

The cell bodies of vestibular afferents lie in Scarpa's ganglion that is close to the internal auditory meatus, while the dendritic terminals of those afferents densely innervate the vestibular neuroepithelium and receive inputs from hair cells. There are two types of terminals: as described in the previous part, calyx terminals that surround type I hair cells and bouton terminals that contact type II hair cells (Figure 1.2). For one given afferent, it can contain only calyx terminals (referred as calyx-only afferents), or only bouton terminals (referred as bouton-only afferents), or a mixture of both terminals (referred as dimorphic afferents). One calyx ending sometimes can embrace more than one type I hair cells with a shared wall in between, and this type is referred to as complex calyx. Using immunostaining methods, in the vestibular ganglion neuron population of rodents, ~20% are calyx-only afferents based on calretinin staining(Desai et al., 2005a, Desai et al., 2005b) and ~5% are bouton-only afferents based on peripherin staining(Lysakowski et al., 1999). In addition, based on a study in which randomly sampled afferents were morphologically reconstructed, 32% were calyx-only afferents, 66% were dimorphic and 2% were bouton-only afferents (Baird et al., 1988). Although these estimations may not be precise, results from these studies using different methods agree that the majority of afferents are dimorphic.

These different types of hair cells and afferent terminals are not evenly distributed in the vestibular epithelium. Based on the distribution of these neuronal elements, the crista can be divided into a central zone and a peripheral zone, and the macula can be divided into a striola and extrastriola zone. An intermediate zone and juxtastriola zone have been suggested in some studies, however, the definition is not consistent. The central zone and striola zone are located in the center of the neuroepithelium. In rodents, the most obvious feature of the central zone and striola zone is that they contain calyx-only terminals, especially complex calyx terminals, while these types of terminals are missing in the peripheral and extrastriola zones (Desai et al., 2005a, Desai et al., 2005b). Because of this property, calretinin has been used as a marker for the central/striola zone, as it labels calyx-only afferents (Although it also labels dimorphic afferents in turtles (Jordan et al., 2015)). Compared to the peripheral/extrastriola zone, the central/striola zone has a slightly lower hair cell density and slightly higher type I hair cell to type II hair cell ratio(Desai et al., 2005a, Desai et al., 2005b). Despite the benefit of having a better anatomical separation of the vestibular neuroepithelium, do the central/striolar zone and the peripheral/extrastriola zone have any differences in functions? Perhaps the major difference is that the firing pattern of afferents in the central/striola zone is much more irregular than those in the peripheral/extrastriola zone, and I will discuss the physiological meaning of these patterns later. The cupula and otolithic membrane may also exert different mechanical forces in the center versus the surrounding of the neuroepithelium. Moreover, the central/striola zone and peripheral/striola zone may

project to different central targets in the brain, as indicated in a recent study using retrograde tracers in the cerebellum and the brain stem (Maklad et al., 2010).

The vestibular afferents with terminals in the periphery are from cell bodies located in the Scarpa's ganglion. The axons of those ganglion cells enter the brain in the vestibular division of the eighth cranial nerve and target ipsilaterally on secondary neurons in the vestibular nuclei and cerebellum. Unlike the auditory or the visual system where topographic representations of the peripheral sensory inputs are present at the first relay in the brain, vestibular nerves from all five organs are already mixed in the path to the secondary neurons. No separate regions committed to processing information from a single end organ have been identified. This anatomical arrangement indicates that although head motion information is deposed into different components and detected by different end organ at the periphery, these components are integrated at an early stage to reconstruct the head movements. The vestibular nuclei and cerebellum then send projections to numerous targets and are involved in many important physiological functions. As the focus of this thesis study is on the peripheral vestibular system, I will not go into the details of those central pathways.

The peripheral vestibular system not only relays information to the brain, it also receives a feedback efferent projection from the brain stem. In mammals, the efferent neurons are located in three groups of neurons. The major group is referred to as group e, which is a slender column of neurons extending rostrocaudally between the abducens and superior vestibular nuclei (reviewed in (Holt et al., 2011)). Those efferents project

bilaterally and innervate all five end organs. At a cellular/synaptic level, those efferents synapse on to type II hair cells and afferents (Figure 1.2). The efferent synapse onto type II hair cells has a postsynaptic membrane specialization – a near-membrane endoplasmic cistern, while no obvious specialization is detected for the efferent synapse onto afferents, suggesting that the efferents may have distinct actions on these two targets.

### 1.3 Computation at each stage of the vestibular peripheral circuitry.

Hair cells are the first stage where head motion signals are transformed into neuronal activities. Head movement can induce a relative displacement between the accessory structure (cupula or otolithic membrane) and the neuroepithelium, and result in deflection of hair bundles. The hair bundle deflection can open or close mechanotransduction channels located in the hair bundles and lead to depolarization or hyperpolarization of hair cells. The properties of mechanical transduction current in vestibular hair cells are comparable to those of cochlear hair cells, including a slow adaptation (Holt et al., 1999, Songer and Eatock, 2013). Type II hair cells have similar composition of voltage-dependent channels as typical hair cells (Rusch et al., 1998). Displacement of hair bundles can lead to transduction currents of ~200 pA and a ~20 mV change of membrane potential (Holt et al., 1999) in type II hair cells. Responses to mechanical stimulation are also similar in immature type I hair cells. The frequency dependence of receptor potentials of type II and immature hair cells suggest that they mainly act as low-pass filters with corner frequencies around 30-40 Hz, although with

slight attenuation for stimulations below 2 Hz, possibly due to adaptation of the mechanotransduction channels (Holt et al., 1999, Songer and Eatock, 2013). However, mature type I hair cells (> postnatal day 8 in mice) have an unusually large resting potassium conductance mediated by low threshold delayed rectifier potassium channels ($g_{K,L}$) (Rusch et al., 1998). Such a large conductance gives type I hair cells a very hyperpolarized resting membrane potential, low gain for mechanical inputs due to low membrane resistance and a fast membrane time constant. As expected then, mechanical stimulation is less effective for type I hair cells – only a maximum peak-to-peak membrane potential change of less than 10 mV can be reached. On the other hand, due to the fast membrane time constant, the frequency dependence of receptor potentials allows type I hair cells to behavior more like a high-pass filter and to perform better at detecting high frequency inputs (with a high-pass corner frequency of $\sim$ 5 Hz (estimated from (Songer and Eatock, 2013)). These drastic differences between type I and type II hair cells in response properties for mechanical stimulation indicate that they may have distinct functions in vestibular sensation.

Both type I and type II hair cells form ribbon synapses with afferent terminals. In electron micrographs, those presynaptic ribbons sites are evident as an electron-dense body surrounded by many vesicles filled with transmitters. Ribbon synapses have been considered as a common mechanism that allows continuous synaptic transmission, and they are found to function in many sensory cell types including various types of hair cells, retinal photoreceptors and bipolar cells, and etc. Interestingly, there seems to be a trend

for fewer ribbons per hair cells with climbing the “the evolutionary ladder”: in turtles, there are ~30 ribbons per type I hair cells and ~40 ribbons per type II hair cells (Holt et al., 2007); in rodents, there are ~20 ribbons per type I hair cells and type II hair cells (Lysakowski and Goldberg, 1997, Sadeghi et al., 2014); in squirrel monkeys, there are ~10 ribbons per type I hair cells and ~20 ribbons per type II hair cells (Lysakowski and Goldberg, 2008). In neurons using ribbon synapses, vesicular release of transmitters usually induces quantal excitatory postsynaptic currents (qEPSCs) mediated through glutamate receptors in postsynaptic neurons. Indeed, spontaneously occurring and stimulation evoked qEPSCs have been observed in bouton-only afferents in chickens(Yamashita and Ohmori, 1990), in bouton afferents and calyx-bearing afferents in turtles(Holt et al., 2006b, Holt et al., 2007, Highstein et al., 2014, Highstein et al., 2015), in isolated HC containing calyx terminals of gerbils (Rennie and Streeter, 2006), in a subset of immature calyx-bearing afferents in the mouse utricular macula (Songer and Eatock, 2013), and in calyx-bearing afferents in rats(Sadeghi et al., 2014), suggesting that ribbon synaptic transmission also occur at vestibular hair cell synapses. Those qEPSCs can be abolished by blockers of ionotropic glutamate receptors(Holt et al., 2006b, Holt et al., 2007, Highstein et al., 2014, Sadeghi et al., 2014), indicating that they are mediated by glutamatergic transmission. Because synaptic release from ribbons is triggered by intracellular calcium concentration and hence is coupled with the membrane potential of hair cells, such a quantal form of synaptic transmission can be effective in transferring the presynaptic receptor potential into changes in the postsynaptic membrane

potential. However, besides qEPSCs, it has been observed that mechanical stimulation of hair bundles also induces more steady non-quantal currents in calyx-afferents of chicken(Yamashita and Ohmori, 1990), bouton afferents and calyx-bearing afferents of turtles (Holt et al., 2007, Highstein et al., 2014) (Holt et al., 2006b) and a subset of immature calyx-bearing afferents at the mouse utricle macula(Songer and Eatock, 2013). It has been shown that the glutamate receptor blocker CNQX (6-cyano-7-nitroquinoxaline-2, 3-dione) has no effects (Highstein et al., 2014) or small blocking effects (Holt et al., 2006b, Holt et al., 2007) on such non-quantal responses. As the non-quantal responses are unique to vestibular afferents of amniotic vertebrates, it has been speculated that they may be generated at the specialized calyx terminals (Goldberg, 1996), but the direct evidence for that is still missing. Moreover, the identity of the non-quantal currents remains mysterious. As characterization of this non-quantal transmission is a main subject of this thesis study, more detailed discussion will be present later.

Hair cell receptor potentials are translated into spikes in vestibular afferents and then relayed to the brain. In the peripheral vestibular physiology field, afferents are usually classified into irregular and regular firing types based on the distribution of inter-spike-intervals obtained for a given afferent. Regularity of firing is considered as an important characteristic of a given afferents, because it is independent of the firing rate and is consistently associated with other physiological properties (reviewed in (Goldberg, 2000)). Irregular firing afferents are mostly calyx-only afferents and dimorphic afferents with terminals in the central/striola zone. They have a thicker fiber diameter and larger

responses to galvanic currents and efferent stimulation. Regular firing afferents are mostly bouton-only afferent(s) and dimorphic afferents with terminals located in the peripheral/extrastriola zone. Our knowledge of the physiology of bouton-only afferents in mammals is extremely limited; as there has been only one such recording of morphologically identified bouton-only afferents (Baird et al., 1988), possibly due to the scarcity of this afferent type.

It has been investigated for decades for whether regular and irregular afferents encode different vestibular information. In general, irregular afferents have much higher gain for head rotation (Goldberg, 2000). However, calyx-only afferents are the exception as they exhibit low rotational gain but have the most irregular firing patterns (Baird et al., 1988). Perhaps response dynamics over different frequency domains can be another indicator of functional differences between regular and irregular afferents. Those analyses suggest that the gain of regular afferents is quite constant over different frequencies, indicating that they have a more "tonic" feature and transfer head motion signals regardless of frequencies. On the other hand, the gain of irregular afferents grows rapidly for higher frequencies, indicating that they have a more "phasic" feature and are more sensitive to high frequency head motion signals (Goldberg and Fernandez, 1971).

The mechanisms underlying difference in firing regularity are not fully understood. The regularity is likely to be an intrinsic property of the afferent fiber itself rather than resulting rom synaptic inputs (Goldberg and Holt, 2013), and neuromodulators may be able to alter the regularity of afferents(Kalluri et al., 2010).

Despite the fact that regularity has been widely used to classify vestibular afferents, it appears that most secondary neurons receive inputs from both regular and irregular (reviewed in (Goldberg, 2000)). As the timing of those inputs is integrated in the secondary neurons, it is of questionable whether the regularity itself is physiologically important.

The activity of hair cells and afferents are also influenced by efferent inputs from the brain stem. In mammals, electrically stimulating efferents *in vivo* exclusively induces an increase of background firing rates of afferents, and such excitation is especially large in irregularly firing afferents (Goldberg and Fernandez, 1980, Marlinski et al., 2004). Activation of efferents also leads to a decrease of rotational gain in afferents (Goldberg and Fernandez, 1980, Plotnik et al., 2005). Additionally, efferent-mediated rotational responses can be observed in the otolith afferents that do not themselves respond to head rotations (Goldberg and Fernandez, 1975), and in canal afferents when positioning the head to the null plane (Sadeghi et al., 2009). However, in other species, efferent stimulation can not only cause excitation but also cause inhibition or a mixed excitation and inhibition in vestibular afferents, suggesting that different mechanisms may be involved in these species (reviewed in (Holt et al., 2011)). Although not much study of response properties of efferent neurons has been conducted in mammals, in other species those efferent neurons have been shown to respond to vestibular stimulation, somatosensory stimulation, visual stimulation and possibly active body (reviewed in

(Holt et al., 2011)). Therefore, the integrated multimodal information can impact the vestibular sensation through efferent inputs to the periphery.

In the periphery, efferents provide synaptic inputs to type II hair cells and afferents neurons. Acetylcholine is the major neurotransmitters released by efferent terminals (reviewed in (Holt et al., 2011)), although other transmitters such as CGRP (calcitonin gene-related peptide) may also play a role(Luebke et al., 2014). Using pharmacological approaches, recent studies in turtle vestibular afferents indicate that efferent induced excitation is mediated by α4, α6, and β2 nicotinic acetylcholine receptors; while efferent induced inhibition is mediated by α9 nicotinic acetylcholine receptors and calcium dependent SK potassium channels (Holt et al., 2006a, Holt et al., 2015). Although those channels and receptors are also expressed in the vestibular periphery of mammals(Hiel et al., 1996), it is not clear whether similar mechanisms can apply. As the mechanism underlying efferent inputs to the mammalian vestibular periphery is one subject of this thesis study, I will discuss this topic in more detail in later chapters.

**1.4 Challenges of detecting head movements at the periphery.**

Many behaviors require the vestibular system to provide real time information about head movement. Therefore, the peripheral vestibular system must be able to rapidly and reliably detect head motion. Let's take an overview of the processing of vestibular information at the periphery: head motion is first transferred into displacement of

accessory structures. Such displacement is then detected by hair cells through the mechanotransduction process. The membrane potential of hair cells determines their synaptic outputs to postsynaptic vestibular afferents. In the last step, afferents encode the synaptic signals into spikes and then relay the head motion information to the brain. As the information flows from the hair cells to the afferents and then to the brain, the transfer functions of hair cells and afferents must be able to guarantee the reliability and sensitivity needed for detecting head movement.

To understand the challenges of detecting head movements through the peripheral vestibular neuronal circuitry, here I use the semi-circular canal system as an example. Studies with different psychophysical methods reveal that humans are extremely sensitive to angular acceleration with a threshold for perception of 0.1 deg/s$^2$ (Clark and Stewart, 1968, Miller and Graybiel, 1975). Given that the angular acceleration of most head movements fall into the range between 2,000 to 10,000 deg/s$^2$(Armand and Minor, 2001), such sensitivity is remarkable, indicating that the peripheral vestibular system has the capacity to detect angular acceleration that is across a wide range that differs ~100,000 fold in intensity! As most active head movements happen in the frequency domain of 8-12 Hz(Armand and Minor, 2001), one may argue that in this range of frequencies canals serve as angular-velocity transducers. Most psychophysical tests have had an observation period of ~20 s, hence that gives a threshold for detecting differences in head velocity at ~ 2 deg/s. Peak angular velocity for most active head movements is in the range of ~400 - 1000 deg/s (Grossman et al., 1988, Armand and Minor, 2001), therefore, the ability of the

peripheral vestibular system to encode head velocities is still quite impressive, across a ~500 fold difference in intensity.

Like other sensory systems, the peripheral vestibular system must maintain a high signal-to-noise ratio in the signal detection process for best sensitivity, while avoiding being saturated for large inputs. It is not known whether such capacity lies at the individual neuronal level through mechanisms of the mechanotransduction, synaptic transmission, spike generation, or in the circuitry level through integrating convergent inputs from many neurons. Perhaps, both neuronal and circuitry level mechanisms account for the remarkable ability of the peripheral vestibular system has to detect head movements. Different neuronal elements such as type I and type II hair cells, calyx-only, dimorphic, and bouton afferents likely play distinct roles in deciphering different components of head movements while operating in concert to produce vestibular sensation. Knowledge of the functional roles of these neuronal elements has been gained through decades of investigation including this thesis study. However, many decades of work are still ahead of us to understand fully the mechanisms of peripheral vestibular sensation.

**1.5 Objectives of this thesis study.**

The peripheral vestibular system has a tremendous ability to detect head movements, yet the mechanisms underlying such power remains mysterious. This thesis study is devoted to improving our understanding of how vestibular information is processed in the periphery through cellular and synaptic level mechanisms.

Among those different neuronal elements, type I hair cell-calyx synapses are the most unique structure evolved for the peripheral vestibular system in reptile, birds and mammals. The presence of such elaborate calyx synapses is unlikely to be an accident, as species appear later in evolution tend to have more type I hair cells and calyx synapses. The question is: what is the functional benefit provided by such specialized neuronal structure? Clues may arise from functional updates required for adapting to life in land. At the same time when type I hair cell-calyx synapses appeared, those land vertebrates also started to have mobile necks. The neck allows animals to move heads more flexibly to explore the surroundings, but also potentially imposes challenges to the peripheral vestibular system for reporting more rapid head movements. Would type I hair cell-calyx synapses play any roles in overcoming these challenges? As described in previous sections, type I and type II hair cells have quite distinct properties. Due to the presence of a large resting potassium conductance, type I hair cells have extremely low resting membrane resistance that allows them to capture rapidly changing inputs as the membrane time constant is lowered by the tiny membrane resistance. However, this fast membrane time constant comes at the sacrifice of gain - the amplitude of membrane potential modulation evoked by mechanical stimulation is exceptionally small. Such low gain limits type I hair cells to operate at a negative membrane potential that is close to the equilibrium potential of potassium. One intriguing question is: if type I hair cells communicate with calyx endings through ribbon synaptic transmission, how can such a negative membrane potential allow for sufficient calcium influx to trigger the release of

transmitters (Bao et al., 2003)? As the membrane potential of type I hair cells may not favor ribbon synaptic release, other possible transmission mechanisms related to the restricted space in the calyx synaptic cleft such as accumulation of potassium and ephaptic coupling have been raised in a theoretical study (Goldberg, 1996). However, despite that potassium accumulation is suggested indirectly from a shift of equilibrium potential in incomplete calyx synapses (Lim et al., 2011, Contini et al., 2012), definitive experimental evidence is still missing. In addition, "non-quantal" synaptic currents in calyx-bearing afferents have been found in a number of studies (Yamashita and Ohmori, 1990, Holt et al., 2006b, Holt et al., 2007, Songer and Eatock, 2013, Highstein et al., 2014). Yet as in these studies either all hair cells are activated or only a subset of calyx bearing afferents show such non-quantal currents, it is not conclusive whether such non-quantal currents happen in type I hair cell-calyx synapses. Furthermore, if synaptic signals provided by type I hair cells and type II hair cells are highly distinctive, efferent inputs then possibly selectively regulate type II hair cell pathways as they synapse onto type II hair cells and afferents but not onto type I hair cells. By tuning these individual pathways, the question is, what kind of functional impact do efferents exert on vestibular sensation?

As solving these mysteries will provide many insights into understanding the computation of the vestibular peripheral system, this thesis study is mainly focus on addressing two fundamental questions: (1) Do type I and type II hair cells provide functionally distinct synaptic signals to calyx bearing afferents? (2) How do efferents

impact the peripheral vestibular through modulation of the activities of type II hair cells and calyx bearing afferents? To investigate these questions, one prerequisite is to be able to activate hair cells or efferents and record the activities of calyx bearing afferents at high resolution. Therefore, the first goal of this study was to establish methods that make such investigation technically possible, and the results are summarized in **Chapter 2**. In particular, optogenetic methods – a recent technique that allows targeted activation of neurons through engineered light gated ion channels (reviewed in (Deisseroth, 2015)) – are implemented to stimulate vestibular hair cells and efferents. This optogenetic approach enables me to control the activity of hair cells and efferents with great temporal and spatial precision, and therefore is critical for conducting this thesis study. Moreover, this study is among the first a few attempts to apply this cutting edge technique to investigate the neuronal circuitry of the inner ear. Experiences gained through many trials and failures for the successful implementation of optogenetic technique will be beneficial for other researchers and will advance the field.

In **Chapter 3**, results achieved through investigating the signal processing at the hair cell to calyx bearing afferents synapses – the first synapse in the vestibular sensation, are presented. Optogenetic activation of hair cells revealed that calyx bearing afferents had quantal synaptic inputs that are sensitive to glutamate receptor blockade and steady "non-quantal" inputs that are insensitive to those blockers. Selective optogenetic stimulation of hair cells showed that "non-quantal" signals derived solely from type I hair cells while quantal synaptic currents were due to transmitter release from type II hair

cells. Thus, the type I hair cell to calyx connection enables a unique form of rapid, sustained vestibular signaling in amniotes. Furthermore, these "non-quantal" signals could effectively drive afferent activity. Transgenic mice with impaired quantal transmission had normal vestibular –ocular-reflexes (VOR) and unimpaired movement, suggesting that non-quantal signals were sufficient for mediating essential vestibular behaviors.

In **Chapter 4**, results achieved by investigating the synaptic mechanisms underlying efferent inputs to vestibular type II hair cells and calyx-bearing afferents are presented. In type II hair cells, electrical stimulation of efferents revealed that efferent inputs had weak basal synaptic strength but can be greatly facilitated during high frequency repetitive efferent stimulation. The efferent inputs were cholinergic and mediated through α9 nicotinic acetylcholine receptors and SK calcium activated potassium channels in type II hair cells. Facilitated efferent inputs could strongly hyperpolarize type II hair cells, resulting in reduced outputs from this hair cell type. In contrast, in calyx-bearing afferents, optogenetic stimulation of efferents induced inward excitatory synaptic inputs and therefore could cause depolarization. Compared to the efferent currents in type II hair cells, efferent synaptic currents in calyx-bearing afferents had slow kinetics resembling those evoked through volume transmission mode; and those currents were mediated through α4 nicotinic acetylcholine receptors. These results demonstrated that efferents could differentially regulate type II hair cells and calyx-bearing afferents. Therefore, efferent modulation of peripheral vestibular sensation is

conveyed through the summation of these two distinct cellular actions. Interestingly, direct application of acetylcholine solution caused α9 nicotinic receptor mediated currents in calyx-bearing afferents. As α9 receptors were not detected in calyx-bearing afferents, these currents are thought to be mediated by a "chain reaction" activation of type I hair cells followed by "non-quantal" synaptic transmission to the calyx-bearing afferents, revealing further insights into the properties of type I hair cells and "non-quantal" transmission.

In **Chapter 5**, a discussion based on results achieved in this thesis study is presented. As "non-quantal" signals from type I hair cells and quantal signals from type II hair cells were identified and characterized in this thesis work, these newly discovered functional properties of the first synapse in the vestibular sensation could bring in many new insights into the understanding of the computation performed at the vestibular periphery. Would distinct vestibular information be channeled through these two forms of synaptic transmission? What could be the possible mechanisms underlying the "non-quantal" transmission? As shown by this thesis work, efferent inputs could differentially modulate type II hair cells and calyx-bearing afferents. What would be the functional consequence of efferent modulation? Not only these questions are discussed, but also future work that could expand this thesis study is suggested.

### 1.6 List of abbreviations.

From Chapter 2, abbreviations are used to denote certain terms.

| | |
|---|---|
| 4AP | 4-aminopyridin |
| α-BTX | α-Bungarotoxin |
| α-RgIA | α-conotoxin RgIA |
| ACh | Acetylcholine |
| APV or AP5 | Amino-5-phosphonopentanoic acid |
| ASIC | Acid-sensing ion channel |
| Calyx-afferent | The afferent that contains calyx terminal(s), including both calyx-only afferents and dimorphic afferents |
| CGRP | Calcitonin gene-related peptide |
| ChAT | Choline acetyltransferase |
| ChR2 | Channelrhodopsin - 2 |
| CNQX | 6-cyano-7-nitroquinoxaline-2,3-dione |
| CPP | 3-(2-Carboxypiperazin-4-yl)propyl-1-phosphonic acid |
| DHβE | Dihydro-β-erythroidine hydrobromide |
| Gfi1 | Growth factor independent 1 |
| HC | Hair cell |
| IBTX | Iberiotoxin |
| KO | Knockout |
| LED | Light-emitting diode |
| nAChR | Nicotinic acetylcholine receptor |
| NBQX | 2,3-Dioxo-6-nitro-1,2,3,4-tetrahydrobenzo[*f*]quinoxaline-7-sulfonamide |
| NMDA | *N*-Methyl-D-aspartic acid |

| | |
|---|---|
| MCPG | α-Methyl-4-carboxyphenylglycine |
| PNU-282987 | N-(3R)-1-Azabicyclo[2.2.2]oct-3-yl-4-chloro-benzamide monohydrochloride |
| Pr | Probability of release |
| PX | Postnatal day X; X is a number |
| QX-314 | *N*-(2,6-Dimethylphenylcarbamoylmethyl)triethylammonium |
| Rm | Membrane resistance |
| Ra | Access resistance |
| TBOA | *Threo*-β-Benzyloxyaspartic acid |
| VgluT | Vesicular glutamate transporter |
| Vh | Holding potential, usually in the unit mV |
| Vm | Membrane potential, usually in the unit mV |
| VOR | Vestibular – Ocular – Reflexes |
| WT | Wildtype |
| ZD-7288 | 4-Ethylphenylamino-1,2-dimethyl-6-methylaminopyrimidinium chloride |

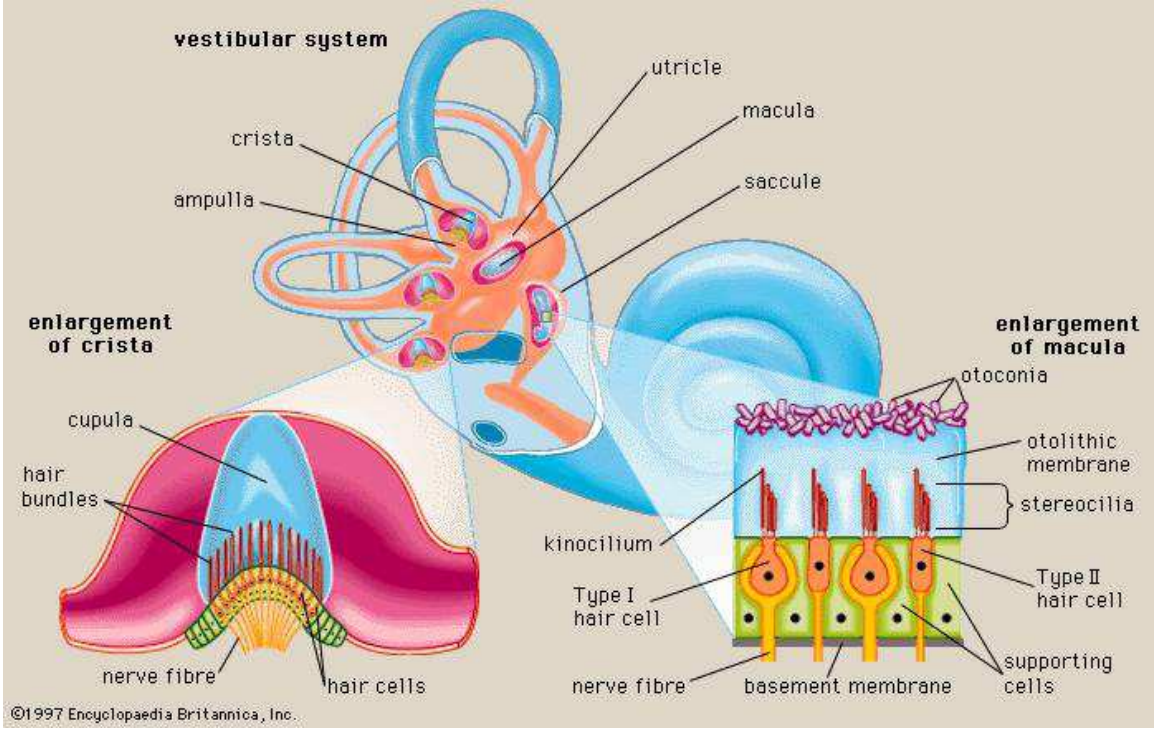


**Figure 1.1 The structure of the peripheral vestibular system.** ©1997 Encyclopaedia Britannica, Inc. The peripheral vestibular system consists of three semicircular canals, utricle and saccule. For the three semicircular canals, the neuroepithelium (crista) is located at the bottom of each canal (ampulla). A gelatinous accessory structure (cupula) sits on top of each crista. For the utricle and saccule, the neuroepithelium (macula) is flattened. The accessory structure for macula is otolithic membrane, which has calcium carbonate crystals (otoconia) embedded. The accessory structures couple the mechanical force generated by head motion to the movement of hair bundles of sensory receptors, triggering the vestibular information processing.

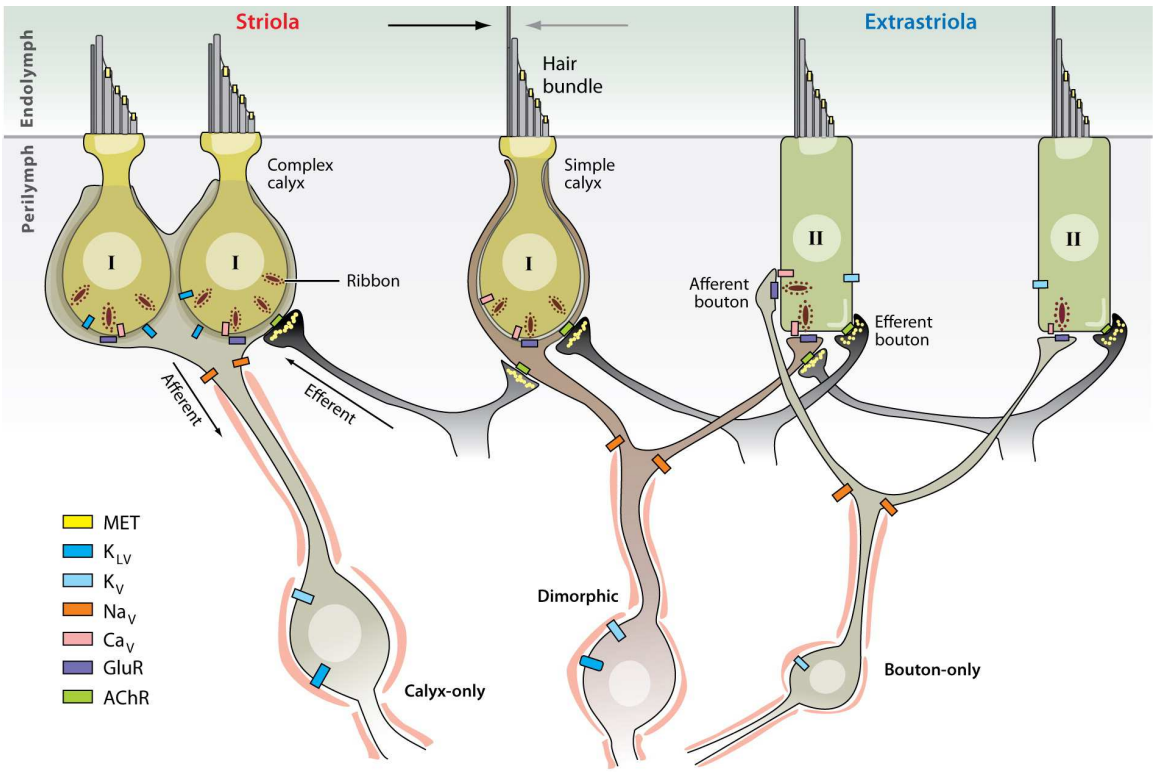


**Figure 1.2 Hair cells, primary afferents and efferents at the vestibular epithelium.** Modified from (Eatock and Songer, 2011). Here using the macula as an example, this figure shows in the vestibular neuroepithelium: (1) there are two types of hair cells, type I hair cells are those contacted by calyx-shape afferent terminals while type II hair cells are those contacted by bouton-shape afferent terminals; (2) Vestibular afferents can have calyx-shape terminals only (calyx-only) or bouton-shape terminals only (bouton-only) or both (dimorphic); (3) Efferents form synaptic contacts with type II hair cells and afferent terminals.

# Chapter 2 Methods

## 2.1 Animals.

All animals were handled in accordance with animal protocols approved by the Johns Hopkins University Animal Care and Use Committee. 13- to 30-d-old rats and mice of either sex were used for electrophysiology recording and immunohistochemistry experiments. 2-5 month old mice were used for behavioral tests. The rat strain is Sprague-Dawley (Charles River Laboratories). In addition to wild-type (WT) C57BL/6J mice (Jackson Laboratories (JAX) #000664), for different experimental purposes, several transgenic lines were used.

To specifically drive gene expression in vestibular HCs, we obtained Gfi1-Cre mice as a gift from Dr. Lin Gan and Dr. Jian Zuo (Yang et al., 2010). To examine the cre expression pattern in this mouseline, they were crossed with Ai3 mice (from JAX, B6.Cg-Gt(Rosa)26Sor$^{tm3(CAG-EYFP)/Hze}$/J; JAX #007903) (Madisen et al., 2010). To drive the expression of ChR2, they were crossed with Ai32 mice (from JAX, B6;129S-Gt(ROSA)26Sor$^{tm32(CAG-COP4*H134R/EYFP)Hze}$/J; JAX#012569) (Madisen et al., 2010). YFP signals were detected in all vestibular HCs (100%) and only in HCs in Gfi1-Cre; Ai3 and Gfi1-Cre; Ai32 mice at P21- P30 (Figure 2.1A). Additionally, YFP signals were detected in the majority of cochlear HCs (90%) in Gfi1-Cre; Ai32 mice at P6. To selectively activate HCs (details are described in Chapter 3), we also obtained VgluT3-Cre mice (from JAX, Tg(Slc17a8-icre)1Edw/SealJ, JAX#018147) to achieve sparse or random expression of genes in HCs. YFP signals were detected in only a small percentage of

vestibular HCs (~10%) in VgluT3-Cre; Ai3 and VgluT3-Cre; Ai32 mice at P21- P30 (Figure 2.1B). To eliminate glutamatergic quantal synaptic transmission, I used VgluT3 knockout mice (from JAX, B6;129S2-Slc17a8$^{tm1Edw}$/J, JAX# 016931) (Grimes et al., 2011). As described previously (Seal et al., 2008), these mice were deaf and showed no startle reflexes to sound. In addition, to examine the expression of VgluT1 and VgluT2, we obtained VgluT1-Cre mice (from JAX, B6;129S-Slc17a7$^{tm1.1(cre)Hze}$/J, JAX#023527) (Harris et al., 2014) and VgluT2-Cre mice (from JAX, Slc17a6$^{tm2(cre)Lowl}$/J, JAX#016963) (Vong et al., 2011). In VgluT1-Cre; Ai3/Ai32 mice, a small subset of vestibular afferents were EYFP positive (Figure 2.2A). In VgluT2-Cre; Ai3/Ai32 mice, the majority of vestibular afferents were EYFP positive (Figure 2.2B). Occasionally I found a few HCs that were EYFP positive in VgluT2-Cre; Ai3/Ai32 mice (n=3 litters (at least two mice each litter) were examined for each genotype).

To specifically drive gene expression in vestibular efferents, we obtained ChAT-Cre mice (B6;129S6-Chat$^{tm2(cre)Lowl}$/J; JAX#006410). YFP signals were detected in efferents only in ChAT-Cre; Ai32 mice at P21-P28 (Figure 2.1C). A gradual increase of YFP positive fibers was observed for mice between P13-P18. α9 knockout mice (originally as CBACaJ;129S-Chrna9$^{tm1Bedv}$/J; JAX#005696) (Vetter et al., 1999) were used to explore the functional role of α9 nAChRs in efferent modulation. To examine the expression pattern of α9 nAChRs in the vestibular periphery, α9-GFP mice were generously provided by Dr. Jian Zuo (Zuo et al., 1999)(Figure 4.6A).

**2.2 Tissue preparation.**

This procedure was described in (Sadeghi et al., 2014). Mice or rats were deeply anesthetized by isoflurane inhalation and decapitated. The inner ear tissue was removed from the temporal bone and placed into extracellular solution. The bony labyrinth was opened and part of the membranous labyrinth was dissected, including ampullae of horizontal and superior canals and Scarpa's ganglion. The efferent fibers in the preparation were cut off from their somata located in the brainstem. The membranous labyrinth was then opened above the cristae and utricle and remaining cupulae located on top of hair cells were removed to expose the neuroepithelia.

**2.3 Electrophysiology recording.**

The preparation was secured on a coverslip under a pin, transferred to the recording chamber, and perfused with extracellular solution at a rate of 1.5 -3 ml/min. The extracellular solution contained (in mM): 5.8 KCl, 144 NaCl, 0.9 $MgCl_2$, 1.3 $CaCl_2$, 0.7 $NaH_2PO4$, 5.6 glucose, 10 HEPES, 300 mOsm, pH 7.4 (NaOH). In some experiments, to increase the extracellular $K^+$ concentraion up to 40 mM, equimolar NaCl was replaced with KCl. In some experiments, the external solution was heated close to body temperature (32 °C) through an inline heater (ThermoClamp-1). To perform patch-clamp recording, tissue was visualized with a 40X water-immersion objective, differential interference contrast (DIC) optics (Axioskop2 microscope, Zeiss) and viewed on a

monitor via a video camera (Dage MTI LSC 70 or IR1000). For targeted recording of fluorescent structures, a wide-field excitation lamp (X-Cite 120) was used as light source.

Patch-clamp recording pipettes were fabricated from 1mm inner diameter borosilicate glass (WPI). Pipettes were pulled with a multistep horizontal puller (Sutter), fire polished, and coated with Sylgard (Dow Corning). Pipette resistances were 5-8 MΩ. The intracellular solution for HC and calyx–afferent recordings contained (in mM): 20 KCl, 110 K-methanesulfonate, 0.1 $CaCl_2$, 5 EGTA, 5 HEPES, 5 $Na_2$ phosphocreatine, 4 MgATP, 0.3 Tris-GTP, 290 mOsm, pH 7.2 (KOH). To improve voltage control during recordings from voltage-clamp recording from calyx-afferents at positive holding potentials (> 0 mV), in a subset of experiments, CsCl based internal solution was used, containing 135 CsCl, 3.5 $MgCl_2$, 0.1 $CaCl_2$, 5EGTA, 5 HEPES, 2.5 $Na_2$ATP, 280 mOsm, pH7.2 (CsOH). To reconstruct the morphology of recorded cells, 0.25-0.3% biocytin (Sigma) was included in the internal solution.

Whole-cell patch-clamp recordings were performed in HCs and calyx-afferents of cristae of either superior or horizontal canals. Cell-attached recordings were performed in some calyx-afferents. All measurements were acquired using pCLAMP10.2 software in conjunction with a Multiclamp 700B amplifier (Molecular Devices), digitized at 50 kHz with a Digidata 1440A, and filtered at 10 kHz. Putative type II HCs were distinguished from putative type I HCs by the absence of calyx-terminal surroundings, a structure that could be visualized as thickened double layer under DIC optics. Type I hair cells were exposed by separating the surrounding calyx terminals with positive pressure. The profile

of voltage dependent conductances of HCs was examined for each HC by applying a voltage-clamp protocol consisting of a hyperpolarization step from -70mV to -130 mV followed by depolarization steps to different potentials from -129 mV to -9 mV (Figure 2.3A). The resulting currents were similar to those of utriclar HCs in previous studies (Rusch et al., 1998)(Figures 2.3B, 2.3C). In particular, in both mice and rats, in putative type II HCs the hyperpolarizing step activated inward currents of a few hundred pAs that were likely mediated by $I_{K1}$, a class of delayed rectifier currents and hyperpolarization activated $I_h$ currents (Rusch et al., 1998); in contrast, in type I HCs, the hyperpolarizing step triggered huge slowly inactivating currents of several nAs, resembling $I_{K,L}$ mediated by delayed rectifier potassium channels (Rusch et al., 1998). Consistent with previous studies in utricle, $I_{K,L}$ was a marker for type I HCs here. As morphologically the presence of calyx terminals could be compromised in the in-vitro preparation, only putative type II HCs that lacked the large and inactivating $I_{K,L}$ were considered type II HCs for the subsequent study. The same voltage-clamp protocol was also applied to calyx-afferents, in which the depolarization step could evoke large inward transient likely mediated by sodium channels (Figure 2.3D). For whole-cell recordings, a voltage clamp protocol contained a 50-ms long, 10 mV hyperpolarization step from -75 or -80 mV was applied to examine membrane resistance (Rm) and access resistance (Ra). Only recordings that had Ra smaller than 25 MΩ were included in data analysis. Membrane resistance of different cell types is reported in Table 2.1.

Drug solution was either applied to the bath directly or to the tissue focally. Focal application of solutions was performed using a gravity-driven flow pipette (~100 μm in diameter) placed near the recorded calyx, connected with a VC-6 channel valve controller (Warner Instruments, Hamden, CT). Amiloride hydrochloride, Iberiotoxin(IBTX), Apamin, 4-aminopyridine (4AP), ZD-7288, DHβE, D-AP5, NMDA, D-Aspartic acid, QX-314 chloride, NBQX, CNQX, (RS)-CPP, (RS)-MCPG, were purchased from Tocris Bioscience. α-CGRP (mouse, rat) was purchased from Bachem. Acetylcholine chloride, PNU-282987, α-Bungarotoxin (α-BTX), Strychnine hydrochloride, (+)-tubocurarine hydrochloride and barium chloride ($BaCl_2$) were purchased from Sigma. α-RgIA was provided by Dr. J.M. McIntosh (Ellison et al., 2006).

**2.4 Electrical stimulation of vestibular efferents.**

Monopolar electrical stimulation of efferents was delivered through a glass micropipette (the same size as the patching pipette) that was placed about 100 μm beneath the targeted hair cells. An electrically isolated constant current source (model DS3, Digitimer Ltd, Welwyn Garden City, UK) was triggered via the data acquisition computer to generate pulses up to 8-50 mA, 20-40 μs long to activate efferents. The position of the stimulation pipette was slowly adjusted so that the electrical pulses could evoke synaptic events with minimal contamination of artifacts. To ensure that the stimulation strength was sufficient to reliably trigger synaptic events, I monitored the release probability by delivering 100 – 200 pulses at 2 Hz at each testing amplitude. The

stimulating amplitude was set at a value where no further increase of release probability was detected at an amplitude that was two times bigger.

**2.5 Optogenetic stimulation.**

Blue light pulses was delivered through an optical fiber (diameter: 910μm, Thorlab) coupled to a LED light source (Xlamp, 485nm, Cree). The intensity and timing of light pauses was controlled through a LED driver (Mightex) that can operate under the command of the data acquisition computer. The maximum output light intensity reached by this system is ~80-100 $mW/mm^2$. For stimulating axons, brief light pulses of 3-5 ms were applied. For activating hair cells, light pulses of 1 s were applied. Synaptic responses evoked by optogenetic stimulation were compared with responses evoked by electrical stimulation in some experiments included in **Chapter 4**.

**2.6 Immunohistochemistry and imaging.**

Freshly excised temporal bone tissue with bony labyrinth opened or tissue after electrophysiology recording was dropped to 4% paraformaldehyde (PFA) for fixation of 1hr to 24 hrs at 4°C and then rinsed in PBS solution. In some experiments, Scarpa's ganglion were then isolated and cryo-sectioned as described (Hiel, 2009). For cryo-sectioning, tissue was transferred to 30% sucrose PBS and rocked overnight at 4°C. The tissue was placed in optimal cutting temperature medium (OCT medium) and fast frozen.

Tissue embedded in OCT block was then cryo-sectioned into slices of 30-50 μm thickness and collected onto slides. Slides were warmed at 45-55°C for 1 hr to dry.

For antibody-based immunolabeling, samples including both whole mount tissue and cryo-sections were first incubated in blocking buffer (PBS with 10% normal donkey serum, 0.3% Triton X-100) for 1 hr. Samples were then incubated in primary antibody diluted in blocking buffer for 24-48 hrs at 4°C. Samples were rinsed in PBS before incubation in secondary antibody diluted 1:500 – 1:750 in blocking buffer for 2 hrs. After rinsing in PBS for 3-5 times, samples were mounted on glass slides in FluorSave™ Reagent medium (EMD Millipore). Primary antibodies used in this work included the following: goat anti-GFP (1:5000, SicGen), mouse anti-TUJ1(1:250, BioLegend), mouse anti-MyosinVIIa (1:250, Sigma), rabbit anti- MyosinVI (1:250, Sigma), rabbit anti-TUJ1(1:250, BioLegend), guinea pig anti-VgluT3(1:500, originally from Dr. Robert Edwards, provided by Dr. Omar Akil). Secondary antibody used in this work included the following: Alexa Fluor® (488, 555, or 595) conjugated donkey anti-goat IgG(H+L) (ThermoFisher), Alexa Fluor®(488, 568 or 647) conjugated donkey anti-rabbit IgG(H+L) (ThermoFisher), Alexa Fluor®(488, 568, or 647) conjugated donkey anti-mouse IgG(H+L) (ThermoFisher), Alexa Fluor®594 AffiniPure donkey anti-guinea pig IgG(H+L) (Jackson ImmunoResearch), and Rhodamine Red ™-X(RRX) donkey anti-guinea pig IgG(H+L) (Jackson ImmunoResarch).

For labeling biocytin filled HCs and vestibular afferents, tissue was either stained by incubating with Alexa Fluor® 488 or 568 conjugated strepdavidin (ThermoFisher) for

2hrs (Figure 2.3C1) or by diaminobenzidine (DAB) peroxidase (HRP) histochemistry reaction (Figures 2.3D1, D2). To be processed for DAB-HRP staining, tissue was quenched in 1%hydrogen peroxide for 10 mins, permeabilized in 2%Triton X-100 in PBS for 1 hr, incubated for 2 hrs using solution mixed with VECTASTAIN ABC kit (Vector laboratories), and finally in DAB substrate (ImmPACT DAB EqV Peroxidase Substrate, Vector laboratories) for 10 mins or until tissue turned dark. After these steps, tissue was rinsed and mounted.

Fluorescence images were acquired using a laser scanning confocal microscope (LSM700, Zeiss) under the software control of ZEN. Imaged Z-stacks were collected under near saturating laser intensities for each channel. Images of DAB-HRP stained tissue was acquired with a Nikon E600 compound microscope coupled with a CCD camera (Q-Imaging MicroPublisher).

**2.7 Data analysis and modeling.**

For some experimental results, certain features of electrophysiology data, such as amplitude, area and etc were extracted and analyzed using Clampfit (Molecular Devices). For applying similar analysis to many recordings, performing computation intense analysis and simulating models, Matlab (MathWorks) scripts were written. The function to read in ABF 2.0 files was adapted from abfload.m contributed by Harald Hentschke, Forrest Collman and Ulrich Egert. In general, threshold for detecting signals was set as mean plus or minus three times the standard deviation. Search steps were overlapped and

the length was usually set as 5 data points (equal to 0.5 ms) and values were calculated by averaging 10-500 data points (equal to 1- 50 ms). Spikes were automatically detected with a threshold set manually. Synaptic events were analyzed using Minianalysis (Synaptosoft). All synaptic events were detected by eye. Parameters of these events were calculated by built-in routines in Minianalysis, and at least 5 points were averaged for a peak value. Decay phase of synaptic events was fitted with single exponential and only fitting results with coefficient of determination (R squired) >0.85 was considered as a good fit and included for further analysis. For those well fitted events, 10-90 % $\tau_{decay}$ was calculated. Igor Pro (WaveMetrics) was used for making plots. An IgorPro script written by Dr. Juan Goutman was used to read in ABF 1.8 files. Most data are reported as mean±SE.

**2.8 VOR measurements.**

These experiments was entirely conducted by Dr. Takashi Kodama, previously described in (Faulstich et al., 2004). In brief, mice were deeply anesthetized, and headposts for restraining the head were implanted onto the skull. After a recovery period of at least 48 hrs after the surgery, mice were subject to eye movement recordings. Vestibular stimulation was applied by rotations of the turntable. Eye movements were monitored and acquired by a miniature infrared video camera.

**Table 2.1 Membrane resistances of vestibular HCs and calyx-afferents**

| Rm (MΩ) | Type I HC | Type II HC | Calyx-afferents |
|---|---|---|---|
| **Rats, at RT** | 50.0 ± 12.7 | 528.6 ± 62.0 | 107.7 ± 16.1 |
| **Mice, at RT** | 43.2 ± 6.0 | 957.0 ± 39.4 | 122.5 ± 14.9 |
| **Mice, at 32°C** | 32.4 ± 4.1 | 749.7 ± 163.4 | 122.2 ± 59.0 |

RT: room temperature

$n \geq 3$ for each testing condition

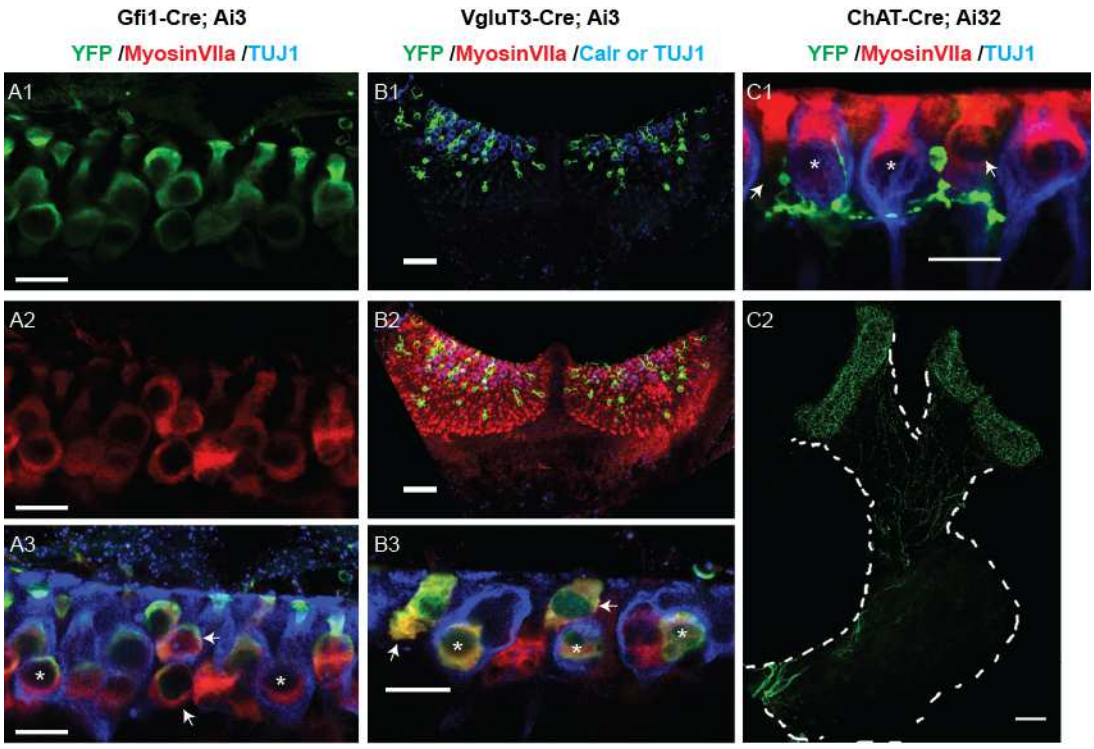


**Figure 2.1 Cre mouse lines used for driving ChR2 expression in this thesis study.** A. Expression pattern in cristae of Gfi1-Cre; Ai3 mice. YFP (A1-A3, stained against YFP (green)) signals were present in all HCs (A2 and A3, stained against MyosinVIIa (red)), regardless of cell types (A3, merged image of A1 and A2 with labeling of afferents for TUJ1 (blue)). B. Expression pattern in cristae of VgluT3-Cre; Ai3 mice. YFP (B1-B3, stained against YFP (green)) signals were presented in a subset of HCs (B2 and B3, stained against MyosinVIIa (red)) in both central zone (B1 and B2, with labeling of calyx-only afferents by staining against calretinin (blue)) and peripheral zone, including both type I and type II HCs (B3, with labeling of afferents by staining against TUJ1). C. Expression pattern in the vestibular periphery of ChAT-Cre; Ai32 mice. YFP positive efferent fibers (C1 and C2, stained against YFP (green)) formed synaptic contacts onto

HCs (C1, stained against MyosinVIIa (red)) and afferents (C1, stained against TUJ1 (blue)). Asterisks: type I HCs; arrows: type II HCs. Scale bar: A1-A3, B3, C1: 10 μm; B1 and B2: 50 μm; C2: 100 μm.

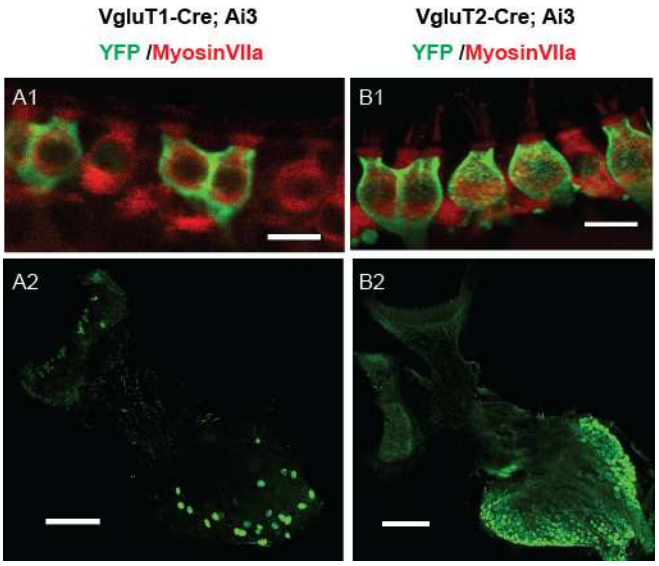


**Figure 2.2 Cre mouse lines used for identifying gene expression in this thesis study.** A. Expression pattern in crisate of VgluT1-Cre; Ai3 mice. YFP (A1 and A2, stained against YFP (green)) signals were present in a small percentage of vestibular afferents (A1, with labeling of HCs by staining against MyosinVIIa (red)). B. Expression pattern in crisate of VgluT2-Cre; Ai3 mice. YFP (B1 and B2, stained against YFP (green)) signals were present in the majority of vestibular afferents (B1, with labeling of HCs by staining against MyosinVIIa (red)). Scale bar: A1 and B1: 10 μm; A2 and B2: 200 μm.

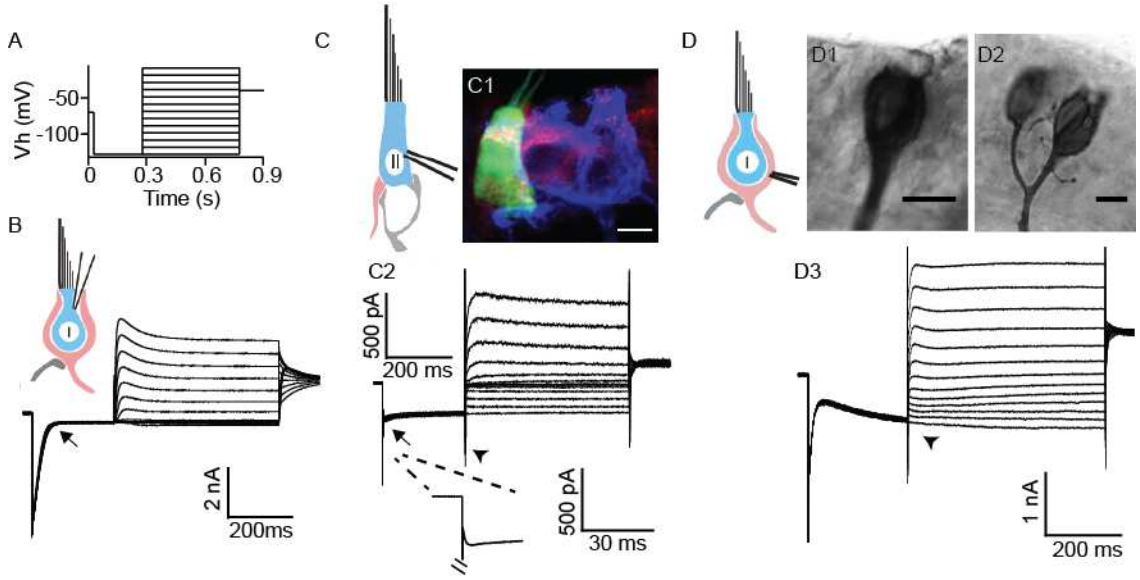


**Figure 2.3 Identification of cell types for whole-cell patch clamp recording.** A. The voltage clamp protocol used to determine voltage dependent channel conductance. B. Recorded currents during the test protocol in a type I HC. Arrow: inactivation phase of $I_{K,L}$. C. Type II HCs were recognized as those HCs without calyx surroundings (C1, a type II HC (green) was filled with biocytin during recording, with labeling of HCs (stained against MyosinVIIa (red)) and afferents (stained against TUJ1 (blue)). Type II HCs lacked $I_{K,L}$ (C2), but instead have a small hyperpolarization activated conductance (C2, inset). Type II HCs had moderate level inward transient currents following the depolarization (C2, arrow head). D. Calyx-afferents included both calyx only (D1) and dimorphic (D2) afferents (filled with biocytin during recording). Calyx-afferents typically exhibited large inward transient currents following the depolarization (D3, arrowhead).

# Chapter 3 Type I and type II hair cells provide functionally distinct synaptic signals to mediate the peripheral vestibular sensation

Vestibular HCs of amniotes are differentiated into highly distinct type I and type II HCs. Each type of HCs is associated with their elaborate synaptic structure – type I HCs are ensheathed by calyx-like terminals while type II HCs are contacted by bouton-like terminals, implying that different forms of synaptic transmission are present with type I and type II HCs. To illustrate what kind of signals are provided by these different synapses, in this chapter, synaptic transmission from type I and type II HCs to calyx-afferents was investigated at high resolution using the optogenetic approach. Distinct non-quantal and quantal signals are shown to originate from type I and type II HCs respectively. Moreover, I show that the atypical non-quantal signals are sufficient to drive activities of vestibular afferents and to mediate vestibular behaviors.

## 3.1 Activation of vestibular HCs induces both quantal and non-quantal signals at calyx-afferents.

To specifically activate vestibular HCs, Gfi1-cre mouse line (Yang et al., 2010) was used to drive the expression of ChR2 coupled with the fluorophore EYFP (**Figure 2.1 A**). In Gfi1-Cre; Ai32 mice of P21-P29, every HC tested could be excited by blue light pulses (n = 32). One second long light pulses reliably depolarized type I (1.1±0.3 mV) and type II (21.9±1.7 mV) HCs with rapid onset (Type I HC: 1.9±0.3 ms; Type II

HC: 1.3±0.4 ms) and little trial-to-trial variation (standard deviation: Type I HC:0.005±0.001 mV; Type II HC: 0.109±0.024 mV; for 10 trials) at near saturating levels (85%-95%) of illumination (n = 7, each type) (**Figure 3.1**). Type I HCs had very hyperpolarized resting membrane potentials (-76.9±1.5 mV) and could only be depolarized to -75.8±1.6 mV, while type II HCs could be depolarized more effectively from -73.9±2.4 mV to -53.0±1.2 mV (n=7, each). This differential depolarization is similar to that reported for hair bundle displacement (Holt et al., 1999, Songer and Eatock, 2013) presumably due to the large resting membrane conductance mediated by the opening of delayed rectifier potassium channels (gK,L) in mature type I HCs (Rusch et al., 1998).

One second long light pulses reliably produced steady postsynaptic currents with rapid onset in calyx-afferents (n = 27, holding potential (Vh) at -90 mV) (Figures 3.2 A,B,C and D) with waveforms similar to the 'non-quantal' responses that were reported for calyx-afferents in cristae of turtles and in the utricle of immature mice(Songer and Eatock, 2013, Highstein et al., 2014). Non-quantal postsynaptic currents were observed in all calyx-afferents tested (n = 27) in contrast to previous studies (Songer and Eatock, 2013, Highstein et al., 2014), indicating that the presence of calyx terminals was sufficient for non-quantal signaling. In addition to non-quantal responses during light stimulation of HCs, fluctuating quantal excitatory postsynaptic currents (qEPSCs) increased in calyx-afferents (n= 14, 3.35±0.79 Hz vs. 0.04±0.01 Hz (in stimulus vs. background), p = 0.001, paired t-test). These qEPSCs had widely varying decay kinetics

(tau = 6.9±0.5 ms, n = 14)(Figure 3.2C inset), consistent with previous observations (Sadeghi et al., 2014, Highstein et al., 2015). Light-evoked non-quantal and quantal currents were comparable in peak amplitude (Figure 3.2 E). However, compared to qEPSCs, the non-quantal currents had little trial-to-trial variation (p=0.05), activated more rapidly (non-quantal: 5.4±0.7 ms; quantal: 284.9±49.5 ms, p <0.0001) and produced a much larger total charge transfer (non-quantal: 35.37±5.14 pC; quantal: 0.79±0.22 pC, p<0.0001), suggesting that they might be mediated by distinct mechanisms.

The kinetics of qEPSCs resembled those from glutamate-releasing ribbon synapses, and previous studies showed that qEPSCs in vestibular afferents could be blocked by antagonists of glutamate receptors (Holt et al., 2007, Highstein et al., 2014, Sadeghi et al., 2014, Highstein et al., 2015). Consistent with those findings, all qEPSCs evoked optogenetically were also completely blocked by a cocktail of antagonists toAMPA/Kainate receptors (25 uM NBQX, 25 uM CNQX), NMDA receptors (25 uM CPP) and mGluRI/II receptors (500 nM MCPG) (n = 6) (Figure 3.2 G). On the other hand, studies of calyx-afferents in turtles suggested that CNQX and APV had less or no effects on non-quantal currents(Holt et al., 2007, Highstein et al., 2014). In agreement with that, the glutamate receptor blocker cocktail used here did not affect the evoked non-quantal currents (in blockers vs. control, -20.7 ± 6.0 pA vs. -18.5 ± 6.3 pA, n= 6, p = 0.25), suggesting that they were not mediated by those traditional glutamate receptors (Figure 3.2 G). The distinct pharmacological properties of non-quantal and quantal

responses not only suggested different underlying mechanisms, but also provided a method to isolate these two responses by glutamate receptor blockade.

### 3.2 Type I HCs and type II HCs contribute to non-quantal and quantal signals respectively.

If quantal and non-quantal responses shared a common upstream cellular origin, their strength might show some degree of correlation. However, the amplitude of non-quantal responses was not significantly correlated with either the amplitude or the increase in frequency of quantal EPSCs (Correlation of amplitude: R = 0.1708, p-value = 0.14; frequency: R: = 0.0093, p-value = 0.97, n = 14, Figure 3.2 F), suggesting that these two modes of transmission arose from independent sources.

One possibility was that the quantal and non-quantal signals were differentially contributed by type I and type II HCs. To dissect the outputs from each individual type of HCs, I took advantage of sparse expression in VgluT3-Cre (Grimes et al., 2011); Ai32 mice to achieve selective excitation of type I or type II HCs. Unlike Gfi1-cre; Ai32/Ai3 mice where every HC was EYFP positive, VgluT3-Cre only drove expression in an apparently random minority of type I and type II hair cells (~ 10%, Figure 2.2B, Figure 3.3A1). Nevertheless, one second long light stimulation could depolarize EYFP positive type I HCs by 1.4±0.5 mV (n=3) and EYFP positive type II HCs by 22.4±2.8 mV (n=4) in VgluT3-Cre; Ai32 mice (Figures 3.3A2 and A3), comparable to light evoked depolarization achieved in Gfi1-Cre mice.

Thus, three testing scenarios were carried out in the crista of VgluT3-Cre; Ai32 mice, according to the distribution of sparse EYFP-positive type I and type II HCs by eye and later verified by immunostaining: (1) “Type I only” calyx-afferents which had at least one EYFP-positive type I HC in calyces and no nearby (within 10μm) EYFP-positive type II HCs (Figure 3.3B1). (2) “Type II only” calyx-afferents which had no EYFP-positive type I HCs in calyces but at least one EYFP-positive type II HC nearby (Figure 3.3C1). (3) “mix of type I and type II” calyx-afferents which had both EYFP+ type I HC(s) in calyces and EYFP+ type II HC(s) nearby. These three conditions allowed us to analyze outputs from type I or type II HCs or both: during light stimulation, “type I only”, “type II only” and “mix of type I and type II” calyx-afferents would receive evoked outputs from type I HC(s), type II HC(s) and a combination of type I and type II HCs respectively.

Remarkably, with the 1s light stimulation protocol, in all “type I only” calyx-afferents only non-quantal synaptic responses were observed (-19.5±2.5 pA, n = 15, Vh = -90mV), with no significant increase of qEPSCs (Figure 3.3B2)(in stimulus vs. background, 0.10 ± 0.06 Hz vs. 0.14±0.06 HZ, P=0.14, n = 15 (n=5 had morphology reconstructed)), suggesting that type I HCs provided only non-quantal signals in this testing condition. Also, only evoked non-quantal responses but not qEPSCs were observed when this same experiment was repeated at near-physiological temperature (32°C) either (n = 4), so those data were combined here. Furthermore, these non-quantal responses remained in the presence of the glutamate receptor blocker cocktail (Figure

3.3B3) (in blockers vs. Ctrl, -17.1 ± 3.5 pA vs. -18.6±2.6 pA, n = 11, p = 0.32, paired t-test), confirming that their pharmacological identity was the same as non-quantal responses determined previously.

In contrast, "type II only" calyx-afferents showed no responses (8 out of 14 tested, possibly due to connectivity between type II HC and calyx-afferents) or were dominated by increases of qEPSCs (Figure 3.3 C2-C5) (In stimulus vs. background, 4.77 ± 1.30 Hz Hz vs. 0.13 ± 0.08 Hz Hz, n = 6 out of 14 tested, p = 0.015; (n=4 had morphology reconstructed). Notably, these qEPSCs resulting from depolarization of type II HCs also exhibited a wide range of decay kinetics (Figure 3.3C2). Responses of those afferents exhibited a slight steady component (-3.3 ± 2.2 pA, n = 6) (Figure 3.3C4). However, compared to the non-quantal responses coupled with the activation of type I HCs, this steady component was much smaller, without a rapid onset and was proportional to the frequency of qEPSCs (Figure 3.3C3)(R = -0.891, p = 0.017, n = 6). The cocktail of glutamate receptor blockers completely eliminated all light evoked responses in "type II only" calyx-afferents, including both qEPSCs and the steady component (Figure 3.3C6), indicating that the steady component here resulted from summed effects of qEPSCs. Thus, outputs from type II HCs were mediated by glutamate and only in the form of qEPSCs. As expected, "mix of type I and type II" calyx-afferents showed both light-evoked quantal and non-quantal responses (n=3). Therefore, by selectively activating type I and type II HCs, I demonstrated that non-quantal signals were from type I HCs while quantal signals were from type II HCs. Since qEPSCs

presumably resulted from glutamate release from ribbon synapses, the lack of qEPSCs from type I HCs was not entirely unexpected. The small depolarization of type I HCs with quite negative resting membrane potentials in our condition would be unlikely to trigger significant calcium influx to drive synaptic release(Bao et al., 2003).

As these experiments were done in VgluT3-Cre; Ai32 mice, one concern was that our conclusion might be biased toward VgluT3 expressing HCs. Two pieces of evidence suggested that VgluT3 was widely expressed in vestibular HCs and the Cre expression was non-selective: (1) Almost all HCs were immunopositive for VgluT3 (Figure 3.5A) while only a small subset of VgluT3-positive HCs were EYFP-positive in VgluT3-cre; Ai32/Ai3 mice (Figure 3.3A1); (2) the percentage of HCs that were EYFP-positive varied widely among individual mice indicating that VgluT3-Cre expression was turned on randomly. Given the similarity of light-evoked depolarization in HCs in Gfi1-cre; Ai32 and VgluT3-cre; Ai32 mice, I could combine results achieved from these two lines of experiments. As all calyx-afferents tested here showed both quantal and non-quantal responses in Gfi1-cre; Ai32 mice, having identified the origins of those two types of transmission in the VgluT3-Cre; Ai32 mice, I conclude that most calyx-afferents normally receive inputs from type I and type II HCs.

### 3.3 Non-quantal signals from type I HCs effectively drive spiking activities in calyx-afferents.

The non-quantal and quantal signals differed in their cellular origins, kinetics and dependence on glutamate transmission. To evaluate the impact of these signals on calyx-afferent transmission, I examined effects of HC stimulation in Gfi-Cre; Ai32 mice where all HC were synchronously activated - a situation more representative of physiological conditions. First, I measured HC-evoked currents in calyx-afferents while holding these afferents at different membrane potentials (Figure 3.4A1). Both quantal and non-quantal currents remained inward until 0 mV (Figure 3.4A2), indicating that they were both excitatory to calyx-afferents. No significant non-quantal currents were observed above 0 mV, possibly reflecting the nature of this transmission mode. In contrast, quantal EPSCs reversed at 0 mV, consistent with mediation by ionotropic glutamate receptors. As non-quantal signals were from type I HCs and quantal signals were from type II HCs, to understand how the intensity of these two types of signals reflected the activity level of their source HCs, the relation between HC membrane potentials and their corresponding output synaptic signals measured at different light intensity was investigated (Figure 3.4B)(n=12 in each condition). The amplitude of non-quantal signals was linearly proportional to the membrane potential of type I HCs. Similarly, a linear relationship between the frequency of quantal signals and the membrane potential of type II HCs was also identified. Therefore, both non-quantal and quantal signals could faithfully encode the information detected at HCs with almost constant gain, at least within the testing condition of this study.

Although the size of both quantal and non-quantal responses was moderate, optogenetic activation of HCs reliably increased the firing rate of calyx-afferents. Measured in cell-attached recordings at physiological temperature (32°C), in all calyx-afferents examined, the firing rate exhibited an increase from 10.4±8.9 Hz (baseline) to 40.4±12.9 Hz during light stimulation of hair cells (n = 6, p =0.017) (Figures 3.4C and E). To dissect the contribution from non-quantal signals mediated by type I HCs and quantal signals mediated by type II HCs, I examined spiking activities of calyx-afferents in the cocktail of glutamate receptor blockers; as this should completely abolish quantal signals while leaving non-quantal signals intact. In the presence of glutamate receptor blockade, the majority of calyx-afferents with various degree of spiking regularity still showed a strong increase of firing rate during optogenetic stimulation of HCs (Figures 3.4D and E) (In stimulus vs. baseline, 37.2±13.5 Hz vs. 13.7±13.0 Hz, n= 6, p = 0.036), suggesting that non-quantal inputs are sufficient to generate spikes in calyx-afferents. Compared to the control condition where both quantal and non-quantal signals depolarized calyx-afferents, the increase in firing rate resulting from non-quantal signals alone was not significantly different (Figure 3.4 E) (Ctrl vs. in blockers, 30.0±8.6 Hz vs. 23.5±8.3Hz, n =6, p = 0.183, paired t-test), indicating that non-quantal signals from type I HCs play a major role in driving activities in those calyx-afferents. Consistent with this conclusion, selectively activating type I HCs in VgluT3;Ai32 mice also led to increased firing in some calyx-afferents (n = 4). Notably, in a small percentage of calyx-afferents (n=1, recorded at room temperature, and n = 1 recorded at physiological temperature),

glutamate receptor blockers eliminated all spiking activities both during stimulus or baseline, indicating that firing activities of these afferents mainly depended on quantal signals under our testing conditions. Nevertheless, all the foregoing results together demonstrated that non-quantal signals from type I HCs were sufficient in themselves to change firing rate in the majority of calyx-afferents.

### 3.4 Non-quantal synaptic transmission alone is sufficient for basic vestibular functions.

If the activity of calyx-afferents could be dominated by non-quantal inputs from type I HCs, non-quantal synaptic transmission should play a critical role in vestibular sensation. To evaluate the behavioral significance of non-quantal transmission, I collaborated with Dr. Takashi Kodama to examine vestibular function in VgluT3 knockout mice. VgluT3 had been shown to be essential for glutamate transmission in ribbon synapses of HCs, including cochlear inner HCs(Seal et al., 2008) and HCs of zebrafish (Obholzer et al., 2008). Moreover, the VOR was absent in VgluT3 mutant zebrafish larvae (Obholzer et al., 2008).

Immunostaining showed that VgluT3 was highly expressed in vestibular HCs, and immunoactivity was particularly strong in type II HCs which were the source of the quantal transmission (Figures 3.5A1-A4) (n=4 preparations from two litters). The expression of the other two types of vesicular glutamate receptor transporters, VgluT1 and VgluT2, was also examined in knockin VgluT1-Cre and VgluT2-Cre mice crossed

with reporter line Ai3 or Ai32. No EYFP signals were detected in VgluT1-Cre;Ai3 or Ai32 mice; and only sporadic expression of EYFP was detected in several HCs in VgluT2-Cre; Ai3 or Ai32 mice (Figure 2.2), indicating that these two type of transporters were unlikely to serve critical functions. Thus Vglut3 was the predominant type of vesicular glutamate transporter for vestibular HC synaptic transmission. Indeed, in Vglut3 KO mice, no qEPSCs could be evoked (0/16, from n= 8 mice) by depolarizing HCs using external solution containing a high concentration of potassium (at 15, 25 and 40 mM respectively), while this solution could reliably induce quantal EPSCs in wildtype mice and heterozygous (VgluT3+/-) littermate (11/13, from n = 7 mice) and rats (Sadeghi et al., 2014) (Figures 3.5 B). Therefore, Vglut3 KO mice could serve as an experimental model in which quantal synaptic transmission from vestibular HCs to calyx-afferents, and presumably to bouton-only afferents as well, was abolished.

Although VgluT3 KO mice were found to be deaf (Seal et al., 2008) and showed no startle reflexes to sound, surprisingly, the VOR appeared to be normal in these mice (Figures 3.5C and D, performed by Dr. Takashi). Those VgluT3 KO mice exhibited VOR gain and phase comparable to that of WT mice during sinusoidal vestibular stimulation at different frequency and velocity, indicating that mice without quantal glutamate transmission from vestibular HCs could perform the VOR without detectable deficits. As non-quantal transmission was the only way to receive vestibular information from HCs in VgluT3 KO mice, these results suggested that non-quantal signals from type I HCs were sufficient for driving the basic vestibular function - VOR. This also explained differences

from the behavior outcome of VgluT3 mutant zebrafish larvae, as they didn't have the type I HC-calyx synaptic specializations and depend solely on conventional quantal transmission for the vestibular function.

### 3.5 Novel mechanisms may underlie synaptic transmission at type I HC to calyx synapses.

Although the only output signals from type I HCs identified with the optogenetic approach were non-quantal, type I HCs had the machinery for vesicular glutamate release. In particular, spontaneous synaptic events were recorded in isolated calyx terminals of gerbils (Rennie and Streeter, 2006), suggesting that qEPSCs could originate from type I HCs. As neither optogenetic nor mechanical stimulation could lead to sufficient depolarization in type I HCs, external solution that contained high concentration of potassium (40 mM $K^+$) was used to activate type I HCs (Sadeghi et al., 2014). Theoretically, 40 mM $K^+$ could shift the equilibrium potential of potassium ($E_k$) from ~ -82.7 mV to ~ -33.1 mV (calculated as with 5.8 or 40 mM external $K^+$, 145 mM internal $K^+$, at 298K). As external solution that contained 25 mM $K^+$ could depolarize type I HCs to -43 mV (n=2), 40 mM $K^+$ should push type I HCs above the threshold for allowing sufficient calcium influx and vesicular glutamate release.

In collaboration with Dr. Soroush Sadeghi (data was reported in (Sadeghi et al., 2014)), by recording from calyx-afferents in rats, we found that EPSCs recorded in 40 mM $K^+$ had significantly larger amplitude and slower decay time (from 4.9±0.6 ms in 5.8mM $K^+$ to 8.5±1.7 in 40 mM $K^+$, n=17, paired t-test, p = 0.03). Notably, as shown in

**3.1** and **3.2**, at least a portion of these EPSCs should arise from type II HCs. Since synaptic currents mediated by NMDA receptors normally exhibited a slow decay, I tested whether these slow ESPCs were resulted from activation of NMDA receptors by applying 20 μM CPP, an NMDA receptor antagonist. Even with the removal of $Mg^{2+}$ blockade (all $Mg^{2+}$ was substituted with $Na^{+}$) and in the presence of co-agonist D-serine (40 μM), CPP had no effects on the waveform of EPSCs ($\tau_{decay}$: at Vh= -80 mV, in CPP vs. Ctrl: 3.26 ms vs. 3.25 ms, paired t-test, p = 0.21, n = 4; at Vh= 60 mV, in CPP vs. Ctrl: 3.90 ms vs. 4.19 ms, paired t-test, p = 0.33, n =3)(Figure 3.6A), indicating that NMDA receptors had little or no contribution to these EPSCs. Another possible mechanism for those slow EPSCs is that of glutamate spillover to receptors located at a distance from the release site (DiGregorio et al., 2007). In agreement with that possibility, Dr. Sadeghi and Dr. Pyott showed that antibody labeled ribbons (by staining against CTBP2) and postsynaptic glutamate receptor clusters (by staining against GluR2/3) were not directly juxtaposed at the inner face of calyx terminals. Finally, in this recently published study(Sadeghi et al., 2014), ATP (at ~100 μM or higher) was used to elevate the synaptic release rate, and effects of the glutamate transporter TBOA were tested on those evoked synaptic currents. However, in subsequent experiments, I found that the amount of ATP induced depolarization was small in type I HCs, as the same concentration of ATP could at most depolarize type I HCs to ~ -67 mV at most (n=2) and may not be sufficient for triggering vesicular release from type I HCs. Therefore, we should be cautious about interpreting ATP induced synaptic events as arising from type I HCs.

Although the depolarization of type I HCs might cause those slow EPSCs in calyx-afferents, we were unable to clearly distinguish them from EPSCs originated from type II HCs. As shown in 3.1 and 3.2, activation of type II HCs also led to similarly slow EPSCs. Nonetheless, the calyx synaptic structure could lead to unusual mechanisms of neurotransmission. In particular, these terminals may act as a diffusion barrier so that ion concentrations and electrical potentials inside the cleft could be different from those of the external solution. Recordings from type I HCs in presumably semi-intact calyces revealed that depolarization of HCs could shift $E_k$ possibly due to a change of inner cleft concentration of potassium (Lim et al., 2011, Contini et al., 2012). In one study, two voltage-clamp recordings of calyx-afferents exhibited a shift of potassium reversal potential following different levels of action currents (Contini et al., 2012). These observations suggested that the potassium concentration in the cleft might be shifted by the activity of type I HCs and calyx-afferents, although they could also possibly be explained by a combination of different channel conductances. If activity-dependent changes in ion composition were occurring at the calyx synaptic cleft as these studies suggested, EPSCs from type I HCs might exhibit a distinct reversal potential. However, by measuring EPSCs at different holding potentials in calyx-afferents, I found that both spontaneously occurring and 40 mM $K^+$ induced EPSCs reversed near 0 mV (Figures 3.6B and C). The polarity of EPSCs recorded at any given holding potential was the same without detectable heterogeneity, indicating that those EPSCs, whether from type I HCs and type II HCs, did not differ in their reversal potential. To explain this unchanged

reversal potential, one or more of the following must occur: (1) prolonged depolarization of calyx-afferents by voltage clamping to positive membrane potentials did not change the total concentration of relevant cations inside the cleft; (2) no EPSCs were generated in the cleft; or (3) type I HCs stopped vesicular release when postsynaptic calyx terminals were depolarized above 0 mV. Neither of the first two explanations was supported by existing studies, and the third one had not been assessed. To test hypothesis (1), a more precise measurement of ion concentration inside the cleft is required; to test hypothesis (2) and (3), methods to provide strong and specific activation of type I HCs are needed (more discussion **in Chapter 5**).

Perhaps the nature of non-quantal transmission was even more mysterious. As I showed in 3.1 and 3.2, type I HC-calyx synapses were both sufficient and necessary for non-quantal signals. Because of the extensive, narrow cleft space between type I HC and the calyx, it has been proposed that accumulation of protons and potassium and/or ephaptic coupling might underlie those unusual non-quantal signals (Goldberg, 1996, Highstein et al., 2014). Among these theories, the accumulation of protons was experimentally measured in calyx-afferents of turtles (Highstein et al., 2014). The main evidence that support the proton theory was that (1) pH imaging showed a build-up of protons around HCs after bundle displacement; (2) Changing the strength of extracellular pH buffer modulated the kinetics of non-quantal currents; (3) Immunoreactivity for proton sensitive ASICs was detected in the crista (Highstein et al., 2014). However, neither of these observations was sufficient for establishing a casual relationship between

the increase of protons and non-quantal responses. To test whether non-quantal currents were resulted from activation of ASICs by proton release from HCs, calyx-afferent responses evoked by optogenetic activation of HCs were measured in the presence of the ASIC blocker amiloride (100 μM) (Figure 3.6D). No detectable effects of amiloride were found on non-quantal currents (non-quantal amplitude: In amiloride vs. control, -44.5 pA vs. -43.4 pA, n=2, paired t-test, p=0.90), rejecting the possibility that non-quantal currents were mediated by activation of amiloride-sensitive ASICs via increased proton concentration.

Ephaptic coupling occurs through modulation of the electrical potential of the extracellular space and such effects have been experimentally assessed (reviewed in (Anastassiou and Koch, 2015)). Although effects of ephaptic coupling fit some properties of non-quantal signals, such as rapid onset and sustained amplitude, the magnitude of known ephaptic effects were usually small, at about tens of μV, and not exceeding 0.5 mV, significantly smaller than non-quantal signals that I measured here (non-quantal responses recorded in current clamp mode: 3.0±0.7 mV, n = 7). Theoretical calculation of ephaptic coupling (in collaboration with Dr. Eric Young) using parameters that reflected realistic geometry of calyx terminals indicated that 10 mV depolarization of type I HCs could cause a 0.06 mV increase in membrane potential in calyx terminal. The maximum effects would not exceed 0.3 mV under extreme conditions, consistent with a previous study (Goldberg, 1996). Though I have not incorporated realistic membrane conductance in this model, such an upper bound is unlikely to increase significantly and account for

the measured non-quantal responses. Thus, the possibility that non-quantal currents were resulted solely from ephaptic coupling is low.

Given that amiloride had no effects on the non-quantal signals I observed, and that the effects of ephaptic coupling were insufficient to explain nonquantal currents, by exclusion, would accumulation of potassium become a more likely candidate to mediate the non-quantal signals? As discussed earlier, indirect evidence hinted at potassium accumulation inside the hair cell to calyx cleft. Elevated potassium concentration in the cleft might effectively depolarize calyx terminals, as potassium channels are present at the inner face of calyces (Lysakowski et al., 2011). To directly examine the effects of potassium accumulation, I used 5 mM 4AP to block potassium channels. 4AP at this concentration has been shown to effectively eliminate the large resting potassium conductance ($g_{K,L}$) expressed in utricular type I HCs (Rusch et al., 1998). Indeed, $I_{K,L}$ was abolished by 4AP in type I HCs recorded in cristae as well, and subsequently the membrane conductance was reduced and resting membrane potential was elevated (Figure 3.6F). However, no significant effects of 4AP were observed on non-quantal currents activated optogenetically were observed (amplitude of non-quantal currents: in 4AP vs. Ctrl: -34.4±8.4 pA vs. -33.7±7.9 pA, n =5, paired t-test, p = 0.81)(Figure 3.6E). These results argue against the potassium accumulation theory, as reduced potassium outflow should decrease the amplitude of non-quantal responses. But later I found that the optogenetically induced depolarization was also elevated in type I HCs (In 4AP vs. control, 0.53 mV vs. 1.78 mV, n =2)(Figure 3.6F). Therefore, the total outflow of

potassium might not be changed, because the potassium conductance decrease might be balanced by an increase of driving force. And this could explain the unchanged non-quantal currents in 4AP observed experimentally. Thus, these results only rule out the possibility that non-quantal currents were solely dependent on $g_{K,L}$, but provided no further information to support or reject the potassium accumulation theory.

One prediction from the ephaptic coupling or potassium accumulation hypotheses is that neither of these two actions would result in opening or closing of a membrane conductance. To experimentally test this possibility, I applied brief (50 ms, 10 mV) hyperpolarization steps in voltage clamp mode to assess the membrane conductance of calyx terminals before and during non-quantal responses with quantal response eliminated (Figure 3.6G). Interestingly, although only two afferents were tested, an increase of membrane conductance of 0.3 nS was identified during light activation (In stimulus vs. Ctrl, 20.0 nS vs. 19.7 nS, n=2). Assuming the reversal potential of this increased conductance was 0 mV, as reflected by the I-V curve in **3.3**, that gave a driving force of 90 mV for such a conductance when holding potential was at -90 mV, and the resulting currents would be 24.3 pA (conductance multiplied by driving force). This amplitude was similar in magnitude with the measured amplitude (28.7±4.6 pA, n = 14), suggesting that such conductance was sufficient to account for the measured non-quantal currents. If non-quantal currents were indeed mediated by this mysterious conductance, many questions still remain, such as what is the neuronal substrate for this conductance,

how could it be activated by type I HC depolarization, and etc. (more discussion in **Chapter 5**).

The exact nature of synaptic transmission between type I HCs and calyx-terminals is still unclear. Nonetheless, many valuable clues were revealed by this thesis study. In summary, this study showed: (1) large depolarization of type I HCs might result in slow EPSCs with a 0 mV reversal potential in calyx afferents, possibly due to spillover of glutamate; (2) Proton sensing ASICs were unlikely to mediate non-quantal signals; (3) Ephaptic coupling could only account for a very small fraction of the non-quantal responses; (4) Non-quantal signals were not dependent on $g_{K,L}$. (5) An increase of membrane conductance in calyx-afferents was associated with non-quantal signals. Although these discoveries did not solve the mechanism of type I HC synaptic transmission, they point to possible directions for future studies (**Chapter 5**). Noteworthy, one prerequisite for the above interpretations of experimental results is that antagonists/agonist could reach the inner face of calyx terminals. The proof for this point will be presented in **Chapter 4**.

### 3.6 Summary.

In this chapter, by targeted activation of vestibular HCs, this thesis study revealed that most calyx-afferents received highly distinct non-quantal synaptic signals from type I HCs and quantal signals from type II HCs, in cristae of mature mice. While both inputs were excitatory, non-quantal inputs could strongly drive firing activities in downstream

calyx-afferents. Moreover, this relatively novel form of non-quantal signals alone was sufficient for mediating basic vestibular function VOR. All together, these findings suggested that highly differentiated synaptic signals are associated with type I HC and type II HCs neuronal pathways in mediating vestibular function at the periphery. Nevertheless, many questions still remain: what is the functional significance of having both quantal and non-quantal signals? What is the underlying mechanism of these unusual non-quantal signals? A discussion of these questions is presented in **Chapter 5**.

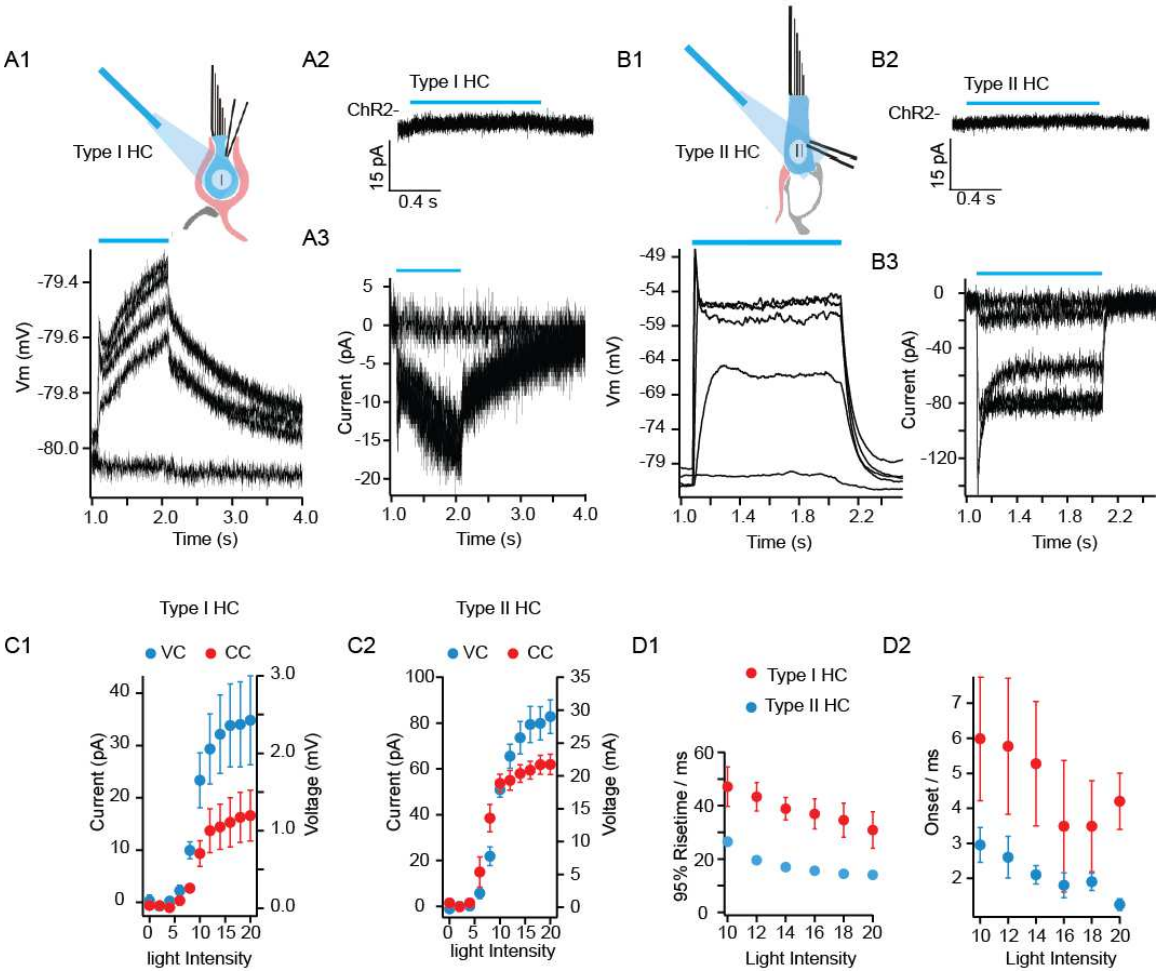


**Figure 3.1 Optogenetic activation of HCs in Gfi1-Cre; Ai32 mice.** A. Type I HCs could be depolarized with 1-s light pulse at different intensities (A1: in current clamp

mode; A2 and A3 in voltage clamp mode, Vh= -90 mV). B. Type II HCs could be depolarized with 1-s light pulse at different intensities (B1: in current clamp mode; B2 and B3 in voltage clamp mode). Light stimulation had no effects on HCs without ChR2 expression (A2 and B2, from WT mice). C and D. To activate HCs with proper light intensity, light level dependent activities in type I and type II HCs were assessed. In both type I (C1) and type II (C2) HCs, our illumination could reach saturating level (amplitude was calculated from the middle-point of response traces). Rise-time (D1) and Onset (D2) were faster in stronger light stimulation (measured from current clamp recordings). Light stimulation was indicated as a blue bar.

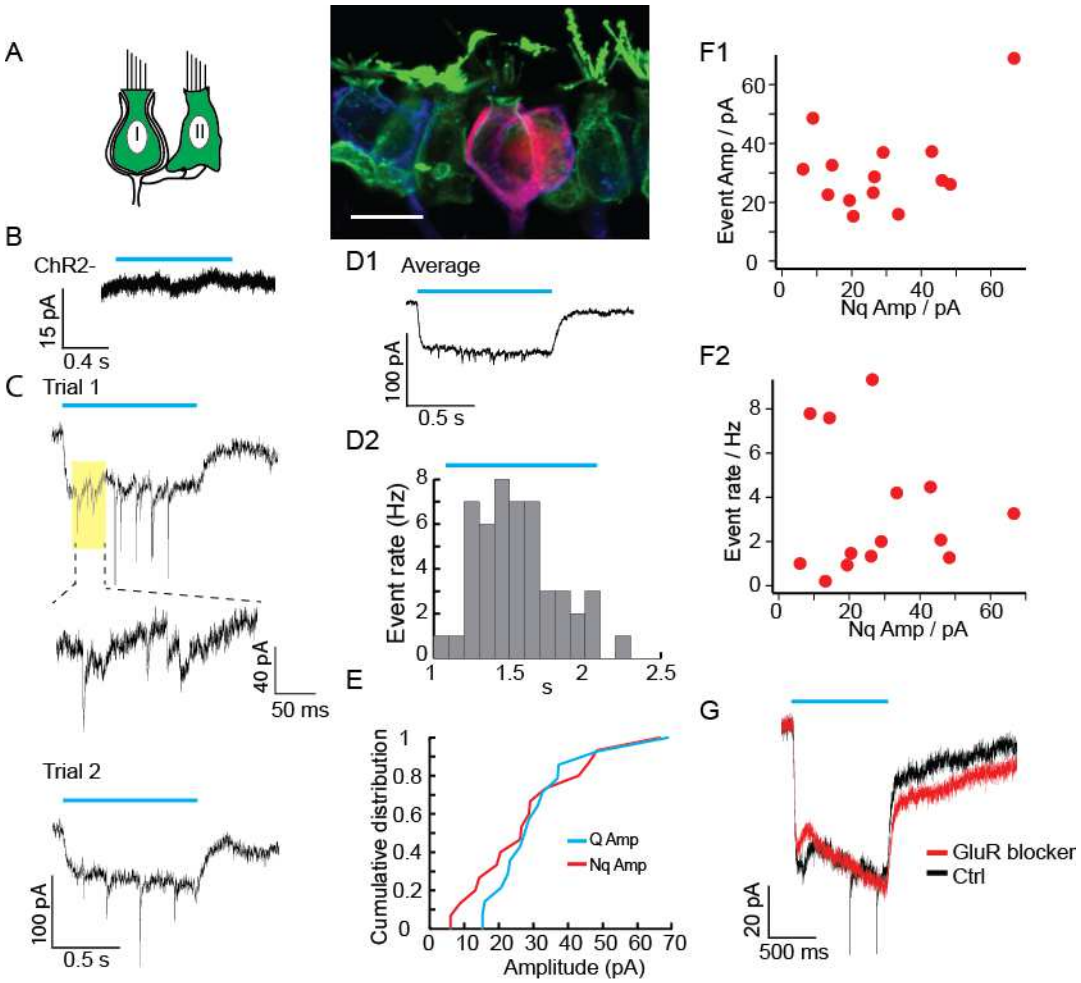


**Figure 3.2 Responses in calyx-afferents due to HC activation.** A. In Gfi1-Cre; Ai32 mice, calyx-afferents (filled with biocytin (red)) were surrounded by ChR2-YFP positive HCs (stained against YFP (green)). B. Light stimulation had no effects on calyx-afferents in ChR2 negative mice. C. Light pulses reliably induced both quantal and non-quantal currents. Notably quantal events exhibited different kinetics (inset from trial 1). D. Non-quantal currents became more prominent after averaging (D1, from 10 trials). The increase of quantal event rate followed the light stimulation (D2, from 10 trials). E. Non-quantal and quantal currents were comparable in amplitude, as reflected by the cumulative distribution (n=14). The amplitude non-quantal currents were calculated from

the midpoint of the averaged response (at least from 10 trials). The amplitude of quantal currents was calculated as the averaged peak amplitude of quantal events. F. The amplitude of non-quantal currents was not correlated with the size (F1) or the amplitude (F2) of the quantal events (n=14). G. Cocktail of glutamate receptor blockers eliminated all quantal events but leaving non-quantal responses unaffected (individual trials). All plots were based on voltage clamp recordings at holding potential of -90 mV. Scale bar in A: 10 μm. Light stimulation was indicated as a blue bar.

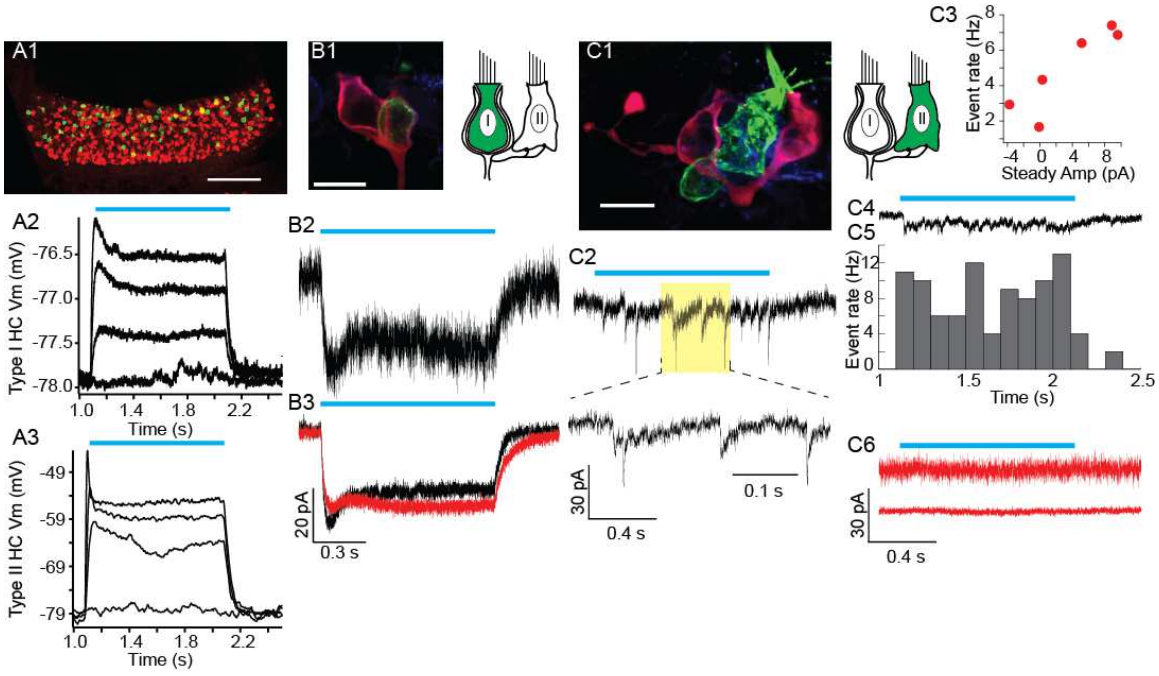


**Figure 3.3 Responses in calyx-afferents due to selective HC activation.** A. VgluT3; Ai32 mice allowed us to selectively depolarize type I or type II HCs. A1. ChR2-YFP (stained against YFP (green)) was expressed sparsely in a subset of HCs expressing VgluT3 (stained against VgluT3 (red)). Light pulses could induce depolarization in YFP

positive type I HCs (A2) and type II HCs (A3) at different intensity. B. “Type I only” calyx-afferents (B1, the recorded calyx-afferent was labeled with biocytin (red)) were defined as those only contacted ChR2-YFP positive type I HCs (B1, stained against YFP (green), with labeling of afferent by staining against TUJ1 (blue)). Light stimulation resulted in only non-quantal responses in this type of calyx-afferents (B2, individual trial; B3, black, averaged response from 10 trials). Non-quantal response were not affected by glutamate receptor blockers (B3, red, averaged response from 10 trials). C. “Type II only” calyx-afferents (C1, the recorded calyx-afferent was labeled with biocytin (red)) were defined as those only contacted ChR2-YFP positive type II HCs (B1, stained against YFP), with labeling of afferent by staining against TUJ1 (blue)). Light stimulation resulted in an increase of quantal events rate (C2: Individual trial; C5: event timing histogram from 10 trials). Those events exhibited different kinetics (C2, inset). Averaged responses sometime revealed a steady component (C4, from 10 trials), with amplitude proportional to the event rate (C3, n=6). Such steady component could be eliminated by glutamate receptor blockers (red, C6, upper trace: individual trial; lower trace: averaged response from 10 trials). All plots (except for A2 and A3) were based on voltage clamp recordings at holding potential of -90 mV. All subplots of panel B and C belonged to the came calyx afferents respectively. Scale bar: A1: 50 μm; B1 and C1: 10 μm. Light stimulation was indicated as a blue bar.

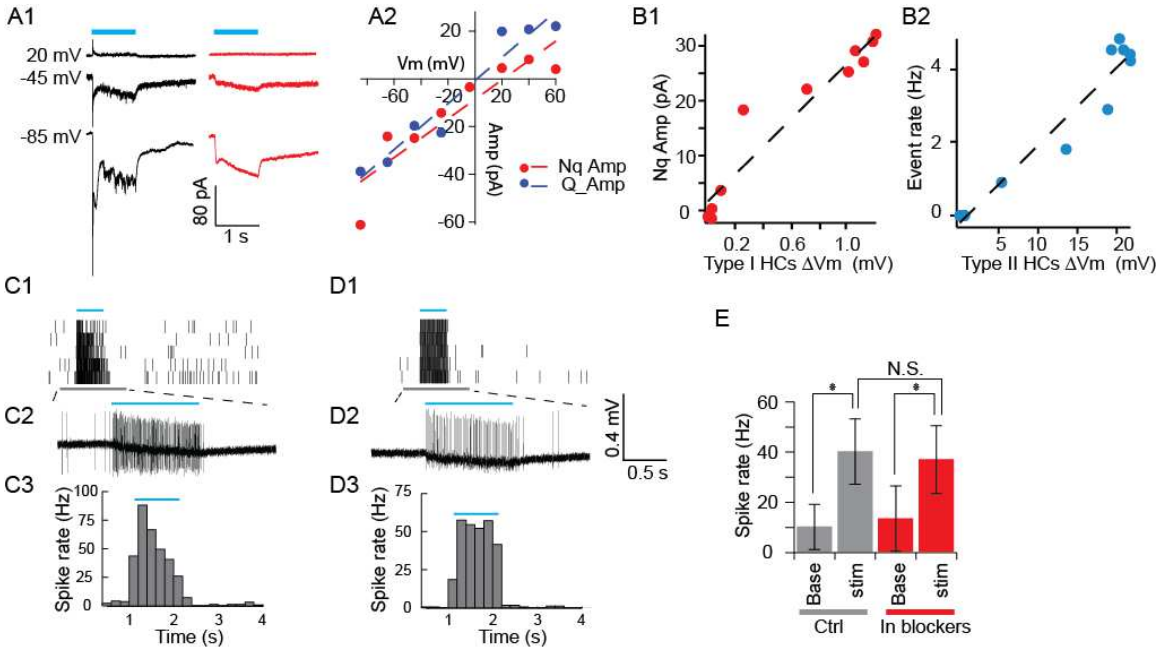


**Figure 3.4 Modulation on calyx-afferent activities due to HC activation.** A. Reversal potential of non-quantal and quantal currents (A1, left, black, in control conditions; right, red, in gluR blockers). A2.Quantal currents reversed near 0 mV (blue dots), non-quantal currents exhibited rectification near 0 mV (red dots) (dashed line: fitted with linear line, n = 4). B. The amplitude of non-quantal signals (B1) and the frequency of quantal signals (B2) were linear to the membrane potential of type I HCs and type II HCs respectively (n=12, R-sqr > 0.9). C. Depolarizing HCs increased firing rate in a calyx-afferent. (C1: raster plot of 5 trials; C2: example trace collected in cell-attached recording mode; C3: PSTH of spikes). D. (the same afferent as in C): With quantal signals blocked by gluR blockers, non-quantal signals were sufficient to induce an increase of spikes. (D1-D3,same setting as C1-C3). E. Inputs from HCs or non-quantal signals from type I HCs alone could significantly drive spike activities in calyx-afferents, while the amount of

increase did not differ significantly with and without blocking quantal signals (n = 6). Light stimulation was indicated as a blue bar.

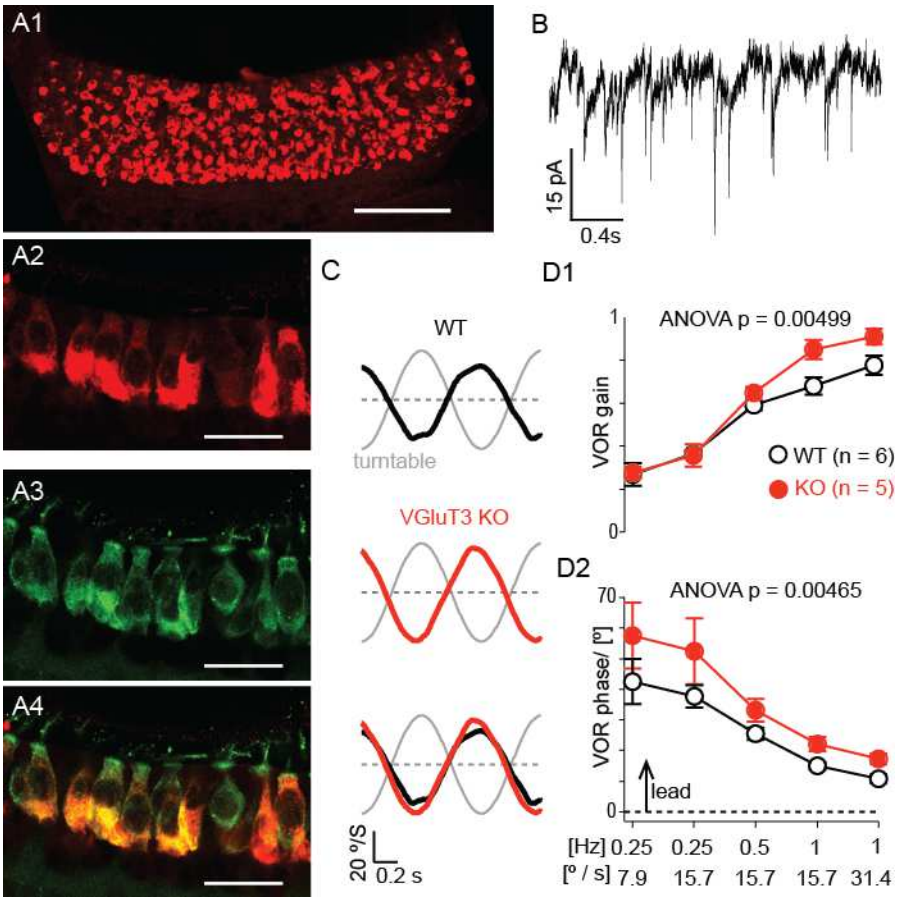


**Figure 3.5 VOR of mice with quantal transmission impaired.** A. VgluT3 (A1 and A2, stained against VgluT3 (red)) was widely expressed in HCs (A2 and A3, stained aginst MyosinVIIa, (green)) in the crista. A4. Overlaying of A2 and A3 revealed that all HCs were VgluT3 positive, although the basal part of type II HCs had more intense VgluT3 immuno signals. B. Most calyx-afferents showed increased EPSCs during elevation of extracellular potassium concentration. C. Average eye velocity traces from representative animals during sinusoidal whole-body rotation (1Hz ± 31.4°/s) in the dark. Grey lines showed velocity of a turntable (i.e. stimulation). Horizontal dotted grey lines

corresponded to 0°/s. D. Average gain and phase of the VOR was plotted against different stimulation frequency and velocity. Scale bar: A1: 100 μm; A2-A4: 20 μm. C and D were prepared by Dr. Takashi Kodama.

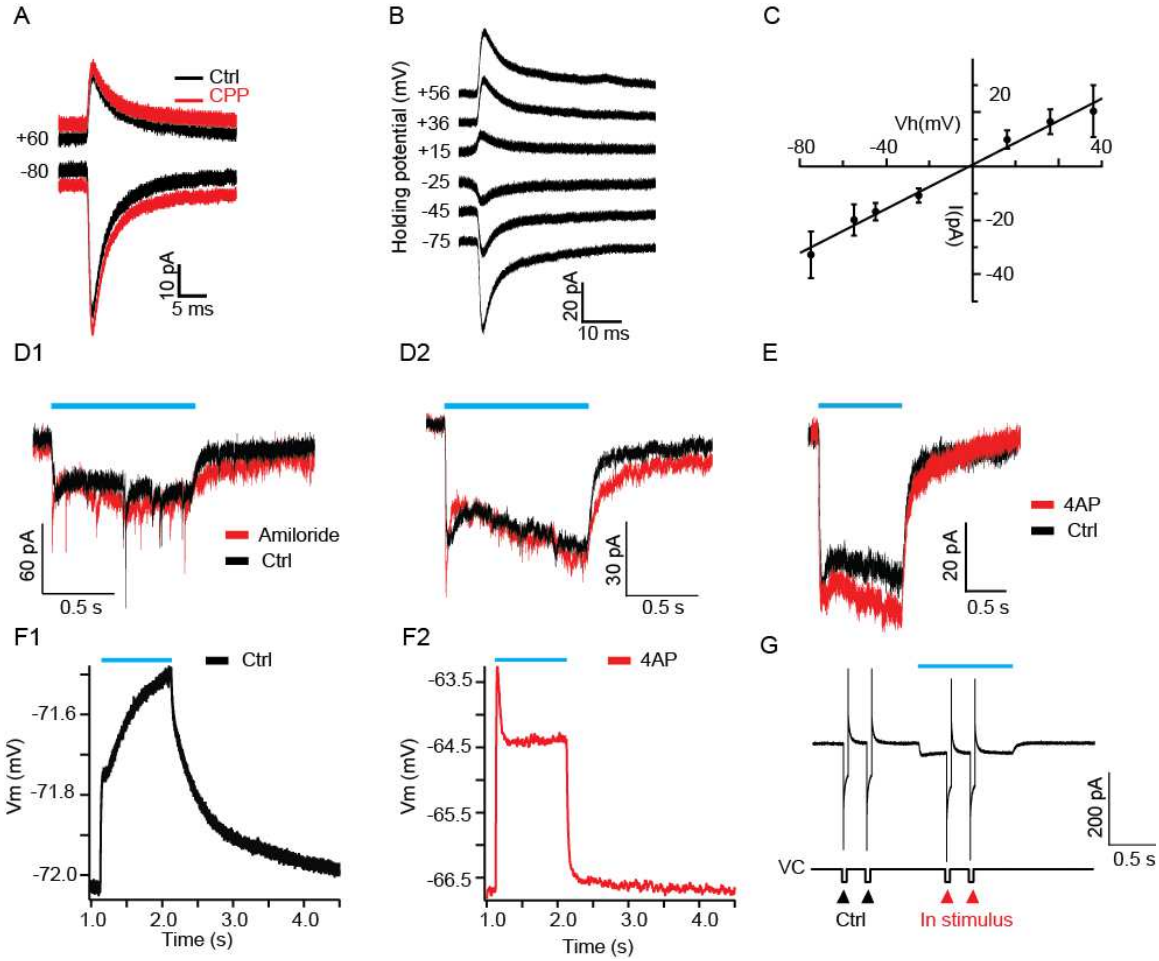


**Figure 3.6 Mechanisms underlying synaptic transmission between type I HCs and calyx-afferents.** A. NMDA receptor blocker CPP had no effect on the EPSC waveform at positive or negative holding potentials. B. Averaged EPSC waveforms recorded at different holding potentials. C. Current voltage relation of averaged EPSCs (n=4) revealed a reversal near 0 mV. D. ASIC blocker amiloride had no effect on quantal or non-quantal currents evoked optogenetically (D1: individual trial; D2: averaged response

from 10 trials). E. Potassium channel blocker 4AP had no effect on non-quantal currents. F. 4AP increased light-evoked depolarizeation in type I HCs (F1, Ctrl; F2, in 4AP). G. Membrane conductances of calyx-afferents were assessed by brief voltage steps before (marked by black triangles) and during non-quantal responses (marked by red triangles) in the absence of quantal resposnes. Light stimulation was indicated as a blue bar.

# Chapter 4 Vestibular efferents differentially modulate activities of type II hair cells and calyx-afferents

In the last chapter, highly distinct non-quantal and quantal signals have been identified as the output signals from type I and type II HCs to downstream vestibular afferents. Those signals are relayed to the central nervous system as the peripherally detected vestibular information. In return, the peripheral vestibular system also receives bilateral efferent inputs from the brain stem. Type II HCs and afferent terminals are primary synaptic targets for such efferent projection. To understand how efferents modulate activities of the vestibular periphery at the cellular/synaptic level, in this chapter, properties of efferent to type II HC synapses and efferent to calyx-afferent synapses have been investigated. We found that although type II HCs and calyx-afferents both receive efferent inputs that exhibit strong short-term facilitation, the effects are inhibitory to type II HCs while excitatory to calyx-afferents, possibly due to distinct underlying postsynaptic mechanisms.

## 4.1 Efferent synaptic inputs to type II HCs can occur spontaneously or by efferent stimulation.

Basal level efferent synaptic events in type II hair cells were measured either as spontaneously occurring events, or as events evoked by electrical stimulation of efferent fibers at low rate.

During recordings, spontaneous synaptic events were seen only rarely (Figure 4.1A). After efferent stimulation had occurred, a subset of type II HCs (n=5 out of 23 tested) exhibited synaptic events that occurred randomly and persisted during time periods without stimulation at a noticeable rate. Such events were described here as "spontaneous" events. At a holding potential (Vh) of -90 mV, those spontaneous excitatory postsynaptic currents (sEPSCs) had amplitude of 21.7 ± 4.3 pA, the 10-90 % rise time of 6.4 ± 0.8 ms and the time constant of decay of 36.4 ± 2.9 ms (n = 5 cells, 527 events analyzed). The EPSC amplitude distribution of all HCs was fit with a single Gaussian distribution, and had a peak at 18.9 ± 0.5pA (R-sqr = 0.84) (Figure 4.1A3).

Electrical stimulation of efferent fibers was delivered by a monopolar glass electrode positioned underneath the epithelium, at about 100 μm distance from the recorded HC (see **Chapter 2**). The stimulation amplitude was gradually increased until the probability of release reached a plateau. At a holding potential of -90 mV, stimulation artifacts were brief in duration allowing the EPSC waveform to be assessed (Figure 4.1B). Synaptic events were induced by electrical stimulation in almost all type II HCs tested (n=22 out of 23 tested). At a stimulation frequency of 1-2 Hz, electrical shocks evoked EPSCs with a low success rate, characterized as probability of release, of about 0.06 % (Pr = 0.056 ± 0.015, n = 8). The release probability was stable at our experimental age range (from P12-P28). The waveform of evoked EPSCs (eEPSCs) was similar to those of spontaneous EPSCs, with amplitude of 22.0 ± 3.0 pA (n = 12) and the time constant of decay of 35.0 ± 3.4 ms (n =7). The eEPSC amplitude distribution of all HCs

was fit by one Gaussian distribution, with peak value at 18.0 ± 0.5 pA (n=515 events, R-sqr= 0.82) (Figure 4.1B3).

Synaptic currents could also be activated by raising extracellular potassium to 40 mM and thereby depolarizing efferent fibers (n=12 out of 14 tested) (Figure 4.1C). The first synaptic event following 40 mM K+ application appeared after a long latency of 38.0 ± 7.4 s (n = 11), consistent with an initial low probability of release.

In summary, I showed here that almost all type II HCs received efferent synaptic inputs. However, those efferent inputs were weak in strength, suggested by small EPSC amplitudes and a low probability of release at basal stimulation rates (1-2 Hz), indicating that at a low activity level, the impact of efferent inputs to type II HCs might be negligible.

**4.2 Efferent inputs are mediated by α9 nAChRs and SK channels in type II HCs.**

To investigate the ionic composition of efferent synaptic currents in type II HCs, as a first step, spontaneous synaptic events were recorded at different holding potentials (Vh) (Figure 4.2A1). Synaptic currents were inward at -90 mV, biphasic at -70 and -60 mV with an inward current followed by an outward current, and outward at -50 mV and above (Figure 4.2A2). The relative total charge transfer of synaptic currents also reversed between -90 and -70 mV, close to the potassium equilibrium potential (~ -83 mV) (Figure 4.2A4), suggesting that a potassium conductance dominated the response. The biphasic waveform and negative reversal potential of the efferent synaptic events in type II HCs

resembled the properties of efferent events observed in cochlear hair cells (reviewed in (Katz et al., 2011)). For cochlear hair cells, it had been demonstrated that efferent synaptic events were mediated by Ca2+-permeable α9-containing nAChRs and subsequent activation of Ca2+-activated (SK or BK) potassium channels. The biphasic synaptic currents there were explained by an initial influx of cations through α9-containing nAChRs and efflux of $K^+$ through $Ca^{2+}$-activated potassium channels (reviewed in (Katz et al., 2011)).

To test whether a similar postsynaptic mechanism might account for efferent responses in type II vestibular HCs, application of 1 mM ACh was used to mimic efferent inputs, as the majority of efferents were likely to be cholinergic (reviewed in (Holt et al., 2011)). All type II HCs tested responded to ACh with inward currents of 103.2 ± 10.6 pA at Vh of -90 mV (n = 22). At Vh positive to -70 mV, outward currents started to appear and became dominant at more positive holding potentials, similar to the findings of synaptic responses (Figure 4.2A2). The relative total charge transfer of the ACh response reversed at -70 mV (Figures 4.2A3, A4), again, close to $E_K$, although slightly more positive compared to the synaptic response.

To test if α9-containing nAChRs mediated the inward ACh response in type II HCs, specific blockers were applied. 10 μM strychnine, an antagonist of α7- and α9-containing nAChRs (Elgoyhen et al., 1994), close to completely and reversibly blocked the ACh response (n = 3, Vh = -81mV, with strychnine: -2.3 ± 0.8 pA; control: -69.0 ± 13.8 pA, p = 0.04, paired t-test) (Figures 4.2B1,B3). 600 nM α-RgIA, a specific

antagonist of α9-containing nAChRs (Ellison et al., 2006), reversibly blocked ACh by ~ 74 % (n = 3, with α-RgIA: -26.6 ± 2.2 pA; control: -102.8 ± 27.0 pA, p = 0.06, paired t-test) (Figures 4.2B2, B3). This blocking effect of strychnine and α-RgIA suggested that the ACh responses were mediated by α9-containing nAChRs. To understand if α9-containing nAChRs played a similar critical role in mediating synaptic responses in type II HCs, I further examined efferent synaptic inputs in α9-/- mice. 40 mM potassium external solution induced synaptic responses in 0/6 type II HCs in α9-/- mice, compared to 4/5 type II HCs in WT mice, indicating that efferent synaptic inputs were cholinergic and indeed mediated by α9-containing nAChRs (p = 0.0006).

To test whether calcium dependent potassium channels were involved in the outward ACh response in type II HCs, blockers for small (SK) and big (BK) conductance potassium channels were applied. Both BK and SK channel blockers had been found to affect ACh responses and efferent synaptic currents in cochlear hair cells, with different effects depending on the apical/basal location of the hair cells along the cochlea (Wersinger et al., 2010). Moreover, based on recordings of dissociated type II HCs it had been suggested that BK channels in combination with muscarinic AChRs might contribute to ACh responses in isolated utricular hair cells (Kong et al., 2005). However, SK channels might be involved in ACh responses in type II HCs in turtle, as apamin, an SK channel blocker, removed efferent induced inhibition in afferents (Holt et al., 2006a).

Here I found that 100 nM IBTX, a BK channel blocker, failed to significantly affect ACh induced outward currents at Vh of -40 mV in type II hair cells (with IBTX:

95.0 ± 17.4 pA; control: 99.4 ± 15.9 pA; n = 5; p = 0.3107, paired t-test) (Figures 4.2C1, C3). However, 300 nM apamin, a SK channel blocker, completely abolished outward currents at -40 mV (with apamin: 44.6 ± 10.0 pA ; control: -13.8 ± 3.4 pA; n = 3, p = 0.0316, paired t-test) (Figures 4.2C2, C3), suggesting that SK channels were coupled to α9-containing nAChRs and accounted for the outward component of ACh responses at negative holding potentials. The remaining inward current uncovered by apamin most likely represented the current through the ACh receptor alone (Figure 4.2C2). To test if outward synaptic currents were also mediated through SK channels, efferent stimulation consisting of three pulses at 100Hz was used to reliably trigger synaptic responses. Outward synaptic currents at -50 mV were completely abolished by 300 nM apamin (n = 3) (Figure 4.2D1), but inward synaptic currents at -90 mV still remained. In one recording with spontaneous synaptic activity, after applying apamin, outward synaptic currents at -50 mV changed into inward currents with shorter duration and smaller amplitude (Figure 4.2D2). These results together suggested that SK channels mediated the outward inhibitory component of efferent inputs to type II HCs.

**4.3 Efferent inputs exhibit short-term facilitation through presynaptic mechanisms.**

Ample studies had indicated that synaptic efficacy is directly regulated by the history of synaptic activity (reviewed in (Blitz et al., 2004)). To demonstrate the relation between the efferent synaptic strength and the activity level of efferents, I first measured the paired-pulse ratio for efferent to type II HC synaptic inputs. Paired electrical pulses

with intervals ranging from 20 to 500 ms were applied to efferents and the amplitude of all responses (averaged across "success" and "failure" trials) following the first pulses (S1) were measured and compared to the amplitude of responses following the second pulses (S2). At 500 ms intervals, no statistical differences were detected between S2 and S1 (S2/S1 = 1.16±0.09, p-value = 0.14, paired *t-test*) (Figure 4.3A1). However, prominent paired-pulse facilitation started to appear with shorter intervals (Figure 4.3A2 - A4). The degree of facilitation was inversely correlated with the duration of intervals, at 20 ms intervals S2 can reach ~4-fold larger than S1 (Figure 4.3B).

Because the amplitude of all responses (S2 and S1) was determined by the probability of release together with the amplitude of EPSCs, to understand whether the observed facilitation was mediated through an increase of release probability which was most likely attributed to presynaptic mechanisms or through an increase of synaptic currents which could also involve postsynaptic mechanisms, I further analyzed the release probabilities (P1 and P2) and amplitude of EPSCs (A1 and A2) following the first and second pulses respectively (Figure 4.3B). P2/P1 increased significantly as the stimulus interval became shorter. In contrast, no significant change of A2/A1 was detected. These results suggested that the efferent paired pulse facilitation is largely due to enhanced release probability, possibly caused by a build-up of calcium concentration at presynaptic terminals.

The paired-pulse ratio test revealed that efferent synaptic strength could be facilitated. I then assessed the impact of such facilitation at efferent firing rates that were

within physiological range. *In-vivo* studies done in toad fishes showed that efferents displayed slow spontaneous firing activity of 4-5 Hz and could reach 80-100 Hz peak rates when fishes were behaviorally activated (Highstein and Baker, 1985). In one *in-vivo* study done in guinea pigs, putative efferent neurons identified by antidromic activation fired spontaneously at 10-50 Hz and could increase that rate up to 150 Hz in response to vestibular or somatosensory stimulation (Marlinsky, 1995, Leijon and Magnusson, 2014). Although the properties of efferent neurons in mammals had not been thoroughly investigated, it is likely that they increased firing rate in response to stimuli. Trains of high frequency efferent stimulation from 50 to 333 Hz were used in a majority of *in vivo* studies and these had been shown to effectively modulate afferent firing rates (Goldberg and Fernandez, 1980, Marlinski et al., 2004). Therefore, to assess synaptic responses during high-level efferent activities, I examined responses while stimulating efferents with 10-pulse train stimulation at frequencies of 25, 50 and 80Hz, which are within the range of physiological firing rates of central nervous system neurons (Figure 4.3C).

Compared to single synaptic events, train stimulation triggered much larger responses. The averaged peak responses were -56.5 ± 17.5 pA, -36.2 ± 12.2 pA, and -28.4 ± 11.0 pA at 80Hz, 50Hz and 25 Hz respectively ($V_h$= -90mV, n = 4). The peak amplitude of averaged responses increased as the stimulation frequencies became higher (80Hz vs. 50Hz, p-value = 0.031; 50Hz vs.25Hz, p-value = 0.007, paired *t*-test). Short-term facilitation of efferent synaptic strength could underlie these potentiated responses, but repetitive efferent activities might also lead to depletion of synaptic vesicles and

result in depression. Therefore, I monitored the change of Pr during the train stimulation. At all frequencies tested, the later pulses in the train had higher Pr and thus were more reliable to trigger synaptic responses (Figure 4.3D). For example, the Pr of the tenth pulse in the 80Hz train stimulation could reach 0.58 ± 0.05 – ~10 fold larger than the baseline Pr. As expected, Pr rose more steeply at higher frequencies, but the increase slowed down and tended to reach a plateau later. In addition, as our data showed the decay time of synaptic responses was slow ($\tau_{decay}$ = 35.0 ± 3.4 ms), synaptic responses were susceptible to summation even at relatively slow stimulation rate. Therefore, the effectiveness of repetitively high frequency efferent stimulation reflected contribution from both facilitation of release probability and summation of synaptic responses.

Other synaptic transmitters besides ACh have also been suggested to function at vestibular efferents (reviewed in (Holt et al., 2011)). Among those transmitters, ATP has been shown to depolarize HCs (Rennie and Ashmore, 1993), and the neuropeptide – calcitonin gene-related peptide (CGRP) has been shown to suppress HC responses to mechanical stimulation in the lateral line organ of Xenopus (Bailey and Sewell, 2000). I have demonstrated that efferent synaptic events at slow stimulation rate were mediated through α9-containing nAChRs. However, it was still possible that those transmitters participated at responses triggered by high-frequency efferent stimulation, as transmitters like neuropeptides had been shown to be preferentially released at high frequency (Dreifuss et al., 1971, Gainer et al., 1986, Muschol and Salzberg, 2000). To test this possibility, I applied 200 nM strychnine while recording responses evoked by 10-pulse

train stimulation at 80Hz. Strychnine reversibly blocked those responses by 85% (Figure 4.3E) with Strychnine -7.6 ± 1.4 pA, Ctrl: -48.3 ± 11.8 pA, p-value = 0.04, paired t-test), indicating that in our experimental condition, efferent synaptic responses were mediated mainly if not exclusively by ACh even for potentiated responses at high stimulation frequency.

High frequency efferent stimulation that lasted for seconds were commonly used *in vivo* to study efferent responses in mammals, but depletion of synaptic release may possibly occur during prolonged stimulation (Goldberg and Fernandez, 1980, McCue and Guinan, 1994, Marlinski et al., 2004). To test this possibility, I examined synaptic responses with 10-s long stimulation at 50Hz (Figure 4.3F). These efferent synapses showed sustained synaptic release throughout the period of stimulation. The plateau of response amplitude (115.0 ± 28.9 pA) was reached with time constants $\tau_{rise}$ of 1.07 ± 0.20 s (fitted with exponential function) after stimulation onset (n = 6), suggesting that efferents were capable of providing sustained inputs to type II HCs. Although synaptic release remained during the stimulation, it showed some relaxation after about 5s (not quantified) in half of cells as the amplitude reduced and events became sparse. In a few cases, I tested the base Pr before and after prolonged stimulation and no obvious changes were detected (n=3), indicating that long stimulation was unlikely to leave long-lasting changes in release probability.

**4.4 Efferent inputs could strongly hyperpolarize type II HCs.**

Vestibular type II HCs provided inputs to downstream afferents through ribbon synapse mediated transmission, which depends on the $V_m$ of type II HCs. To understand how type II HC to afferent signals are affected by vestibular efferent inputs, I sought to characterize the $V_m$ change produced by efferents.

However, artifacts coupled with electrical stimulation overwhelmed synaptic responses at more positive Vh, including in current clamp mode, although they were transient and separable from synaptic responses at Vh of -90 mV where most voltage gated channels were closed. To overcome this, I implemented optogenetic method to stimulate efferents specifically. ChR2 was expressed under the control of the choline acetyltransferase(ChAT) promoter in ChAT-Cre; ChR2 mice. At low magnification, the fluorescently labeled ChR2-YFP positive fibers were thin in diameter and projected to cristae, resembling the anatomy of efferents (Figure 2.1C). No vestibular ganglion neurons showed fluorescence, suggesting that the expression of ChR2 was confined to efferents. At high magnification, those fluorescent fibers were observed to branch extensively and form contacts with type II HCs (Figure 2.1C) (stained by antibodies against MyosinVI), and calyces, (stained by antibodies against TUJ1) as predicted by their efferent identity. Moreover, putative synaptic sites at the bottom of HCs, revealed by staining of synaptic vesicle protein with antibodies against SV2, largely overlapped with terminals of ChR2-YFP positive fibers (Figure 4.4A), indicating that the majority of efferent fibers expressed ChR2.

5-ms blue light pulses were delivered through an optic fiber to activate efferents (details in **Chapter 2**). In 19 out of 20 type II HCs of ChAT-ChR2 mice, light pulses successfully triggered efferent synaptic currents (Figure 4.4B). At a stimulation rate of 2Hz, those ChR2 induced responses had an averaged amplitude of 16.3 ± 1.1 pA (n=9), rise-time of 4.2 ± 0.7 ms (n = 8), decay-time constant of 31.0 ± 3.5 ms (n = 8), and Pr of 0.105 ± 0.018 (n =11) when recorded at Vh of -90mV. To illustrate whether optogenetically evoked events were comparable to those evoked by other methods, I recorded electrically evoked and spontaneous efferent responses in littermates of ChAT-YFP mice. The electrically-evoked or spontaneous efferent responses had averaged amplitude of 17.0 ± 3.7 pA, rise-time of 5.3 ± 0.8 ms, decay-time constant of 33.4 ± 3.4 ms (n = 2 cells for electrically evoked events, n = 1 cell for spontaneous events), and Pr of 0.17 (n = 2), almost identical to optogenetically evoked responses (Figure 4.4B). Similarity in waveforms and Pr of efferent events suggested that optical stimulation was comparable to electrical stimulation. Moreover, as the optical stimulation method only activated cholinergic efferents while the electrical stimulation method activated all efferents, the similar results got from the two methods also confirmed that the efferents onto type II HCs were entirely cholinergic.

Although the Pr for events evoked by both methods was similar, the presynaptic properties of efferent synapses, particularly short-term facilitation, could be altered by the optogenetic method. It had been reported that the optogenetic method could introduce artificial synaptic depression in a cell-type dependent manner, although such depression

usually occurred in virus-mediated expression of ChR2 (Jackman et al., 2014). Therefore, to evaluate the fidelity of the optogenetic method for high-frequency efferent stimulation, I carefully compared the short-term facilitation of optogenetically triggered responses with electrically triggered responses. ChR2 responses also exhibited paired-pulse facilitation. At 20 ms, 40 ms, and 100 ms inter stimulus intervals, the ratio of release probability of the second stimuli to the first stimuli all exceeded 1 ($P<0.05$ for 20ms and 40ms, not significant for 100ms, one-sample t test, $n \geq 4$). Train stimulation with 10 light pulses led to potentiated responses as well (Figure 4.4C1 and C2). However, analysis of release probability for each pulse suggested that Pr rose sharply during the first a few pulses but fell to a plateau level during both electrical and optical stimulation methods, unlike the situation in rats where the $P_r$ grew monotonically during the train stimulation train (Figure 4.4D). This additional slow depression component observed in mice but not in rats possibly reflected differences between species.

Compared to electrically evoked efferent responses, the responses evoked by the optogenetic method showed similar properties including facilitation, suggesting that it could be applied to repetitively activate cholinergic vestibular efferents. Nevertheless, there are several subtle differences between the ChR2 efferent responses and electrical responses. The onset of light evoked synaptic responses had a relatively long delay of 9.0 ± 1.6 ms (calculated from stimulus offset) (n = 4 cells), while the electrically evoked responses followed the stimulus instantly. Also, possibly due to the inactivation of ChR2 by high frequency light stimulation, the depression of Pr was more obvious during later

stimuli in the train, compared to the moderate drop of Pr for the electrical stimulation (Figure 4.4D). Taking into account the pros and cons of optogenetic method, because the optogenetically evoked efferent responses largely preserved the properties of efferent synapses but also showed minor variation during high frequency stimulation, I used this method primarily to study the overall postsynaptic impact of vestibular efferent inputs at depolarized $V_m$ at moderate stimulation frequencies (≤ 50Hz) without going to the details of synaptic release which had been addressed using the electrical stimulation method in previous experiments.

To examine how efferent inputs shift the $V_m$ of type II HCs, I applied stimulation consisted of 10 light pulses at 50 Hz to activate efferent synaptic release and recorded $V_m$ from type II HCs in current clamp mode. To compare the impact of efferents at different $V_m$ levels, currents were injected to type II HCs to set $V_m$ to near -80mV, -60mV, and -40mV, mimicking the hyperpolarized, resting and depolarized membrane potentials respectively. At hyperpolarized $V_m$ (-80mV) which could happen during head movement toward the non-preferred direction, efferent inputs induced moderate depolarization of 2.40±0.50 mV, followed by slow weak hyperpolarization of -0.66±0.18 mV due to opening of SK channels (n = 6) (Figures 4.5A and B). At resting $V_m$ (-60mV) and depolarized $V_m$ (-40mV), efferent inputs induced strong inhibition of 10.47±1.67 mV and 10.60±3.18 mV respectively (n=6) (Figure 4.5A and B). According to voltage clamp recording results, the total charge transfer should be larger at -40 mV, the similar degree

of inhibition of $V_m$ at -60mV and -40 mV was likely due to that cells were leakier and hence had larger membrane conductance at -40 mV.

I also examined the kinetics of the efferent induced membrane potential change. Interestingly, the decay of efferent inhibition was much slower at -60 mV (90-10% decay time: 239.99±55.77 ms), compared to a 90%-10% decay time of 108.18±30.17 ms at -40 mV (P = 0.019, paired *t-test*), and to a much shorter 90% - 10% decay time of 31.98±5.63 ms for the efferent depolarization at -80 mV (n = 6 cells) (Figure 4.5D). As more calcium influx could occur at – 60 mV and possibly induce calcium evoked calcium release (reviewed in (Fuchs, 2014)), possibly, the slower decay time resulted from extended gate opening of SK channels due to higher intracellular calcium concentration.. To test this possibility, I characterized efferent responses in more controlled condition by using the same stimulation paradigms but in voltage clamp mode at holding potentials of -60 mV and -40 mV (Figure 4.5C). 50Hz light stimulation induced responses of 39.36±15.75 pA and 63.36±24.39 pA at -60 and -40 mV respectively. Nevertheless, the 90-10% decay time of responses were 79.32±8.90 ms at -60 mV and 80.32±17.43 ms at -40 mV, and did not differ significantly (paired *t- test*, P =0.92,n= 4 cells) (Figure 4.5D). If calcium entry during the train stimulation in voltage clamp and current clamp configuration was comparable, the similar decay time observed in voltage clamp mode at -60 mV and -40 mV would argue against the possibility that calcium accumulation was involved in shaping the decay of efferent inhibition. In fact, the appearance of slowed decay time in

current clamp but not in voltage clamp mode may favor the participation of additional voltage-dependent conductance.

To completely exclude the possible influence of calcium influx on decay kinetics, I compared efferent synaptic events evoked optogenetically with artificial efferent events evoked by injecting currents with identical waveform of efferent synaptic currents recorded at -40mV and -60 mV (Figure 4.5F1). In current clamp mode (Figure 4.5E), synaptic responses to single stimuli at -60 mV were similar to responses at -40 mV in amplitude (amplitude of averaged responses at -60mV: -7.42±0.70 mV, at -40mV: -6.71±1.51 mV, P=0.25, paired t-test, n=4 cells), but the decay time constants were much longer ($\tau_{decay}$ of averaged responses at -60 mV: 68.03±5.31 ms, at -40 mV: 32.02±3.93 ms, P=0.016, paired t-test, n=4 cells), resembling the slow decay of responses to train stimulation at -60mV recorded in current clamp mode (Figures 4.5E and F2). As predicted, artificial efferent events also exhibited similarly slower decay time at -60 mV (n=6)(Figure 4.5G), suggesting that intrinsic cell conductance alone was sufficient to slow down the efferent inhibition at around -60 mV.

To assess such effect, I tested 200 μM 4AP - a blocker of delayed rectifier potassium channels, which were usually active at depolarized membrane potential, and 200 μM $BaCl_2$ - a blocker of inward rectifier potassium channels, which would usually be active at hyperpolarized membrane potential, on $V_m$ responses induced by efferents and artificial current injection respectively. Bath applying 4AP increased the amplitude and the decay time of efferent induced $V_m$ responses at -40 mV, without affecting responses

at -60 mV(Figure 4.5H). In contrast, bath application of $BaCl_2$ increased the amplitude but speeded up the decay of $V_m$ responses induced by artificial efferent currents injection at -60 mV, without affecting responses at -40 mV (n=3). These results suggested that channel conductance operating at different $V_m$ could effectively shape the kinetics and amplitude of efferent responses, and such modulation strengthened efferent inhibition of type II HCs near resting membrane potentials. Moreover, biological processes that could modify the channel properties might also impact efferent inputs through this mechanism.

**4.5 Efferent synaptic inputs to calyx-afferents exhibit slow kinetics.**

To activate efferent inputs to calyx-afferents, I tried both electrical and optogenetic stimulation methods. Electrical stimulation delivered through a glass pipette placed underneath the epithelium failed to induce synaptic responses that could be resolved from overwhelmingly large artifacts in calyx afferents, possibly because afferents were more susceptible to direct stimulation in our settings. Thus, the optogenetic approach was used here to stimulate efferents in ChAT-Cre;Ai32 mice through ChR2 activation (Figure 4.6B). In 3 out of 9 calyx-afferents, synaptic currents were induced by light stimulation (Figures 4.6B1 and B2). Although most calyx-afferents receive inputs from type II HCs, those efferent synaptic currents observed here were from direct efferent inputs to calyx-afferent rather than from indirect efferent modulation through type II HCs. Because type II hair cells provided inputs to calyx-afferents in the form of qEPSCs, indirect inhibitory efferent effects through type II HCs would be predicted as a decrease of qEPSC rate. As

the baseline level qEPSC rate was close to zero in our recording condition, such indirect efferent effects would be negligible.

In one example, success-responses (17 successes) exhibited remarkably slow rise time, long decay phase, enhanced noise and irregular shapes, with amplitude of 8.5 pA, rise time of 36.6 ms, and decay time of 200.0 ms (Vh = -90mV)(Figure 4.6B2). Such currents were highly distinctive from those fast rising and exponential decaying efferent currents recorded from type II HCs (Figure 4.6C). Although further experimental testing was needed, the slow kinetics and irregular shapes were likely resulted from "volume transmission", where transmitters mainly acted on extrasynaptic receptors through diffusion – a transmission mode common for cholinergic synapses. Unlike phasic transmission, which causes fast responses as transmitters acted on receptors at the synaptic cleft, volume transmission leads to slow and prolonged responses, similar to those efferent currents measured in calyx-afferents here (reviewed in (Sarter et al., 2009).)

The Pr of efferent inputs was only characterized in that one calyx-afferent, as the single-pulse evoked efferent like responses in other two afferents were too small to be resolved from noise. At a slow stimulation rate (2 Hz), Pr measured in this calyx-afferent was 0.17. To evaluate the degree of facilitation, repetitive optogenetic stimulation was applied (Figure 4.6D). 10-pulse train stimulation at 50-80 Hz resulted in an over 10-fold larger response (amplitude of 115 pA, at 50Hz) compared to the response triggered by single stimuli, supporting the presence of facilitation. Although this was just from one example, efferent inputs to calyx-afferents seemed to share similarities with efferent

inputs to type II HCs, such as low basal Pr and short-term facilitation. More data were required to establish whether uniform presynaptic properties were shared at efferent synapses onto calyx-afferents and type II HCs.

### 4.6 Efferent inputs are excitatory and mediated by neuronal type nAChRs in calyx-afferents.

From this study (presented in 4.4), efferent inputs were shown to strongly inhibit type II HCs. However, in *vivo* recording from vestibular afferents showed that efferent stimulation exclusively increased base line firing rate of mammalian vestibular afferents(Goldberg and Fernandez, 1980, Marlinski et al., 2004). In order to account for such excitatory effect, direct efferent synaptic inputs to afferents must be excitatory. To test this possibility experimentally, responses evoked by train stimulation (10 pulses at 50 Hz) were measured at holding potentials of -90 mV and -40 mV (Figure 4.6D). Synaptic currents recorded at these two potentials were both inward. Amplitude of responses was much smaller in -40 mV than in -90 mV, suggesting a reversal potential more positive than -40 mV. Therefore, unlike efferent synaptic currents reversed below -70 mV and were inhibitory to type II HCs, efferent inputs to calyx-afferents were excitatory.

The inhibitory part of efferent inputs to type II HCs were mainly mediated by SK potassium channels coupled to α9* nAChRs. Could the excitatory efferent effects on calyx-afferents be mediated by α9* nAChRs without coupling to SK channels? Controversial evidence for the existence of α9 nAChRs on mammalian vestibular

afferents was present, as immunoreactivity of α9 nAChRs was detected in afferent terminals and somata in one study (Luebke et al., 2005) while mRNA signals of α9 nAChRs were negative in Scarpa's ganglion by RT-PCR and in-situ hybridization (Hiel, 2009). To examine the expression level of α9 nAChRs, a third approach was taken in this study by checking the fluorescent signals in α9 GFP BAC (Zuo et al., 1999) in the vestibular periphery (Figure 4.6A). Consistent with previous studies using *in situ* hybridization and RT-PCR methods, no fluorescent signals were observed in any afferents or vestibular ganglion neurons, while the signals were strong in all vestibular hair cells, indicating that α9 nAChRs were absent from the afferents.

To investigate what other types of nAChRs located at calyx-afferents might mediate those excitatory efferent responses, nAChR receptor antagonists were directly tested on efferent responses evoked by 50 Hz train stimulation. In a preliminary set of experiments (n=2), 3μM DhβE (Dihydro-β-erythrodine hydrobromide), an antagonist against α4β2, α6β2*, and α4β4 nAChRs (Chavez-Noriega et al., 1997, Papke et al., 2008), completely abolished efferent responses at calyx afferents (Figure 4.6E)(In DhβE vs. Ctrl, 1.1pA vs. -18.0 pA, n = 2, Vh=-90mV), indicating that neuronal type nAChRs (α4* and α6* nAChRs) might play a major role in mediating efferent inputs to calyx afferents. Interestingly, efferent responses recorded from calyx-afferents in turtles were also sensitive to DhβE blockade, indicating that postsynaptic mechanisms for mediating efferent inputs to calyx-afferents might be conserved across species.

## 4.7 Acetylcholine induced responses in calyx-afferents reveal insights to unusual properties of type I HC and non-quantal transmission.

Only a small percentage of calyx-afferents showed efferent induced synaptic currents. To test whether such scarcity was caused by sparse expression of functional nAChRs postsynaptically and also to identify nAChRs more efficiently in calyx-afferents, 1mM ACh was applied here to mimic efferent synaptic inputs. Such an approach had allowed successful identification of postsynaptic mechanisms for efferent inputs to type II HCs in 4.2. Focal application of 1 mM ACh resulted in an inward current (average amplitude: 129± 80pA (n=28, measured at -80mV)) in 60% of calyx-afferents in rats (Figure 4.7A). By recording at different holding potentials, the reversal potential of these ACh currents was identified to be near 0 mV (Figure 4.7A). ACh currents could be blocked by 10 μM tubocurarine (nAChR antagonist, n = 3; 84% blockade), 10μM strychnine (α7 and α9 nAChR antagonist, n = 3; 90% blockade), 400 nM α-BTX (selective α7 and α9 nAChR antagonist, n = 3; 67% blockade), 600 nM α-RgIA (selective α9 nAChR antagonist, n = 5; 76.8% blockade), but were not affected by 3 μM DhβE (n =2). Strong blockade effects of α9 nAChR antagonists suggested that ACh responses were mediated by α9 nAChRs. To further validate this conclusion, I tested ACh responses in calyx-afferents of α9 knockout mice. Only 1 out of 3 calyx afferents showed very weak ACh responses (<10 pA) in α9-/- mice, compared to 12 out of 16 calyx afferents that showed responses in wild type mice of the same genetic background (P-value = 0.016), confirming that α9 nAChRs were essential for ACh responses. These

results together seemed to be contradictory to the identified composition of postsynaptic nAChRs for efferent induced synaptic responses. As shown in 4.6, efferent synaptic currents could be blocked by DhβE and possibly through neuronal nAChRs, and α9 nAChRs were absent in calyx-afferents as suggested by the expression pattern in α9-GFP mice and previous histology studies.

One explanation for this discrepancy could be that those α9 nAChRs that mediated ACh responses in calyx afferents were not located at afferents. Histology studies suggested that α9 nAChRs were expressed in type I and type II HCs, and this was in agreement with the strong GFP signal observed in all HCs in α9-GFP mice (Figure 4.6A). Given the similarities in the waveforms between ACh currents and non-quantal currents, could it possible that those ACh currents were in fact non-qunatal currents resulting from activation of type I HCs through opening their α9 nAChRs? The key to test this possibility was to identify the ACh responses in type I HCs. Indeed, 1mM ACh resulted in inward currents in type I hair cells (n=7 out of 9 tested), with amplitude of -48.6 pA (n=2, measured at -90 mV) (Figure 4.7C)(ACh responses were also observed at type I-like HCs by Dr. Sadeghi). Furthermore, those currents were mediated through α9* nAChRs, as they disappeared in α9-/- mice (n=1). The amplitude of ACh currents in type I HCs was larger than that of light induced ChR2 currents (shown in **3.1**). Consistent with this observation, the ACh-evoked currents were larger than non-quantal currents in calyx-afferents. The percentage of type I HCs showing ACh responses (66.7%) also matched well with the percentage of calyx-afferents responding to ACh application (60%). These

results supported the hypothesis that ACh responses in calyx-afferents were due to activation of type I HCs that then elicited and subsequent non-quantal transmission.

Although direct application of ACh to activate type I HCs seemed to have little physiological relevance, the above results revealed important information about type I HCs and calyx-afferents. (1) Functional α9 nAChRs were still present in type I HCs at a relatively mature age. More discussion regarding the physiological significance of α9 nAChRs in type I HCs is presented in **Chapter 5**. (2) Non-quantal transmission also existed in rats. Moreover, α9 nAChR-dependent ACh responses could be an easy assay to test non-quantal transmission without relying on transgenic manipulation or complicated mechanical stimulation, making investigation of such transmission possible in more species. (3) A lesson from this part of study was that careful experiments were needed to be designed to identify whether the primary site of action was on type I HCs or calyx-afferents, as non-quantal currents could be confused with expected responses induced by agonist application or other manipulations. Moreover, this part of the study proved that large size molecules, such as α-BTX (74 amino acid, molecular weight: 8KD), could reach the inner face of calyx terminal to block α9 AChRs of type I HCs in our preparation. Such proof was critical for pharmacological studies of synaptic signaling at the calyx terminals, as it ruled out the possibility that a lack of effects of certain reagent was due to its inaccessibility of calyx synapses.

**4.8 Summary.**

By investigating cellular and synaptic level mechanisms underlying efferent inputs to type II HCs and calyx-afferents, results presented in this chapter revealed that efferent synaptic inputs had low basal release probability but exhibited strong short-term facilitation during repetitive efferent stimulation. Efferents were found to strongly inhibit type II HCs through activation of α9 nAChRs and SK channels, while exciting calyx-afferents possibly through activation of neuronal nAChRs in volume transmission mode. Those cellular level mechanisms were comparable to those identified in turtles. An intriguing question from these results is: although efferent inputs inhibit type II HCs, why does in *vivo* efferent stimulation exclusively increase firing rate of vestibular afferents in mammals? A discussion of this question and functional significance of efferent synaptic inputs is presented in **Chapter 5**.

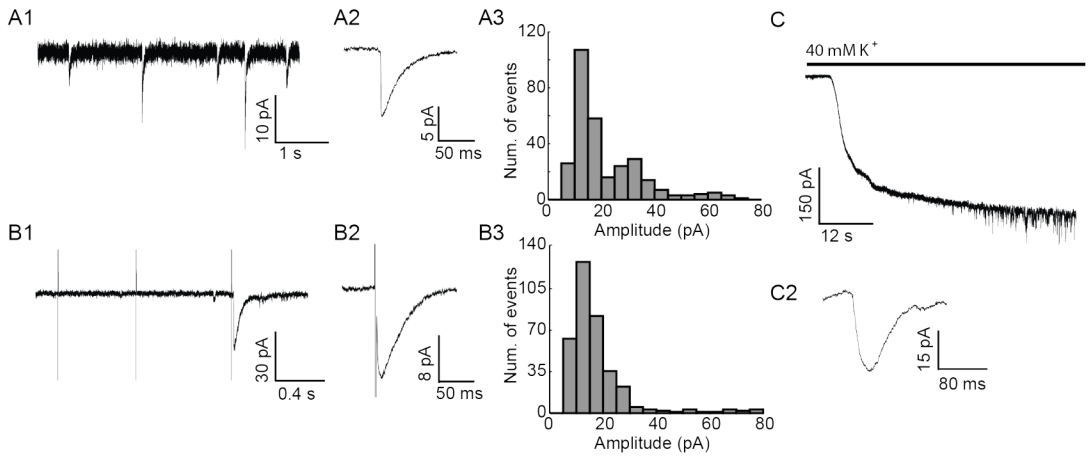


**Figure 4.1 Spontaneous and evoked efferent synaptic responses in type II HCs.** A1. An example of spontaneous efferent synaptic events. A2. Average waveform of spontaneous synaptic events. A3. Amplitude distribution of spontaneous efferent events

from 5 HCs. B1. An example of responses following electrical stimulation. The first two electrical pulses only resulted in transient artifacts, while the third one triggered synaptic response. B2. Average waveform of evoked synaptic events. B3. Amplitude distribution of evoked efferent events from 12 HCs. C. High concentration of potassium external solution also triggered efferent synaptic events. C2. Average waveform of 40mM $K^+$ induced events. (Recordings were performed at $V_h$ = -90 mV in A-D.)

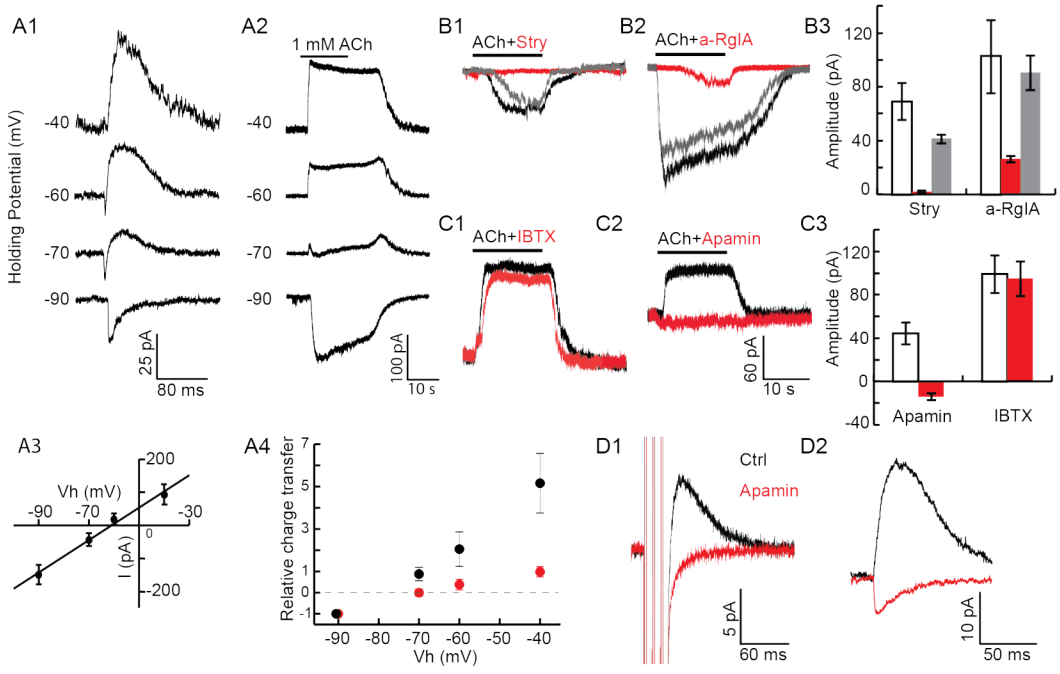


**Figure 4.2 Efferent synaptic responses were mediated through α9* nAChRs and SK channels.** A1. Spontaneous efferent synaptic currents recorded at different Vh. A2. Currents induced by 1 mM ACh application recorded at different Vh. A3. Reversal potential of Ach responses (n=5). A4. Relative total charge transfer (normalized to the

charge transfer at -90 mV) at different Vh for synaptic currents (black)(n=4) and ACh currents (red)(n=5). B1-B2, C1-C2, examples of blockade of ACh responses using antagonists (black: control; red: with antagonists; grey: wash out). (B1-B2: recorded at $V_h$= -90mV; C1-C2: recorded at -40 mV). B3. Bar graph showed strychnine and α-RgIA could block ACh responses (n = 3 each). C3. Bar graph showed apamin could reverse the response polarity of ACh responses while IBTX had litter effects (apamin: n = 3; IBTX: n = 5). (For B3 and C3, white bars: Ctrl; red bars: with antagonists; grey bars: washout). D1. Apamin completely blocked outward evoked synaptic currents at -50 mV. (Three pulses at 100 Hz were used to trigger responses. Traces were averaged from 200 trials.) D2. Apamin reversed the polarity of spontaneous synaptic currents (traces were averaged from 15-20 events).

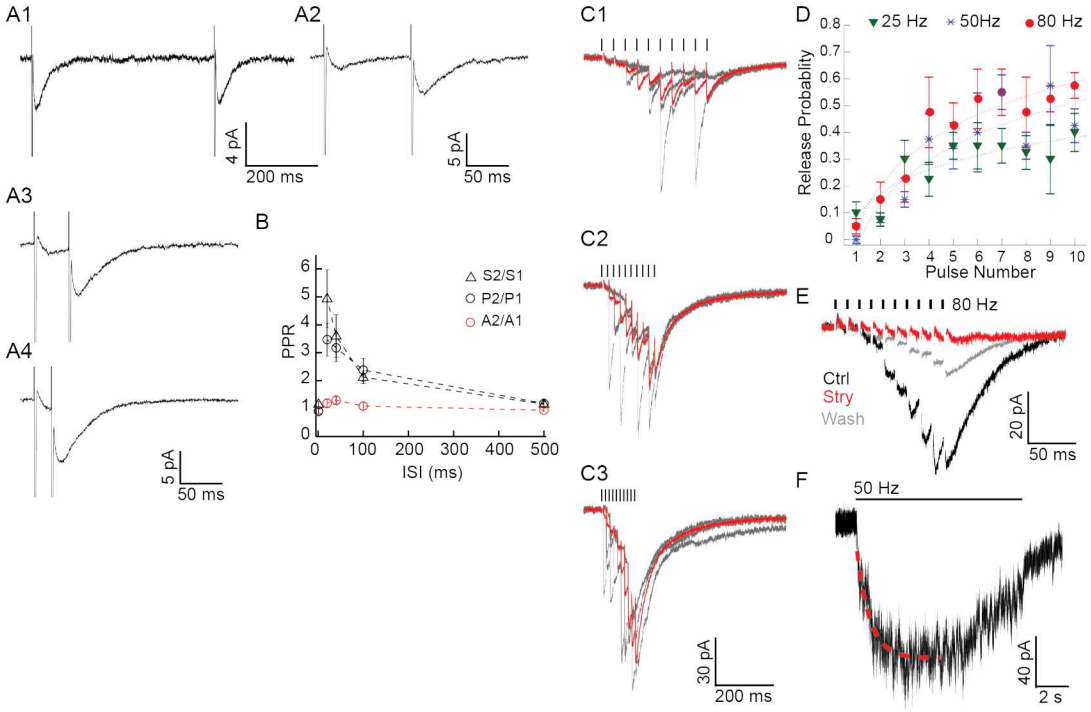

**Figure 4.3 Short-term facilitation of efferent synaptic inputs.** A. Averaged paired pulse responses with inter-stimulus intervals (ISIs) of 500 ms (A1), 100 ms (A2), 40 ms (A3), 20 ms (A4) (averaged across 200 trials). B. Paired pulse ratio inversely correlated with ISIs. The ratio of overall responses (S2/S1, triangle) and release probability (P2/P1, black circle) were enhanced at shorter intervals, while the ratio of amplitudes was unaltered (A2/A1 red circle) (n = 4). (The data points at 0 ms were calculated as the ratio of first responses in tests with different ISIs, reflecting the variance). C. Train stimulation evoked potentiated efferent responses - Examples of synaptic responses evoked by 10 - pulse stimulation at 25 Hz (C1), 50Hz (C2), 80Hz (C3) respectively (Electrical pulses were indicated as black bars), with artifacts removed after recording. Red traces were averaged responses across 10 trials. Grey traces were un-averaged example responses. (C1 – C3 were from the same cell). D. Release probability kept growing during train stimulation (n=6). E. Strychnine almost completely abolished synaptic responses evoked by 80 Hz train stimulation. F. An example of synaptic responses evoked by 50 Hz stimulation that lasted 10s. The rise of the response was fitted with an exponential function (red dashed line). All plots were based on recordings at Vh = -90mV.

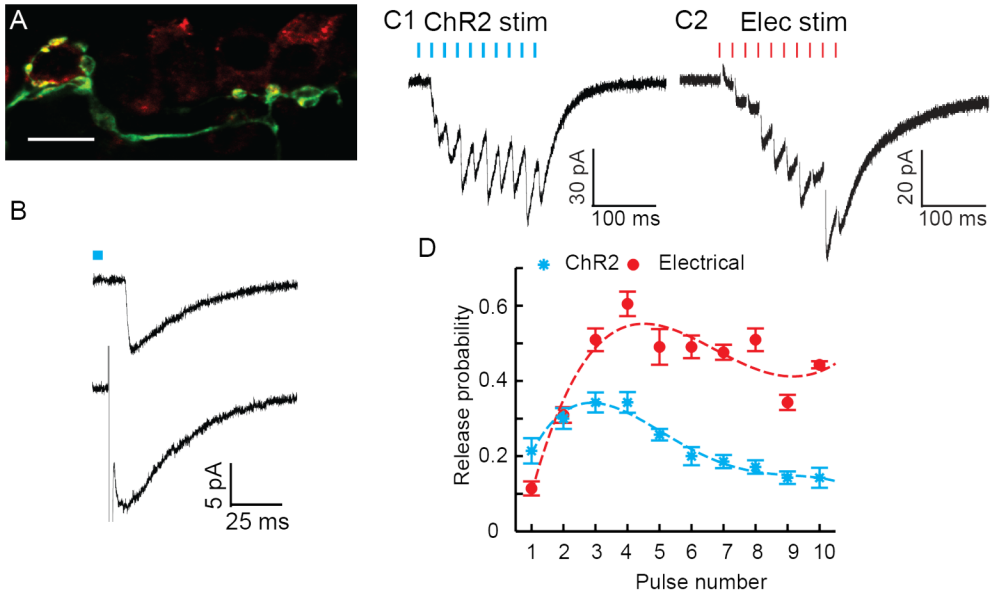


**Figure 4.4 Optogenetic stimulation of efferents.** A. Terminals of ChR2-EYFP positive fibers (stained against YFP, green) colocalized with synaptic vesicle protein SV2 (red). SV2 was also observed to faintly stain cell bodies of HCs. B. Upper trace: an example of averaged response to 5-ms blue light stimuli; lower trace: an example of averaged response to electrical pulse. C1, An example of averaged response (from 10 trials) following train stimulation consisted of 10 light pulses at 50 Hz. C2. An example of averaged response (from 10 trials) following train stimulation consisted of 10 electrical pulses at 50 Hz, with artifacts removed after recording. D. Both optogenetic (blue, n = 6) and electrical stimulation (red, n =3) revealed an increase and then a reduction of release probability for later pulses in the train. All plots were based on recordings at Vh = -90mV.

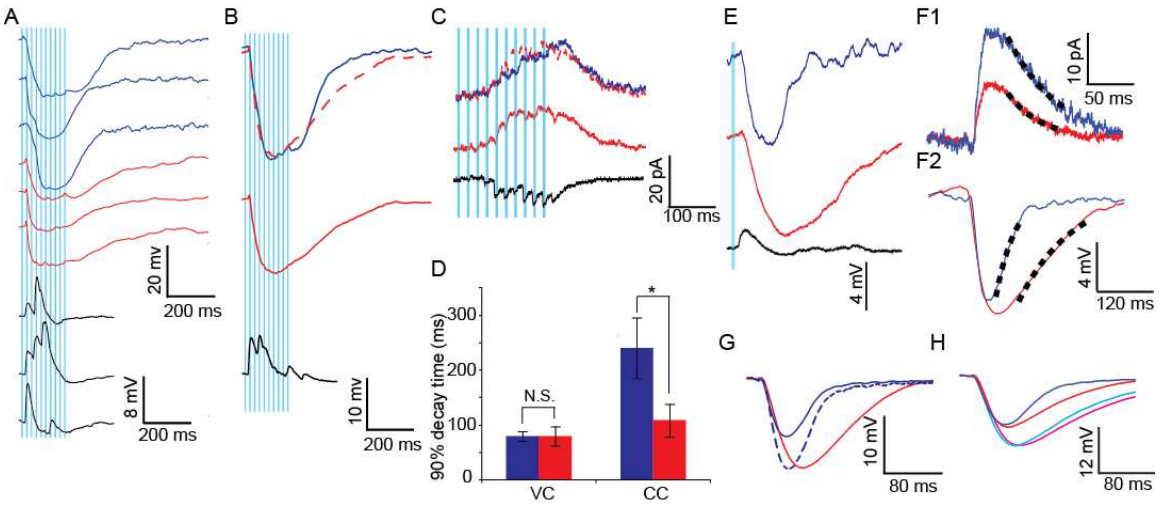


**Figure 4.5 Inhibition induced by efferent stimulation.** A. 50 Hz optical stimulation resulted in strong inhibition for cells that at -60 mV(red), -40mV(blue), and excitation but also flowed by inhibition for cells that at -80mV(black). B. Averaged membrane potential changes (from 10 trials) at -40 mV(blue), -60mV(red), -80mV(black) for the same cell in A. For the upper trace, the response at -60mV (red, dashline) was scaled to the same amplitude to reveal a slowed decay time. C. Averaged currents (from 10 trials) recorded in voltage clamp mode at -40mV (blue), -60mV (red), -90mV (black). For the upper trace, the response at -60mV (red, dash line) was scaled to the same amplitude to reveal a slowed decay time. D. The decay time for efferent induced inhibition was significantly longer at -60mV (blue), compared to the inhibition at -40mV (red). But no changes were detected for the currents measured at the two potentials (n=6). E. An example of membrane potential change evoked by single light pulse at -80mV (black), -60mV (red), and -40 mV (blue). F1. Averaged efferent induced currents at -60 mV (red) and -40 mV (blue); F2. Averaged efferent induced membrane potential change at -60 mV (red) and -

40 mV (blue). Traces in F1 and F2 were averaged from 100 – 200 trials and fitted with single exponential function (dash line). G. Injecting currents resemble efferent induced currents in F1 also revealed slowed kinetics near resting membrane potential. (Averaged response at -40mV (blue solid line) and at -60 mV (red line); the response at -40 mV was scaled for comparison (blue dash line)(averaged from 100-200 trials). H. Efferent inhibition was prolonged in the presence of 4-AP at -60mV (magenta) and at -40 mV (cyan), compared to the inhibition in control condition at -60mV (red) and at -40mV (blue). 4-AP also eliminated the differences of kinetics between responses at -60mV and -40 mV (traces were averaged from 100-200 trials).

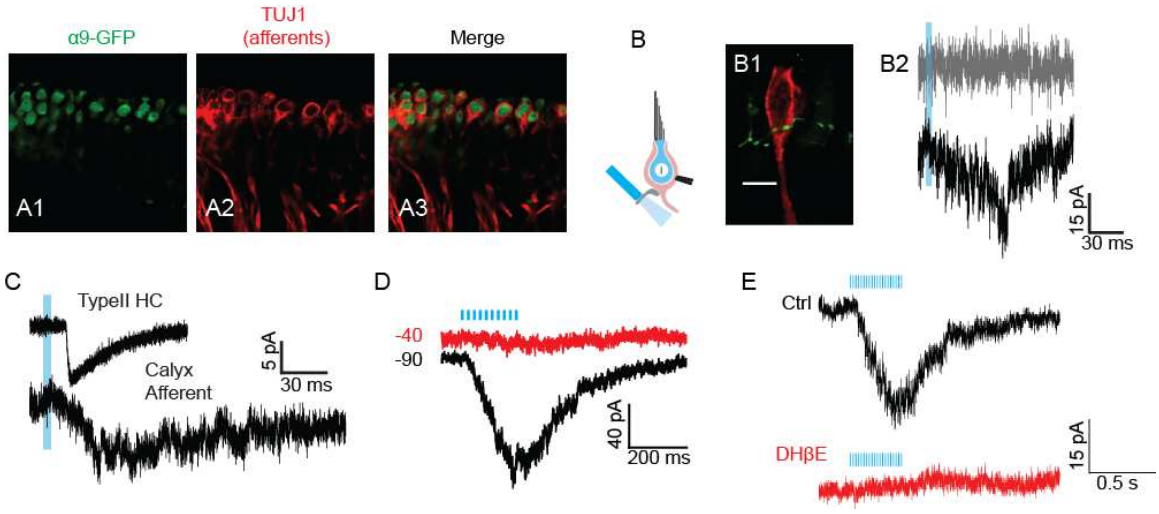


**Figure 4.6 Efferent synaptic inputs to calyx-afferents.** A. GFP signals (A1, stained against GFP, green) were detected in HCs, but not in calyx-afferents (A2, stained against TUJ1, red). (A3: an overlay of A1 and A2). B. Single pulse light stimulation could induce inward synaptic current (B2: upper trace (grey), failure; lower trace (black), success) in calyx-afferents (B1, filled with biocytin) in ChAT-Cre; Ai32 mice (B1, YFP signals

(stained against YFP, green) were present at efferents). Scale bar: 10 µm. C. Efferent synaptic currents recorded from type II HCs and calyx-afferents had distinct waveforms (averaged from 100-200 trials). D. Averaged efferent synaptic responses (from 10 trials) evoked by train stimulation consisted of 10 light pulses were recorded at -40 mV and -90 mV. E. Train stimulation (of 20 light pulses) evoked efferent responses could be blocked by DHβE.

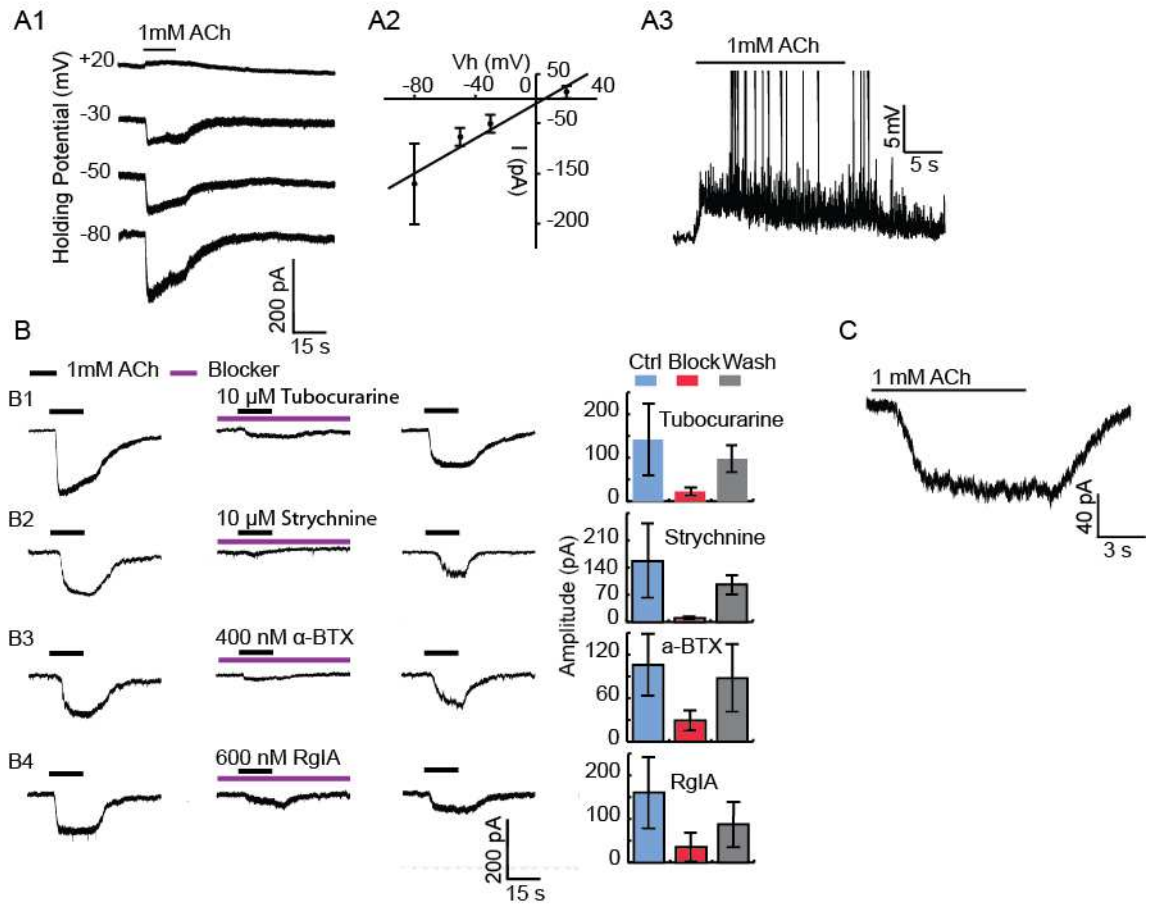


**Figure 4.7 ACh responses of calyx-afferents.** A. 1mM ACh induced currents in a subset of calyx-afferents at different holding potentials (A1). ACh responses in calyx-afferent

reversed near 0 mV (n = 5) and were excitatory (A2, n = 4-5), sufficient for triggering an increase of firing rate in calyx-afferents (A3). B. ACh response in calyx-afferent could be reversibly blocked by tubocurarine, strychnine, α-BTX and α-RgIA (n≥4). C. 1 mM ACh induced inward currents in type I HCs.

# Chapter 5 Discussion

Presented in **Chapter 3** and **Chapter 4**, findings from this study demonstrate many interesting features of signal processing mediated by various types of synaptic transmission at the vestibular periphery. Type I HCs and type II HCs supply non-quantal and quantal synaptic signals to downstream vestibular calyx-afferents respectively, and vestibular efferents provide excitatory synaptic inputs to calyx-afferents but inhibitory inputs to type II HCs. These highly diverse types of signals grant the peripheral vestibular system a strong capacity for encoding head movements. In this chapter, I will review how findings from this thesis study can improve our understanding of the computation performed by the peripheral vestibular system and some future directions following this study.

### 5.1 Mechanisms underlying HC to calyx-afferent synaptic transmission.

In **Chapter 3**, I showed by targeted activation of vestibular HCs that in mature mice, most calyx-afferents received highly distinct non-quantal synaptic signals from type I HCs and quantal signals from type II HCs. While both inputs were excitatory, non-quantal inputs could strongly drive firing activities in downstream calyx-afferents. Moreover, this relatively novel form of non-quantal signals alone was sufficient for mediating basic vestibular function VOR.

The type I HC-calyx synapse is the most unique structure that evolved for the peripheral vestibular system in amniote vertebrates (reptiles, birds and mammals). Such

elaborate calyx synapses likely provide functional benefits for adapting to life in land, as species appear later in evolution tend to have more type I HCs and calyx synapses(Lysakowski, 1996, Lysakowski and Goldberg, 1997, 2008). After migrating to land, another common feature acquired by amniotes is a mobile neck. More flexible head movements enabled by the neck impose challenges to the vestibular system for detecting faster head motion. The unusually large resting potassium conductance of type I HCs maybe a specialization for such functional requirement, as it shortens membrane time constant and likely enables better capture of rapidly changing inputs (Songer and Eatock, 2013). However, this large membrane conductance greatly lowers the membrane potential gain and limits type I HCs to operate at negative membrane potential, which is not in favor of ribbon synaptic transmission. Therefore, it is speculated that type I HC-to calyx-synapses have implemented other forms of synaptic transmission(Goldberg, 1996). Highly diverse 'non-quantal' and quantal synaptic responses have been reported in a number of studies (Yamashita and Ohmori, 1990, Holt et al., 2006b, Holt et al., 2007, Songer and Eatock, 2013, Highstein et al., 2014). Yet as in these studies either all HCs were activated or only a subset of calyx bearing afferents showed such non-quantal responses, and it was therefore not conclusive whether non-quantal responses were indeed from type I HC-calyx synapses. Here, this thesis study demonstrates that inputs from type I HCs are necessary for non-quantal signals, as activating type II HCs only leads to quantal signals; and sufficient for non-quantal signals, as activating type I HCs results in non-quantal signals in every calyx-afferent tested. Non-quantal signals are rapid

and reliable, following the activity of type I HCs with high fidelity. These properties of non-quantal transmission are consistent with the presumed role that type I HCs play in detecting the fast component of head motion. The amplitude of non-quantal signals may appear rather small, but I showed that they could effectively induce firing-rate increase in calyx-afferents, indicating that action potential generation was sensitive to small input currents near resting membrane potential. As the majority of vestibular afferents have calyx terminals (Baird et al., 1988, Lysakowski et al., 1999), non-quantal signals could play a critical role in peripheral vestibular coding.

Type II HCs are more prototypical and are the only type of HCs functioning in fishes and amphibians. In mammals, while dimorphic and bouton-only afferents can receive inputs from type II HCs via bouton terminals, ~20% of afferents only have calyx-terminals (Desai et al., 2005a). Although it has been shown using electron microscopy that type II HCs can form ribbon synapses onto the outer wall of calyx terminals, the number of these synapses appears low(Lysakowski and Goldberg, 1997, 2008). Here I showed that in mice every calyx-afferent tested received quantal synaptic inputs from type II HCs, indicating that those outer face synapses were consistent sites for transmission. Those qEPSCs that resulted from activation of type II HCs exhibited a wide range of kinetics, consistent with EPSCs observed in previous studies (Sadeghi et al., 2014, Highstein et al., 2015). It has been suggested that the slow EPSCs were due to glutamate spillover inside the calyx terminal(Sadeghi et al., 2014). As qEPSCs in this study were from type II HCs, spillover may happen at type II HCs synapses as well and

lead to prolonged decay time. Possibly dendritic filtering and other mechanisms also may account for highly variable EPSC kinetics.

Our data indicate that type I HCs provide non-quantal signals that are distinct from quantal signals resulting from vesicular glutamate synaptic releases. However, type I HCs have ribbons and synaptic vesicles(Lysakowski, 1996, Lysakowski and Goldberg, 1997, 2008). Although I observed only non-quantal signals by optogenetic activation of type I HCs, quantal synaptic transmission could not be ruled out from type I HC-calyx synapses, as the threshold for vesicular synaptic transmission might not have been reached by those type I HCs in the specific experimental conditions. To strongly depolarize type I HCs, 40 mM $K^+$ solution was applied to the preparation in another set of experiments in this study. qEPSCs evoked by such an approach are likely to result from both type I and type II HCs. However, no significant heterogeneity that might reflect such different origins could be identified. By comparison to those qEPSCs evoked by activating type II HCs solely, no obvious differences were detected either. One possibility is that EPSCs resulting from ribbon synaptic vesicular release were similar regardless from which type of HC produced them. However, given the geometry of calyx-synapse and the positioning of ribbons and postsynaptic receptors, it is hard to believe that the resulting glutamate accumulation and spillover does not affect EPSC kinetics. Perhaps, the difference may be subtle and lost in our analysis as I could not distinguish the origins of those 40 m$MK^+$ evoked EPSCs. Nevertheless, it is intriguing to know how type I HCs can be depolarized enough to release transmitters in the presence

of such unusually large resting potassium conductance in physiological conditions. Since mechanical stimulation of hair bundles also failed to depolarize type I HCs to above -70 mV (Songer and Eatock, 2013), possibly only extremely large head movements may be sufficient. There is a trend toward decreasing numbers of ribbon synapses in species during evolution (Lysakowski and Goldberg, 1997, Holt et al., 2007, Lysakowski and Goldberg, 2008), suggesting that quantal transmission from type I HCs declines in importance. Another possibility is that those ribbon synaptic releases may occur during development before the potassium conductance is fully acquired in type I HCs. Indeed, a recent study showed that immature type I HCs could be depolarized by ~20 mV by mechanical stimulation and this resulted in an increase of qEPSCs in calyx-afferents(Songer and Eatock, 2013).

There are many theories regarding the possible mechanisms for synaptic transmission at the large contact surface between type I HCs and calyx terminals(Goldberg, 1996). Some of them, such as ephaptic coupling or accumulation of potassium (Lim et al., 2011, Contini et al., 2012), protons (Highstein et al., 2014) and/or other transmitters, may account for the non-quantal currents in calyx-afferents. Our study did not completely resolve the underlying mechanism but revealed a number properties of non-quantal signals that result from weak depolarization (~1mV) of type I HCs: extremely fast onset (< 5ms), very little variation among trials, inward at negative membrane potentials and insignificant above 0 mV, not affected by blockers against typical glutamate receptors or amiloride (blockers for ASICs) or 4AP (blockers for $I_{K,L}$),

and coupled with opening of an unknown conductance. From these features, I can probably deduce that: (1) the possibility of glutamate as transmitters underlying such non-quantal signals is low; (2) If protons were transmitters here, they are not acting through ASICs; (3) If non-quantal currents were caused by potassium accumulation, they do not depend on $g_{K,L}$; (4) there is a change of membrane conductance associated with non-quantal responses. Moreover, from theoretical modeling, I know that effects of ephaptic coupling should be too small to account for the non-quantal responses. It is not clear whether the increased membrane conductance is related to accumulation of potassium or protons. Thus, it appears that identifying this unknown conductance is key to resolving the non-quantal mechanisms.

**5.2 Mechanisms underlying efferent synaptic transmission.**

Activities of type II HCs and afferent terminals are directly regulated by feedback efferent inputs from the brain stem. In **Chapter 4**, I investigated the efferent synaptic responses in type II HCs and calyx-afferents at cristae of rodents. Our data suggest that efferent inputs to type II HCs are mainly mediated by α9* nAChRs and SK channels while efferent inputs to calyx-afferents are mediated by neuronal nAChRs. These efferent inputs exhibited a high degree short-term facilitation and facilitated inputs could strongly inhibit type II HCs but excite calyx-afferents.

Properties of efferent synapses onto HCs seem to be highly conserved across different species and sensory systems, reflecting a common origin in evolution. α9*

nAChRs have been studied extensively for mediating efferent inputs to cochlear HCs (Elgoyhen et al., 1994) and have been shown to exist in vestibular epithelia of various species(Hiel et al., 1996, Luebke et al., 2005, Holt et al., 2006a). Our study further confirms their functional role at efferent responses in type II HCs. Usually, α9* nAChRs are associated with SK channels to induce inhibition in HCs (Yuhas and Fuchs, 1999, Glowatzki and Fuchs, 2000, Holt et al., 2006a). Our results suggest that this is also the case for efferent – to – type II HCs synapses. However, it has been shown that at the basal turn of the cochlea, BK channels instead of SK channels underlie efferent inputs to outer hair cells (Wersinger et al., 2010, Rohmann et al., 2015). I did not detect the participation of BK channels, but it remains possible that a small subset of type II HCs use BK channels for efferent (Kong et al., 2005). Not only similar in postsynaptic mechanisms, presynaptic properties such as low basal release probability and short term facilitation revealed in this study also resemble presynaptic properties demonstrated for efferents input to inner HCs and outer HCs in immature rodents(Goutman et al., 2005, Ballestero et al., 2011). Notably, compared to cochlear efferent synapses, the basal release probability of efferent-to-type II HC synapses is even lower, although after facilitation the release probabilities of these synapses are comparable. Due to these similarities, mechanisms underlying presynaptic short-term plasticity found at cochlea efferent-to-HC synapses could possibly hold true at vestibule efferent-to-HC synapses. On the other hand, our results indicated that the inhibition was stronger near the resting membrane potential (-60 mV), caused by higher membrane resistance near that potential

as well as other voltage-dependent conductance. A similar phenomenon was also observed in one study performed in the turtle cochlea(Art et al., 1984). Hence, a stronger inhibition near resting membrane potential can be expected at cochlea HCs in mammals if those HCs possess similar profile of channel conductances, although this idea remains to be tested.

Type II HCs contains ~ 10-20 ribbon synapses per cell, and supply inputs to bouton terminals as well as to calyx terminals through their outer wall(Lysakowski and Goldberg, 1997). In **Chapter 3**, I showed that every calyx-afferents receives inputs from type II HCs through quantal transmission. In **Chapter 4**, our results indicated that efferent inputs could strongly hyperpolarize the membrane potential of type II HCs: efferent stimulation at 50 Hz could decrease the membrane potential by ~ 7 mV (maximum: ~20 mV) when HCs are at rest (-60 mV) or in an excitatory state (-40 mV). The transfer function for the membrane potential and the output of type II HCs, obtained by measurements of capacitance and calcium currents, seems to be most sensitive or dynamic in the range between -70 to -20 mV(Bao et al., 2003, Dulon et al., 2009). Therefore, the amount of efferent inhibition can effectively reduce or even shut down the output of type II HCs to the ganglion neurons. In addition, I found efferent inhibition was prolonged near the resting membrane potential (-60 mV), indicating that efferent inputs may delay the onset of vestibular responses by keeping the HCs below the threshold for transmitter release. Based on the powerful efferent inhibition I observed, it is likely that one function of efferents is to switch the peripheral vestibular system from a two-channel

system receiving inputs from both type I and type II HCs to a one-channel system receiving inputs only from type I HCs, by suppressing the vestibular information gated through type II HCs. If so, as the vestibular sensation is mediated mainly by type I HCs during activation of efferents, it might have lower gain. And indeed, a reduced rotational gain has been observed in in-vivo recordings of vestibular afferents during efferent stimulation(Goldberg and Fernandez, 1980, Marlinski et al., 2004).

According to results from this thesis study, direct efferent synaptic inputs to calyx-afferents could be completely blocked by DhβE and were excitatory, consistent with findings from calyx-afferents in the crista of turtles (Holt et al., 2006a, Holt et al., 2015). DhβE is a nAChR blocker selective for α4β2, α6β2* and α4β4 types. Pharmacology experiments with more specific blockers confirmed the functional role of α6-containing nAChRs, and immunostaining results indicated the presence of α4 and β2 subunits in those turtle calyx-afferents (Holt et al., 2015). Although it remains to be tested, α6, α4 and β2 might also function at the mammalian efferent to calyx-afferent synapses. Additionally, in this study, efferent synaptic currents recorded at calyx-afferents exhibited slow kinetics, possibly due to volume transmission. Interestingly, in calyx-afferents of turtles, nicotinic receptor mediated efferent responses lasted for seconds after brief stimulation, consistent with the slow kinetics caused by volume transmission. However, more experiments are required to confirm the existence of volume transmission. Other than nAChRs, the presence of mAChRs at vestibular afferents has also been suggested by previous studies(Wackym et al., 1996, Perez et al.,

2009), yet nAChR antagonists could block the majority of efferent induced responses in calyx afferents in this study and studies done in turtles.

By recording ACh induced responses from calyx-afferents, I unexpectedly discovered that at least a subset of type I HCs could also respond to ACh solution, suggesting that functional nAChRs (α9* nAChRs likely) were present at type I HCs at a relatively mature age. However, type I HCs do not receive direct efferent inputs, although they might be contacted during development (Dememes and Broca, 1998). Therefore, the functional significance of these nAChRs in type I HCs remains mysterious.

**5.3 Functional significance of diverse synaptic signals in the vestibular periphery.**

Type I HC and type II HC pathways likely play distinct roles in detecting head movements at the vestibular periphery. Type I HCs have a large resting membrane conductance due to $g_{K,L}$, and therefore have a much lower membrane potential gain for mechanical stimulation, compared to type II HCs. Additionally, in **Chapter 3**, I revealed that two types of synaptic signals – non-quantal and quantal signals functioned at type I HC and type II HC to calyx-afferents pathways respectively. However, studies that investigated the functional implication of the diverse type I and type II HC pathways are very preliminary. In **Chapter 3**, I found that mice with only non-quantal transmission (VgluT3 KO) exhibited normal VOR. Although such results prove the sufficiency of non-quantal transmission, they may not represent the real contribution from non-quantal transmission and the type I HC pathway because compensation may happen in the VOR

circuitry. Nevertheless, studies showed that selectively eliminating type I HCs by administrating gentamicin could effectively reduce vestibular function (Hirvonen et al., 2005, Lyford-Pike et al., 2007), supporting the notion that non-quantal transmission from type I HC to calyx-afferents is crucial. Additional inputs from type II HCs seem to enhance the gain, as dimorphic afferents have higher gain than calyx-only afferents(Baird et al., 1988). In agreement with this notion, studies have shown that efferent inputs can reduce the rotational gain of afferents(Goldberg and Fernandez, 1980, Marlinski et al., 2004) possibly through inhibiting type II HCs (details in **Chapter 4**). These studies only demonstrate that both type I and type II HC pathways contribute to the detection of head movements, yet whether each pathway has its own specialized function is unknown. As the type I HCs have a shorter membrane time constant and non-quantal signals have a rapid onset, I speculate that they might be responsible for detecting fast head motion, but the evidence is still missing.

Although I found the primary effect of efferent inputs to type II HCs was inhibitory in the cristae of mice and rats, activating efferents *in vivo* exclusively lead to an increase in resting discharge rate of vestibular afferents in mammals(Goldberg and Fernandez, 1980, Marlinski et al., 2004). Given that calyx-afferents receive direct synaptic inputs from efferents and type II HCs, to explain the increased discharge rate, excitatory efferent inputs to calyx-afferents must outweigh the inhibitory efferent inputs to type II HCs in terms of determining the firing rate of afferents. However, results from this study showed that only a subset of calyx-afferents responded to optogenetic efferent

stimulation while every calyx-afferent received excitatory synaptic inputs form type II HCs, indicating that efferent excitation may not be able to compensate for the reduction of type II inputs and raise the firing rate. Nevertheless, optogenetic stimulation might not effectively activate all efferent inputs; hence the strength of efferent excitation to calyx-afferents could be underestimated.

The strong efferent inhibition in type II HCs well suits a role in reducing the vestibular gain - a phenomenon also has been observed *in-vivo* by many studies(Goldberg and Fernandez, 1980, Marlinski et al., 2004). As type II HCs may function differently from type I HCs, inhibiting the type II HC pathway might allow the type I HC pathway to dominante the vestibular function, although the exact functional consequence of this action is unclear due to a lack of understanding of the individual contribution from type I and type II HC pathways. It worth pointing out that efferent inhibition may not be the only source of gain reduction. For example, activating nAChRs at efferent to afferent synapses may also reduce the gain by increasing the membrane conductance. While gain modulation might extend the dynamic range for detecting head movements, it is still intriguing that efferents have opposite effects on type II HCs and calyx-afferents. It is unlikely that these seemingly opposite effects just cancel each other. A guess would be that the gain reduction due to efferent inhibition of type II HCs might hyperpolarize calyx-afferents to below the threshold for action potential generation. Therefore, the efferent induced excitation in calyx-afferents might be required to maintain the resting discharge rate, allowing the gain reduction to happen without decreasing sensitivity.

**5.4 Future directions.**

This thesis study provides many insights into how information is processed at the peripheral vestibular system. On the other hand, these findings also raise a number of interesting questions. Perhaps the most curious one would be what is the mechanism underlying synaptic transmission between type I HCs and calyx-terminals. This thesis study is limited by the extent to which the membrane potential of type I HCs can be manipulated and monitored. For instance, the optogenetic method could only depolarize type I HCs by 1-2 mV. Such tiny depolarization might not reach the threshold for vesicular glutamate release and prevent us from studying possible quantal synaptic transmission from type I HCs. Also, pharmacological manipulations of synaptic transmission might impact type I HCs and calyx-afferents simultaneously (e.g. 4AP, in **Chapter 3**). Although we can record type I HC and calyx-afferents in separate experiments, type I HCs in intact calyx-terminals might behave differently from those exposed. Without knowing the exact membrane potential changes in type I HCs, it is difficult to interpret just based on recordings from calyx-afferents. Moreover, as the calyx synaptic cleft might have isolated electrical potential and ion concentration, it is key to assess these conditions when investigating synaptic mechanisms. Usually measurements of these conditions require to precisely manipulate and monitor the activities of type I HCs and calyx-afferents. Maybe dual patch-clamp recordings from type I HCs and calyx-afferents could provide such accuracy. However, the calyx-synaptic structure might be damaged when approaching type I HCs. Possibly, such damage could be evaluated by

comparing to results obtained through optogenetic approach. If it is considerably small, then such dual recording approach can provide many advantages in studying synaptic transmission at calyx-afferents. In addition, stronger ChR2 expression in type I HCs might be achieved by crossing with other Cre mouse lines. If I can selectively activate type I HCs to above the threshold of vesicular synaptic release, I would know if type I HCs could provide quantal signals to calyx-afferents.

Another interesting yet unsolved question is: what is the functional role of non-quantal and quantal transmission in mediating vestibular sensation and behavior? The mouse model studied in Chapter 3 (VgluT3 KO) had quantal synaptic transmission impaired. However, compensation in the vestibular system may happen at various stages and prevent us from dissecting out the contribution from quantal signals and non-quantal signals in physiological conditions. If the elimination of quantal transmission can be more temporally and spatially restricted, we can provide a better answer to this question. Therefore a mouse line that allows inducible knockout of VgluT3 in vestibular HCs is desirable. Moreover, if we could have a handle on the mechanism of non-quantal transmission and could eliminate such transmission, we could obtain a better understanding of functional roles of these various forms of synaptic signals in vestibular sensation as well.

The functional role of efferent inputs is also mysterious, although I showed that efferents could inhibit type II HCs and excite calyx-afferents at the synaptic level. Part of the mystery lies in the functional properties of efferent neurons. Little is known about the

behavioral context in which efferent neurons might be activated in mammals. Nevertheless, as I identified that α9 nAChRs mediate efferent inputs to type II HCs and the expression of α9 nAChR subunit is quite restricted to HCs(Zuo et al., 1999), the α9 KO mouse line could be a tool to evaluate the behavioral significance of efferent inputs to type II HCs.

# Bibliography


Anastassiou CA, Koch C (2015) Ephaptic coupling to endogenous electric field activity: why bother? Current opinion in neurobiology 31:95-103.

Armand M, Minor LB (2001) Relationship between time- and frequency-domain analyses of angular head movements in the squirrel monkey. Journal of computational neuroscience 11:217-239.

Art JJ, Fettiplace R, Fuchs PA (1984) Synaptic hyperpolarization and inhibition of turtle cochlear hair cells. J Physiol 356:525-550.

Bailey GP, Sewell WF (2000) Calcitonin gene-related peptide suppresses hair cell responses to mechanical stimulation in the Xenopus lateral line organ. J Neurosci 20:5163-5169.

Baird RA, Desmadryl G, Fernandez C, Goldberg JM (1988) The vestibular nerve of the chinchilla. II. Relation between afferent response properties and peripheral innervation patterns in the semicircular canals. Journal of neurophysiology 60:182-203.

Ballestero J, Zorrilla de San Martin J, Goutman J, Elgoyhen AB, Fuchs PA, Katz E (2011) Short-term synaptic plasticity regulates the level of olivocochlear inhibition to auditory hair cells. J Neurosci 31:14763-14774.

Bao H, Wong WH, Goldberg JM, Eatock RA (2003) Voltage-gated calcium channel currents in type I and type II hair cells isolated from the rat crista. Journal of neurophysiology 90:155-164.

Blitz DM, Foster KA, Regehr WG (2004) Short-term synaptic plasticity: a comparison of two synapses. Nature reviews Neuroscience 5:630-640.

Chavez-Noriega LE, Crona JH, Washburn MS, Urrutia A, Elliott KJ, Johnson EC (1997) Pharmacological characterization of recombinant human neuronal nicotinic acetylcholine receptors h alpha 2 beta 2, h alpha 2 beta 4, h alpha 3 beta 2, h alpha 3 beta 4, h alpha 4 beta 2, h alpha 4 beta 4 and h alpha 7 expressed in Xenopus oocytes. The Journal of pharmacology and experimental therapeutics 280:346-356.

Clark B, Stewart JD (1968) Comparison of three methods to determine thresholds for perception of angular acceleration. The American journal of psychology 81:207-216.

Contini D, Zampini V, Tavazzani E, Magistretti J, Russo G, Prigioni I, Masetto S (2012) Intercellular K(+) accumulation depolarizes Type I vestibular hair cells and their associated afferent nerve calyx. Neuroscience 227:232-246.

Crawford J (1964) Living without a Balancing Mechanism. The British journal of ophthalmology 48:357-360.

Deisseroth K (2015) Optogenetics: 10 years of microbial opsins in neuroscience. Nature neuroscience 18:1213-1225.

Dememes D, Broca C (1998) Calcitonin gene-related peptide immunoreactivity in the rat efferent vestibular system during development. Brain research Developmental brain research 108:59-67.

Desai SS, Ali H, Lysakowski A (2005a) Comparative morphology of rodent vestibular periphery. II. Cristae ampullares. Journal of neurophysiology 93:267-280.

Desai SS, Zeh C, Lysakowski A (2005b) Comparative morphology of rodent vestibular periphery. I. Saccular and utricular maculae. Journal of neurophysiology 93:251-266.

DiGregorio DA, Rothman JS, Nielsen TA, Silver RA (2007) Desensitization properties of AMPA receptors at the cerebellar mossy fiber granule cell synapse. The Journal of neuroscience : the official journal of the Society for Neuroscience 27:8344-8357.

Dreifuss JJ, Kalnins I, Kelly JS, Ruf KB (1971) Action potentials and release of neurohypophysial hormones in vitro. J Physiol 215:805-817.

Dulon D, Safieddine S, Jones SM, Petit C (2009) Otoferlin is critical for a highly sensitive and linear calcium-dependent exocytosis at vestibular hair cell ribbon synapses. J Neurosci 29:10474-10487.

Eatock RA, Rusch A, Lysakowski A, Saeki M (1998) Hair cells in mammalian utricles. Otolaryngology--head and neck surgery : official journal of American Academy of Otolaryngology-Head and Neck Surgery 119:172-181.

Eatock RA, Songer JE (2011) Vestibular hair cells and afferents: two channels for head motion signals. Annual review of neuroscience 34:501-534.

Elgoyhen AB, Johnson DS, Boulter J, Vetter DE, Heinemann S (1994) Alpha 9: an acetylcholine receptor with novel pharmacological properties expressed in rat cochlear hair cells. Cell 79:705-715.

Ellison M, Haberlandt C, Gomez-Casati ME, Watkins M, Elgoyhen AB, McIntosh JM, Olivera BM (2006) Alpha-RgIA: a novel conotoxin that specifically and potently blocks the alpha9alpha10 nAChR. Biochemistry 45:1511-1517.

Faulstich BM, Onori KA, du Lac S (2004) Comparison of plasticity and development of mouse optokinetic and vestibulo-ocular reflexes suggests differential gain control mechanisms. Vision research 44:3419-3427.

Fuchs PA (2014) A 'calcium capacitor' shapes cholinergic inhibition of cochlear hair cells. The Journal of physiology 592:3393-3401.

Gainer H, Wolfe SA, Jr., Obaid AL, Salzberg BM (1986) Action potentials and frequency-dependent secretion in the mouse neurohypophysis. Neuroendocrinology 43:557-563.

Glowatzki E, Fuchs PA (2000) Cholinergic synaptic inhibition of inner hair cells in the neonatal mammalian cochlea. Science 288:2366-2368.

Goldberg JM (1996) Theoretical analysis of intercellular communication between the vestibular type I hair cell and its calyx ending. Journal of neurophysiology 76:1942-1957.

Goldberg JM (2000) Afferent diversity and the organization of central vestibular pathways. Experimental brain research 130:277-297.
Goldberg JM, Fernandez C (1971) Physiology of peripheral neurons innervating semicircular canals of the squirrel monkey. 3. Variations among units in their discharge properties. Journal of neurophysiology 34:676-684.
Goldberg JM, Fernandez C (1975) Responses of peripheral vestibular neurons to angular and linear accelerations in the squirrel monkey. Acta oto-laryngologica 80:101-110.
Goldberg JM, Fernandez C (1980) Efferent vestibular system in the squirrel monkey: anatomical location and influence on afferent activity. Journal of neurophysiology 43:986-1025.
Goldberg JM, Holt JC (2013) Discharge regularity in the turtle posterior crista: comparisons between experiment and theory. Journal of neurophysiology 110:2830-2848.
Goutman JD, Fuchs PA, Glowatzki E (2005) Facilitating efferent inhibition of inner hair cells in the cochlea of the neonatal rat. J Physiol 566:49-59.
Grimes WN, Seal RP, Oesch N, Edwards RH, Diamond JS (2011) Genetic targeting and physiological features of VGLUT3+ amacrine cells. Visual neuroscience 28:381-392.
Grossman GE, Leigh RJ, Abel LA, Lanska DJ, Thurston SE (1988) Frequency and velocity of rotational head perturbations during locomotion. Experimental brain research 70:470-476.
Harris JA, Hirokawa KE, Sorensen SA, Gu H, Mills M, Ng LL, Bohn P, Mortrud M, Ouellette B, Kidney J, Smith KA, Dang C, Sunkin S, Bernard A, Oh SW, Madisen L, Zeng H (2014) Anatomical characterization of Cre driver mice for neural circuit mapping and manipulation. Frontiers in neural circuits 8:76.
Hiel H (2009) In situ hybridization approach to study mRNA expression and distribution in cochlear frozen sections. Methods in molecular biology 493:31-46.
Hiel H, Elgoyhen AB, Drescher DG, Morley BJ (1996) Expression of nicotinic acetylcholine receptor mRNA in the adult rat peripheral vestibular system. Brain research 738:347-352.
Highstein SM, Baker R (1985) Action of the efferent vestibular system on primary afferents in the toadfish, Opsanus tau. J Neurophysiol 54:370-384.
Highstein SM, Holstein GR, Mann MA, Rabbitt RD (2014) Evidence that protons act as neurotransmitters at vestibular hair cell-calyx afferent synapses. Proceedings of the National Academy of Sciences of the United States of America 111:5421-5426.
Highstein SM, Mann MA, Holstein GR, Rabbitt RD (2015) The quantal component of synaptic transmission from sensory hair cells to the vestibular calyx. Journal of neurophysiology 113:3827-3835.

Hirvonen TP, Minor LB, Hullar TE, Carey JP (2005) Effects of intratympanic gentamicin on vestibular afferents and hair cells in the chinchilla. Journal of neurophysiology 93:643-655.

Holt JC, Chatlani S, Lysakowski A, Goldberg JM (2007) Quantal and nonquantal transmission in calyx-bearing fibers of the turtle posterior crista. Journal of neurophysiology 98:1083-1101.

Holt JC, Kewin K, Jordan PM, Cameron P, Klapczynski M, McIntosh JM, Crooks PA, Dwoskin LP, Lysakowski A (2015) Pharmacologically distinct nicotinic acetylcholine receptors drive efferent-mediated excitation in calyx-bearing vestibular afferents. The Journal of neuroscience : the official journal of the Society for Neuroscience 35:3625-3643.

Holt JC, Lysakowski A, Goldberg JM (2006a) Mechanisms of efferent-mediated responses in the turtle posterior crista. The Journal of neuroscience : the official journal of the Society for Neuroscience 26:13180-13193.

Holt JC, Lysakowski A, Goldberg JM (2011) The Efferent Vestibular System. In: Auditory and Vestibular Efferents (Ryugo, K. D. and Fay, R. R., eds), pp 135-186 New York, NY: Springer New York.

Holt JC, Xue JT, Brichta AM, Goldberg JM (2006b) Transmission between type II hair cells and bouton afferents in the turtle posterior crista. Journal of neurophysiology 95:428-452.

Holt JR, Vollrath MA, Eatock RA (1999) Stimulus processing by type II hair cells in the mouse utricle. Annals of the New York Academy of Sciences 871:15-26.

Jackman SL, Beneduce BM, Drew IR, Regehr WG (2014) Achieving high-frequency optical control of synaptic transmission. The Journal of neuroscience : the official journal of the Society for Neuroscience 34:7704-7714.

Jordan PM, Fettis M, Holt JC (2015) Efferent innervation of turtle semicircular canal cristae: comparisons with bird and mouse. The Journal of comparative neurology 523:1258-1280.

Kalluri R, Xue J, Eatock RA (2010) Ion channels set spike timing regularity of mammalian vestibular afferent neurons. Journal of neurophysiology 104:2034-2051.

Katz E, Elgoyhen AB, Fuchs PA (2011) Cholinergic inhibition of hair cells. In: Auditory and Vestibular Efferents, pp 103-133: Springer.

Kong WJ, Guo CK, Zhang S, Hao J, Wang YJ, Li ZW (2005) The properties of ACh-induced BK currents in guinea pig type II vestibular hair cells. Hearing research 209:1-9.

Leijon S, Magnusson AK (2014) Physiological characterization of vestibular efferent brainstem neurons using a transgenic mouse model. PLoS One 9:e98277.

Lim R, Kindig AE, Donne SW, Callister RJ, Brichta AM (2011) Potassium accumulation between type I hair cells and calyx terminals in mouse crista. Experimental brain research 210:607-621.

Luebke AE, Holt JC, Jordan PM, Wong YS, Caldwell JS, Cullen KE (2014) Loss of alpha-calcitonin gene-related peptide (alphaCGRP) reduces the efficacy of the Vestibulo-ocular Reflex (VOR). The Journal of neuroscience : the official journal of the Society for Neuroscience 34:10453-10458.

Luebke AE, Maroni PD, Guth SM, Lysakowski A (2005) Alpha-9 nicotinic acetylcholine receptor immunoreactivity in the rodent vestibular labyrinth. The Journal of comparative neurology 492:323-333.

Lyford-Pike S, Vogelheim C, Chu E, Della Santina CC, Carey JP (2007) Gentamicin is primarily localized in vestibular type I hair cells after intratympanic administration. Journal of the Association for Research in Otolaryngology : JARO 8:497-508.

Lysakowski A (1996) Synaptic organization of the crista ampullaris in vertebrates. Annals of the New York Academy of Sciences 781:164-182.

Lysakowski A, Alonto A, Jacobson L (1999) Peripherin immunoreactivity labels small diameter vestibular 'bouton' afferents in rodents. Hearing research 133:149-154.

Lysakowski A, Gaboyard-Niay S, Calin-Jageman I, Chatlani S, Price SD, Eatock RA (2011) Molecular microdomains in a sensory terminal, the vestibular calyx ending. The Journal of neuroscience : the official journal of the Society for Neuroscience 31:10101-10114.

Lysakowski A, Goldberg JM (1997) A regional ultrastructural analysis of the cellular and synaptic architecture in the chinchilla cristae ampullares. The Journal of comparative neurology 389:419-443.

Lysakowski A, Goldberg JM (2008) Ultrastructural analysis of the cristae ampullares in the squirrel monkey (Saimiri sciureus). The Journal of comparative neurology 511:47-64.

Madisen L, Zwingman TA, Sunkin SM, Oh SW, Zariwala HA, Gu H, Ng LL, Palmiter RD, Hawrylycz MJ, Jones AR, Lein ES, Zeng H (2010) A robust and high-throughput Cre reporting and characterization system for the whole mouse brain. Nature neuroscience 13:133-140.

Maklad A, Kamel S, Wong E, Fritzsch B (2010) Development and organization of polarity-specific segregation of primary vestibular afferent fibers in mice. Cell and tissue research 340:303-321.

Marlinski V, Plotnik M, Goldberg JM (2004) Efferent actions in the chinchilla vestibular labyrinth. Journal of the Association for Research in Otolaryngology : JARO 5:126-143.

Marlinsky VV (1995) The effect of somatosensory stimulation on second-order and efferent vestibular neurons in the decerebrate decerebellate guinea-pig. Neuroscience 69:661-669.

McCue MP, Guinan JJ, Jr. (1994) Influence of efferent stimulation on acoustically responsive vestibular afferents in the cat. J Neurosci 14:6071-6083.

Miller EF, Graybiel A (1975) Thresholds for the perception of angular acceleration as indicated by the oculogyral illusion. Perception & Psychophysics 17:329-332.
Muschol M, Salzberg BM (2000) Dependence of transient and residual calcium dynamics on action-potential patterning during neuropeptide secretion. J Neurosci 20:6773-6780.
Obholzer N, Wolfson S, Trapani JG, Mo W, Nechiporuk A, Busch-Nentwich E, Seiler C, Sidi S, Sollner C, Duncan RN, Boehland A, Nicolson T (2008) Vesicular glutamate transporter 3 is required for synaptic transmission in zebrafish hair cells. The Journal of neuroscience : the official journal of the Society for Neuroscience 28:2110-2118.
Papke RL, Dwoskin LP, Crooks PA, Zheng G, Zhang Z, McIntosh JM, Stokes C (2008) Extending the analysis of nicotinic receptor antagonists with the study of alpha6 nicotinic receptor subunit chimeras. Neuropharmacology 54:1189-1200.
Perez C, Limon A, Vega R, Soto E (2009) The muscarinic inhibition of the potassium M-current modulates the action-potential discharge in the vestibular primary-afferent neurons of the rat. Neuroscience 158:1662-1674.
Plotnik M, Marlinski V, Goldberg JM (2005) Efferent-mediated fluctuations in vestibular nerve discharge: a novel, positive-feedback mechanism of efferent control. Journal of the Association for Research in Otolaryngology : JARO 6:311-323.
Rennie KJ, Ashmore JF (1993) Effects of extracellular ATP on hair cells isolated from the guinea-pig semicircular canals. Neurosci Lett 160:185-189.
Rennie KJ, Streeter MA (2006) Voltage-dependent currents in isolated vestibular afferent calyx terminals. Journal of neurophysiology 95:26-32.
Rohmann KN, Wersinger E, Braude JP, Pyott SJ, Fuchs PA (2015) Activation of BK and SK channels by efferent synapses on outer hair cells in high-frequency regions of the rodent cochlea. J Neurosci 35:1821-1830.
Rusch A, Lysakowski A, Eatock RA (1998) Postnatal development of type I and type II hair cells in the mouse utricle: acquisition of voltage-gated conductances and differentiated morphology. The Journal of neuroscience : the official journal of the Society for Neuroscience 18:7487-7501.
Sadeghi SG, Goldberg JM, Minor LB, Cullen KE (2009) Effects of canal plugging on the vestibuloocular reflex and vestibular nerve discharge during passive and active head rotations. Journal of neurophysiology 102:2693-2703.
Sadeghi SG, Pyott SJ, Yu Z, Glowatzki E (2014) Glutamatergic signaling at the vestibular hair cell calyx synapse. The Journal of neuroscience : the official journal of the Society for Neuroscience 34:14536-14550.
Sarter M, Parikh V, Howe WM (2009) Phasic acetylcholine release and the volume transmission hypothesis: time to move on. Nature reviews Neuroscience 10:383-390.

Seal RP, Akil O, Yi E, Weber CM, Grant L, Yoo J, Clause A, Kandler K, Noebels JL, Glowatzki E, Lustig LR, Edwards RH (2008) Sensorineural deafness and seizures in mice lacking vesicular glutamate transporter 3. Neuron 57:263-275.

Songer JE, Eatock RA (2013) Tuning and timing in mammalian type I hair cells and calyceal synapses. The Journal of neuroscience : the official journal of the Society for Neuroscience 33:3706-3724.

Vetter DE, Liberman MC, Mann J, Barhanin J, Boulter J, Brown MC, Saffiote-Kolman J, Heinemann SF, Elgoyhen AB (1999) Role of alpha9 nicotinic ACh receptor subunits in the development and function of cochlear efferent innervation. Neuron 23:93-103.

Vong L, Ye C, Yang Z, Choi B, Chua S, Jr., Lowell BB (2011) Leptin action on GABAergic neurons prevents obesity and reduces inhibitory tone to POMC neurons. Neuron 71:142-154.

Wackym PA, Chen CT, Ishiyama A, Pettis RM, Lopez IA, Hoffman L (1996) Muscarinic acetylcholine receptor subtype mRNAs in the human and rat vestibular periphery. Cell biology international 20:187-192.

Wersinger E, McLean WJ, Fuchs PA, Pyott SJ (2010) BK channels mediate cholinergic inhibition of high frequency cochlear hair cells. PloS one 5:e13836.

Yamashita M, Ohmori H (1990) Synaptic responses to mechanical stimulation in calyceal and bouton type vestibular afferents studied in an isolated preparation of semicircular canal ampullae of chicken. Experimental brain research 80:475-488.

Yang H, Gan J, Xie X, Deng M, Feng L, Chen X, Gao Z, Gan L (2010) Gfi1-Cre knock-in mouse line: A tool for inner ear hair cell-specific gene deletion. Genesis 48:400-406.

Yuhas WA, Fuchs PA (1999) Apamin-sensitive, small-conductance, calcium-activated potassium channels mediate cholinergic inhibition of chick auditory hair cells. J Comp Physiol A 185:455-462.

Zuo J, Treadaway J, Buckner TW, Fritzsch B (1999) Visualization of alpha9 acetylcholine receptor expression in hair cells of transgenic mice containing a modified bacterial artificial chromosome. Proceedings of the National Academy of Sciences of the United States of America 96:14100-14105.

# Curriculum Vitae

**Zhou Yu**

---

Department of Neuroscience and

Department of Otolaryngology Head and Neck Surgery Tel: (410) 533-9677

The Center for Hearing and Balance Email: yuz04ster@gmail.com

Johns Hopkins University School of Medicine

720 Rutland Ave

Ross 824

Baltimore, MD, 21205

**Education History:**

| | | |
|---|---|---|
| **Ph.D. expected** | 2016 | Neuroscience Graduate Program, Johns Hopkins University School of Medicine, Baltimore, MD<br>Thesis advisor: Elisabeth Glowatzki, Ph.D. |
| **Minor** | 2008 | Department of Computer Sciences, Tsinghua University, Beijing, P.R. China |
| **B.S.** | 2008 | Department of Biological Sciences and Biotechnology, Tsinghua University, Beijing, P.R. China |

**Professional Experiences**

**Research rotations** 2008-2012 Advisors: King-Wai Yau, Ph.D., JHMI

David Linden, Ph.D., JHMI

Marshall Shuler, Ph.D., JHMI

Solange Brown, Ph.D., JHMI

**B.S. Thesis research** 2006-2008 Department of Biological Sciences and Biotechnology

Tsinghua University, Beijing, China

Thesis advisor: Yi Zhong, Ph.D.

**Student Research Training** 2005-2006 Department of Chemistry, Tsinghua University, China

Advisor: Dr. Yauwu Sha

**Honor and Awards:**

| | |
|---|---|
| 2015-2016 | Ruth L. Kirschstein National Research Service Award (NRSA) Individual Predoctoral Fellowship (Parent F31) |
| 2014 | Graduate Student Travel Award |
| 2004-2007 | Tsinghua Scholarship for Academic Excellence |

**Peer-reviewed publications:**

Soroush G. Sadeghi, Sonja J. Pyott, **Zhou Yu**, and Elisabeth Glowatzki (2014)

**Glutamatergic Signaling at the Vestibular Hair Cell Calyx Synapse.** *Journal of Neuroscience 34(44):14536-50. PMID: 25355208*

**Posters and talks:**

**Zhou Yu**, Soroush G. Sadeghi, J.Michael McIntosh and Elisabeth Glowatzki (2015) **Vestibular efferents differentially modulate the activity of vestibular afferents and type II hair cells.** *25th Neuropharmacology Conference, Chicago, IL, USA*

**Zhou Yu**, Soroush G. Sadeghi, J.Michael McIntosh and Elisabeth Glowatzki (Accepted for podium presentation, February 2015) **Mechanisms of Cholinergic Efferent Synaptic Inputs to Vestibular Type II Hair Cells.** *The Association for Research in Otolaryngology, 38th Annual MidWinter Meeting, Baltimore, MD, USA*

**Zhou Yu**, Soroush G. Sadeghi, J.Michael McIntosh and Elisabeth Glowatzki (2014) **Acetylcholine- mediated Ionotropic Currents in Vestibular Calyx Afferents and Type II Hair Cells.** *The Association for Research in Otolaryngology, 37th Annual MidWinter Meeting, San Diego, CA, USA*

**Zhou Yu**, Soroush G. Sadeghi, J.Michael McIntosh and Elisabeth Glowatzki (2014) **Acetylcholine-mediated Ionotropic Currents in Vestibular Calyx Afferents and Type II Hair Cells: Support for Differential Efferent-mediated Responses.** *Society for Neuroscience Meeting, Washington, DC, USA*

Soroush G. Sadeghi, **Zhou Yu**, Sonja J. Pyott and Elisabeth Glowatzki (2014) **Properties of synaptic inputs from hair cells and efferents onto the vestibular afferent calyx terminals.** *Canadian Neuroscience Meeting, Montreal, Canada*

**Service and activities:**

| | | |
|---|---|---|
| 2010 - 2011 | Teaching assistant | Neuroscience journal club, cortical circuitry, Undergrad Neuroscience program, Homewood campus, JHU |